A FINITE ELEMENT APPROACH FOR THE PLANNING AND SIMULATION OF 3D MANDIBULAR OSTEOTOMY FOR ORTHOGNATHIC SURGERY

UNAIZAH HANUM BINTI OBAIDELLAH

FACULTY OF COMPUTER SCIENCE AND INFORMATION TECHNOLOGY UNIVERSITY OF MALAYA KUALA LUMPUR

2006

A FINITE ELEMENT APPROACH FOR THE PLANNING AND SIMULATION OF 3D MANDIBULAR OSTEOTOMY FOR ORTHOGNATHIC SURGERY

UNAIZAH HANUM BINTI OBAIDELLAH

DISSERTATION SUBMITTED IN FULFILMENT OF THE REQUIREMENTS FOR THE DEGREE MASTER OF COMPUTER SCIENCE

FACULTY OF COMPUTER SCIENCE AND INFORMATION TECHNOLOGY UNIVERSITY OF MALAYA
KUALA LUMPUR

2006

UNIVERSITI MALAYA

ORIGINAL LITERARY WORK DECLARATION

Name of Candidate: **UNAIZAH HANUM BINTI OBAIDELLAH**

Registration/Matric No: **WGA040091**

Name of Degree: **MASTERS OF COMPUTER SCIENCE**

Title of Project Paper/Research Report/Dissertation/Thesis ("this Work"):

A FINITE ELEMENT APPROACH FOR THE PLANNING AND SIMULATION OF 3D MANDIBULAR OSTEOTOMY FOR ORTHOGNATHIC SURGERY

Field of Study: **IMAGE PROCESSING, ARTIFICIAL INTELLIGENCE**

I do solemnly and sincerely declare that:

(1) I am the sole author/writer of this Work;
(2) This Work is original;
(3) Any use of any work in which copyright exists was done by way of fair dealing and for permitted purposes and any excerpt or extract from, or reference to or reproduction of any copyright work has been disclosed expressly and sufficiently and the title of the Work and its authorship have been acknowledged in this Work;
(4) I do not have any actual knowledge nor do I ought reasonably to know that the making of this work constitutes an infringement of any copyright work;
(5) I hereby assign all and every rights in the copyright to this Work to the University of Malaya ("UM"), who henceforth shall be owner of the copyright in this Work and that any reproduction or use in any form or by any means whatsoever is prohibited without the written consent of UM having been first had and obtained;
(6) I am fully aware that if in the course of making this Work I have infringed any copyright whether intentionally or otherwise, I may be subject to legal action or any other action as may be determined by UM.

Candidate's Signature: Date:

Subscribed and solemnly declared before,

Witness's Signature: Date:

Name:
Designation:

in the name of Allah, most Gracious, most Merciful

ACKNOWLEDGEMENT

I praise Allah for His consent in completing this dissertation. My gratefulness to the Almighty for good health and compelling strength throughout the research.

First and foremost, I would like to thank Prof. Dr. Ir. Selvanathan Narainasamy for the excellent supervision for which his invaluable spiritual, academic advice, stimulating suggestions, motivating comments and subtle direction of my efforts throughout learning the meaning of 'research' encouraged me to produce better research procedures and a better person as a whole.

I am thankful for the technical support provided by Mrs. Karen Ng Sher Lin, Ms. Chan Wan Kit and Mr. Kenneth Gomez of MSC.Software Company. I am fully indebted to the Fellowship Scheme of University of Malaya for the financial support which has funded the research and dissertation.

I extend my sincere gratitude and appreciation to Prof. Dr. Zainal Ariff Abdul Rahman, Dr. Siti Mazlipah Ismail, Dr. Nor Zakiah Mohamed Zamzam and Dr. Zamri Radzi of the Faculty of Dentistry, University of Malaya for providing data and patiently offered me insights into the clinical topic regarding the case study of this work. To the patient, Mr. Nor Azlan Sulaiman, thank you for sharing the surgery experience and allow me to capture a few photos.

A big thank you is conveyed to Dr. Rosli Salleh, Ms. Mangalam Sankupellay, Mr. Sim Kian Hwa and all staffs at the Faculty of Computer Science for friendly and helpful facilitation throughout the completion of this dissertation. Also, special thanks goes to my comrades, Salhana Amad Darwis, Sara Khanafiah, Sharifalillah Nordin, Sharizal Fadlie Sabri and Zati Hakim Azizul Hasan for their friendship and laughter keeps my sanity within limit.

Last but not least, I wish to express my appreciation to the most important persons in my life. To my parents, Mr. Obaidellah Mohamad and Mrs. Wan Suriati and siblings Ahmad Taufiq, Ahmad Taqiyuddin and Izyan Najla, thank you for the precious care, support and showering love throughout these years. To the one who is always close at heart, Mohd Izzat Latif, thank you for the endless inspiring motivation and sincere friendship all this while.

ABSTRACT

Facial deformities caused by accidents or malformation at birth highly influence the appearance and functionality aspects of an individual. Self-confidence and interpersonal relationships in addition to the ability of breathing, biting and speaking are the few factors affected by facial disharmony. Often corrective surgery known as orthognathic surgery is performed to resolve this issue. Careful and precise surgery planning is mandatory to ensure the success of a surgery that leads to a change in the facial morphology of an individual. The current technique used by craniofacial surgeons for predicting a patient's post operative facial appearance is done by sketches on 2D lateral x-ray images resulting to less-accurate and unrealistic picture, thus leading to the need of a more realistic computerized 3D picture.

Therefore, this dissertation presents a prototype system for the surgery planning involving bone cutting and repositioning particular to the human mandible as well as the prediction of the facial changes through simulation of the virtual orthognathic surgery. Actual preoperative patient data of Asian ethnicity is used and a computerized facial model is derived under the guidance of image processing methods in *Mimics*. The finite element method (FEM) available in *MSC.AFEA* is employed to accommodate numerical solution for mathematical formulations used for representing material properties of biological tissues. In addition, the contact analysis of FEM predicts the facial changes due to the underlying mandibular repositioning through dependant association in between the bone and the tissue. Results of the simulated facial appearance are presented using *Amira* and compared with the actual postoperative photograph.

TABLE OF CONTENTS

LIST OF FIGURES

LIST OF TABLES

LIST OF SYMBOLS AND ABBREVIATIONS

A. List of Abbreviations

2D	2-dimensional
3D	3-dimensional
AFEA	MSC.Advanced FEA
CAD	Computer-aided Design
CAS	Computer-assisted Surgery
CPU	Central Processing Unit
CT	Computer Tomography
CTM	Computer Tomography Modeler
FE	Finite Element
FEA	Finite Element Analysis
FEM	Finite Element Method
LED	Light Emitting Diode
MRI	Magnetic Resonance Imaging
RAM	Random Access Memory
RF	Radiofrequency
RP	Rapid Prototype
SGI	Silicon Graphics, Inc.
STL	Stereolithography (file format)
ZIB	Zuse-Institute Berlin

B. Lists of Symbols

$[E]$	elasticity matrix
[k]	stiffness matrix
{F}	column matrix of the externally applied loads
$N(x)$	shape functions
{u}	column matrix
$u(x)$	unknown field
u, v	displacement components in local coordinates
u_i, v_i	displacement values at element nodes
x, y	point coordinate
x_i, y_i	coordinates of element nodes
K^e , f^e	element matrices
λ, μ	*Lamé* material constants
ξ	local coordinates
e	Element
b	body loads
t	surface loads
E	elasticity modulus, *Young's* modulus
F	concentrated loads
G	shear modulus
ν	*Poisson's* ratio
Ω^e	domain of element
a^e	nodal point unknowns
a_u	unknown nodal values
a_s	specified nodal values
f_a	applied nodal loads
f_r	nodal point reactions

1

INTRODUCTION

1.1. Background

Facial appearance is the first impression that reflects a person's interpersonal relationship during communications. Normal, abnormal, beautiful or aesthetically pleasing faces have been debating issues for a mechanism to be judged as an acceptable facial outlook. Not only has the face represent one's impression on another person's point of view, but also plays a major role in functional systems such as breathing, eating and talking.

The prediction of a balanced and harmony appearance for a patient suffering from facial deformities due to family trait, congenital deformity or trauma in infancy is a rather complex and tedious task to be performed, even by an experienced surgeon. A slight facial malformation of the facial proportion strongly affects the appearance thus determine the aesthetic aspects such as individual beauty (Farkas 1994). These facial deformities fall under the category of maxillofacial and craniofacial disease. The treatment of these abnormalities focuses on functionality and the reconstruction of proportioned aesthetic. Therefore, the use of computer systems to predict a considerable acceptable face due to soft

tissue movement resultant to orthognathic surgery is of critical requirement for both craniofacial surgeons and the patient.

This dissertation deals with the subject on facial soft tissue simulation with a computer. A facial model comprised of skull and facial skin layer is extracted from a type of medical imaging resource. These tissues are obtained from a number of sequential image processing techniques. By employing simplification of anatomical representation in addition to definition of appropriate biomechanical properties of tissue structure that closely characterizes the real face; the model is simulated using the finite element method. The predicted facial appearance is subsequently evaluated with the actual after surgery image of the patient.

1.2. Problem Description

The problem description of this dissertation is to perform surgery planning for mandibular advancement to achieve realignment of the mandible with the upper jaw and simulate the facial soft tissue appearance resultant to forward movement of the mandible. The simulation is carried out by numerical computations done by employing linear elastic solution through the finite element method. The facial model prepared for finite element analysis is highly desired for parameters which define the soft tissue behavior and adequate boundary conditions. The resulting soft tissue deformation has to present at least sufficiently realistic output for comparison and validation with the real postoperative image of the individualized patient.

1.3. Motivation

Over the past 100 years, ever since the discovery of X-ray, the development of medical imaging applications increased exponentially providing enhanced diagnosis, visualization, surgery planning and simulation for almost infinite medical areas. The modern medical imaging technology such as computer tomography (CT) and magnetic resonance imaging (MRI) idealizes the generation of numerous 3D human anatomical models on computer systems. These models are capable of providing meaningful information and thus offer the ability to perform difficult or technically impossible experiments on the computer termed as *in silico*. Thus, computer-assisted surgery (CAS) planning systems have been often used to model and simulate anatomical structures as realistic as it would in reality. In particular, the simulation of soft tissue deformations necessitates integration of numerous field studies such as computer graphics, engineering, biomechanical to possibly obtain acceptable results.

Orthognathic surgery is defined as a type of counteractive facial surgery giving focus on skull and respective facial components performed on patients with malformed facial to correct facial deformities and oral dysfunction. Generally, the current method of planning an orthognathic surgery is performed according to the particular surgeon's experience and intuition by sketches on lateral 2D X-ray radiographs. Most patients are interested to get an initial overview of their predicted postoperative facial appearance if an orthognathic surgery were to proceed for the reasons of confidence and psychological motivation. However, lack of soft tissue information on these lateral X-ray images leaves the patient hesitant and unmotivated for the corrective surgery. Therefore, the computer based system that enables robust, accurate and flexible surgical planning and facial tissue prediction system is of great demand in the area of orthognathic surgery.

Through surgery planning on the computer, surgeons are given the ability to realize interactive simulations of the resulting tissue changes and to improve his planning process. The simulation outcomes are therefore available for analysis and further study. If one simulation does not yield expectation, the surgeon is able to undo the process or perform another virtual operation. Thus, this technique immediately produces better surgical planning as it reduces costs and saves time.

1.4. Requirements

In the view of modeling facial model for the simulation of orthognathic surgery, complex physical based model which includes mathematic equations and advanced numerical computation are required. Listed below are the features adopted for the facial modeling particular for this work.

- The current common methodology used for predicting facial appearance of a corrective surgery is done by sketches on radiographs. Therefore, a computer based planning procedure and simulation results for the predicted soft tissue in the form of three-dimension is desired for craniofacial surgeons and patients.
- In order to realistically model soft tissue simulation, the physics based approach further explained in Chapter 2: Literature review must be employed for the facial models. Hence, a finite element based software program, MSC.AFEA (MSC.Software Corporation 1999) typically used for solving engineering problems is utilized.
- Many works produced by previous researches made use of generic models where patient specific data are registered on the template face for further analysis. In

addition, a number of approaches derive the facial surface from laser range scanners. On the contrary, the facial skull model and the underlying facial skin for this work are extracted from individualized patient CT data.

- A number of biomechanical material parameters responsible for modeling the behavior of facial tissue are incorporated with the facial tissue model. A few examples of them are elasticity, incompressibility and thickness.

1.5. Contributions

The work presented in this dissertation is regarded as a combination of several approaches from previous researches in the field of computer aided craniofacial surgery simulation with combination of a few new techniques to produce better prediction and simulation results. Listed are the contributions of this dissertation.

Anatomy based modeling

In previous works particularly in facial animation (Terzopoulos and Waters 1993, Horace et al. 2000, Kähler et al. 2001, Xia et al. 2001), template based face data are commonly employed instead of actual data sets.

A generic face template is chosen depending on the skull similarities or properties such as ethnicity, gender and age. Subsequently, the skin layer is mapped on the generic model template. Thus, facial appearance deformation is estimated based on the interpolation of the corresponding landmark points of the model skull and the target skull. However, the predicted results would be incorrectly biased according to the chosen template in which unwanted facial appearance is adopted

in the final predicted results. In addition, the use of template-based model produces unspecific reconstruction as the prediction is not face specific.

On the other hand, facial models respectively, the skin surface and the skull structure which are reconstructed from actual and individualized patient data promises specific postoperative prediction. It is also easier to assess the quantitative evaluation because the ground-truth data is readily available. However, due to the complex human facial anatomy, facial models derived based on actual data are always simplified by considering the most vital information such as the skull and the skin layer. Hence, various future researches needs to be undertaken to employ more advanced anatomy such as the facial blood circulation, nerves and muscle anatomy.

Since the skin surface and skull representation are crucial in determining the accuracy of surgical prediction application, the facial models presented in this dissertation are constructed based on merely CT images which were obtained from volume scans. Tissue segmentation technique is utilized to attain different tissue types that range from skull and facial skin.

Case study with real Asian patient data

An important contribution is a thorough investigation on actual patient who are Asians with attention given on the Malay ethnic. A prototype application was built on individual patients in the current clinical environment. This involves the pre and post surgical situations of the patient under clinical treatment. Precise individual parameters such as elasticity, stiffness and bone movement are

incorporated in order to predict the simulated surgery as accurately as possible. Validation between the computed results and actual case are made and the surgical procedures are re-simulated for accurate results.

Surface based facial model

A patient specific surface based model obtained from tissue segmentation is crucial to initiate the craniofacial surgery simulation. Similar approach to (Keeve et al. 1996, Koch et al. 1996, Zachow et al. 2000 and Gladilin 2003), by using the finite element analysis, physics based algorithm the facial deformation for this surface models can be predicted in the sense that deformation on the surface based model is possible through the interpolation of prescribed deformation.

Contact analysis

The derivation of tolerable simplified model is importation in this work. To achieve the contact analysis, the soft tissue simulation is simulated by means of the rigid lower jaw acting towards the elastic deformable facial skin. For each surgical procedure, movements of bones affect the elastic surface. Various attempts with different material parameters and boundary conditions are carried out to determine the optimized chosen approach of contact analysis for the model.

Linear finite element analysis

The linear elastic approach is employed in this work. From previous works (Koch et al. 2000, Zachow et al. 2000, Gladilin et al. 2001a, Schmidt et al. 2004), it is known that the linear elastic approach in soft tissue modeling yields has been mostly used for the approximation of soft tissue behavior. Linear elastic model is

applied due to the complexity of soft tissue behavior, lack of exact and ample data on properties of living tissues. The non-linear approach is more suitable to cater for large soft tissue deformation for which the linear elastic approach is limited for such purpose. Based on finite element approach, the non-linear approach yields more realistic results for modeling of facial soft tissue deformation but high computing powers are necessary to ensure successful results. However, referring to previous researches (Koch et al. 1996, Zachow et al. 2000, Gladilin et al. 2002), the non-linear elastic models yields more realistic and accurate soft tissue prediction and simulation results of large soft tissue deformation. Nevertheless, linear elastic models are still acceptable for small living tissue deformation.

Static soft tissue prediction

The numerical prototype model of the deformable facial soft tissue is applied for the prediction of a patient specific postoperative appearance. Relevant clinical studies are carried out from 3D models derived from individual tomographic data. The predicted results is considered static with attention given on the first impression of the patient's postoperative facial appearance instead of the estimation of patient's facial mimic due to muscular activity which is defined under the dynamic soft tissue prediction. In order to resemble the actual tissue behavior as precise as possible, the 3D facial model is assigned with appropriate material and properties values according to previous researches in the biomechanical field.

1.6. Dissertation Organization

This dissertation consists of six chapters. This section gives an overview of the content of this dissertation.

Chapter 1: Introduction

This chapter introduces the general idea on the entire research project. Motivations that initiates the research is explained followed by the requirements needed for the prototype system development. At the end of the chapter, a number of contributions are given.

Chapter 2: Literature Review

This chapter gives brief explanation on topics researched and studies that are relevant to this project. It is the combination between literature search and literature review. Among the discussed topic are the face anatomy, biomechanics and soft tissue properties, Caucasian bones vs. Asians, three-dimensional medical imaging, surgery planning and simulation, tissue simulation techniques, general idea of the FEM concluded with analysis of previous works contributed by other researches.

Chapter 3: Methodology

This chapter emphasized on the justification of the chosen methods used during the prototype development. Explanation starts with the process of deriving a computer facial model from the acquired data, followed by model improvement steps, surgery planning and preparation for numerical model simulation ended with the analysis setup.

Chapter 4: *Results and Data Analysis*

This chapter presents the results achieved through simulation. Initial results using artificial objects are first described before the actual result is presented. The final results include the dynamic and static output from the respectively MSC.AFEA and Amira.

Chapter 5: *Discussion*

This chapter discusses about the evaluation and validation of the end results. Discussion touches various aspects on the justification of the simulated results achieved in comparison to the actual results.

Chapter 6: *Conclusion and Future Directions*

This chapter summarizes the entire dissertation. An overview of the findings of this research is stated in a sequence order starting from the reconstruction of individualized 3D facial models from computer tomography data until the simulation of the predicted appearance. Comparison remarks are also discussed. Subsequently, a number of suggestions to enhance the current work are elucidated for the future directions. The chapter ends with an overall view of the surgery planning and simulation application in the current state of interdisciplinary research areas.

2

LITERATURE REVIEW

2.1. Overview

This chapter details the basic knowledge about the problem matter of this research. Brief description on the face anatomy is first described. The fundamental properties of biological soft tissues are subsequently introduced followed by comparison of Caucasian bones with Asian bones supported by other researchers' findings. This chapter continues with elementary ideas regarding the three dimensional medical imaging tool, where explanation details on the types of different imaging modalities such as computer tomography and magnetic resonance imaging. Trailing on, the meaning of surgery planning and surgery planning is described. Two common tissue simulation techniques comprised of mass-spring systems and finite element method are presented giving focus on the finite element analysis in which explanation is based on mathematical equations. Finally, prior works of others based on the finite element method and other approaches are discussed.

2.2. Face Anatomy

An accurate face modeling crucial for the planning of surgical operations will determine the degree of realistic behavior of a model. Inadequate with just facial representation, sufficient knowledge about the interaction of facial structure with the surrounding tissues would aid in better understanding of the subject in consideration. The head anatomy is comprised of the skull, muscles responsible for facial expressions and facial function such as the opening or closing of the jaw or eyelid and the skin that represents an individual recognition to others. This section presents brief introduction on the face anatomy in order to gain basic knowledge on the parts utilized for this work.

2.2.1. Bone

The bone that constructs a human face is called the skull where its main functions are to protect the brain and acts as a foundation structure for the face. The skull is divided into two major parts which are the few unmovable bones called cranium located at the upper part of the skull and the remaining bones that forms the frontal face known as the facial skeleton. The cranium which looks like a deformed sphere is pieced together by a number of bones. In addition, the cranium connects head to the body through the neck in the upper part of the back.

As depicted in **Figure 2.1**, the facial skeleton is again partitioned into three distinct divisions whereby the upper region is composed of orbits and nasal bone; the middle region composed of the nasal cavities and maxilla in which the upper teeth resides; and the lower region composed of the mandibular region holding the lower teeth or the only movable

bone structure of the face referred as the mandible. The upper and middle region of the facial skeleton shapes the facial appearance by incorporating the eyes, nose and cheeks. Carrying on, the lower region presents the upper teeth, lower teeth and chin. The lower teeth wherein the mandible known as the only moving bone on the face controls the mouth opening for talking, eating, and expressing emotions. **Figure 2.2** displays the facial structure of a human head.

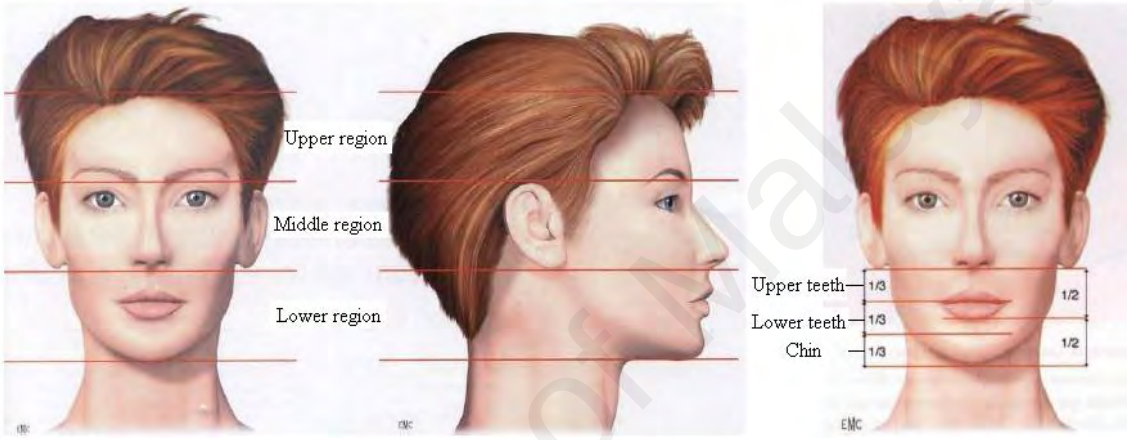

Figure 2.1: The three regions of the face (source: Richter et al. 1998)

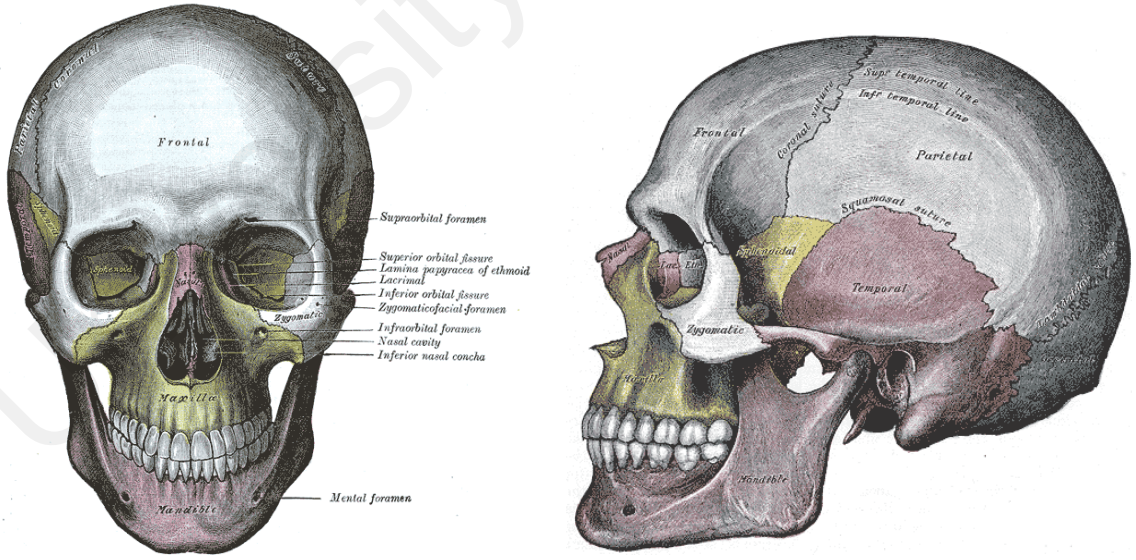

Figure 2.2: Frontal (left) and side (right) view of the human skull (source: Gray 1918)

2.2.2. Muscle

Muscle is the most important tissue responsible for the movement of the body. The muscle functions by contraction and relaxation between the parts they are related to. Four types of muscle connections that initiate motion are attachment by two bones, bone and skin, two different regions of the skin and two organs. The facial muscle is mainly used to execute facial expressions such as moving lips and cheeks. These facial expression muscles are attached to the subcutaneous fat and skin at which the point where they are connected move or slide. Generally, the facial muscles works synergistically rather independently. The motion of the mandible such as forward, backward, mouth opening and closing are affected by sliding of the corresponding muscle of the face. Also, jaw rotation around the joint region in between mandible and maxilla contribute to the movement of the mandible. **Figure 2.3** shows the muscle distribution of the face.

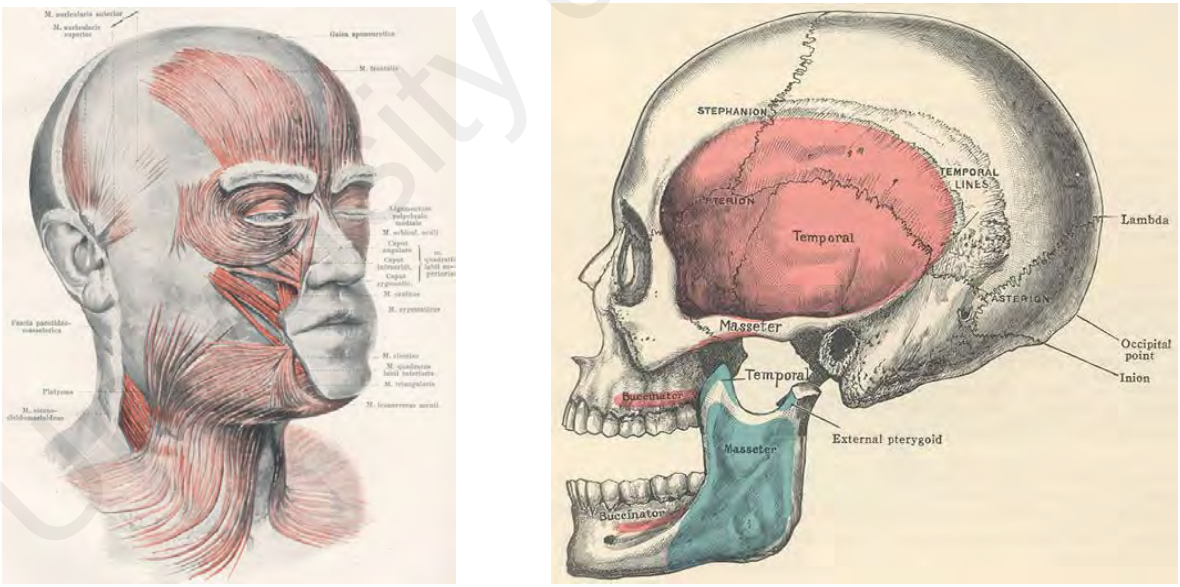

Figure 2.3: Muscular anatomy of the human face (left) and lateral view of facial muscle (right) (source: DataFace 2003)

2.2.3. Skin

The skin externally envelops the entire internal human body and behaves as an interface between the body and its surrounding environment. Skin is composed of interlinked arrangement of *elastin*, *collagen*, nerve fibers, small blood vessels, sweat glands and lymphatics shielded by a layer of *ephitelium* with hairs. The thickness of the skin fluctuates over the entire face. For example, some part of the skin of an older person has wrinkles due to loss of elasticity and underlying fatty tissue. **Figure 2.4** shows the skin anatomy.

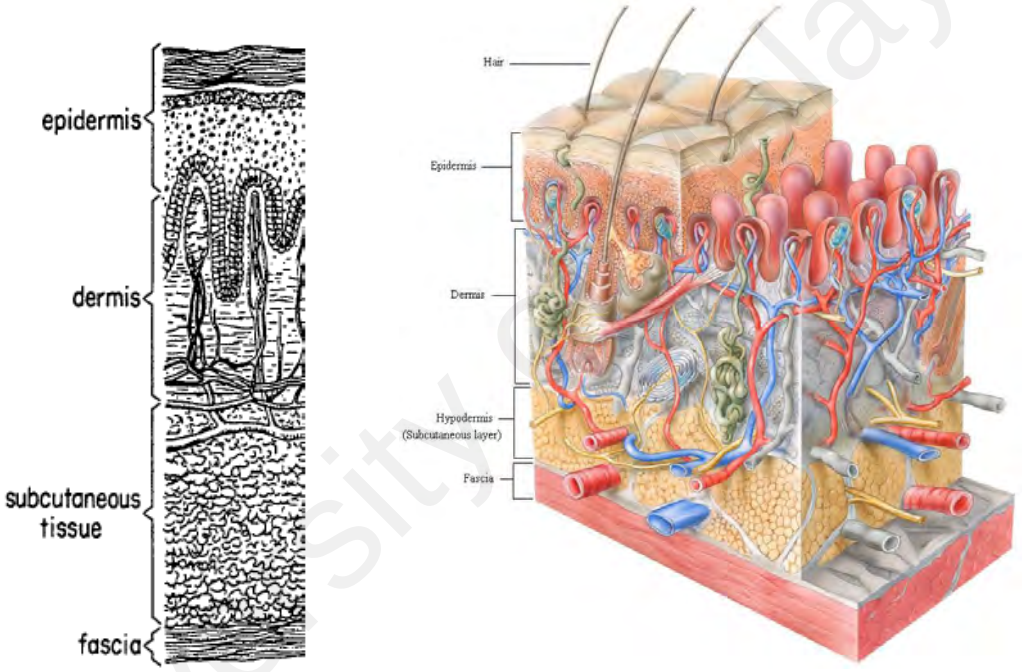

Figure 2.4: The skin tissue structure (source: The Dermis and Epidermis 2003)

In **Figure 2.4**, it is perceived that the skin is structured into two biaxial membranes which are the epidermis, a thin layer of stratified epithelium and dermis, a thicker layer of irregular wavy coiled *collagen* and *elastin* fibers (Danielson 1973). The *elastin* fibers are important in the response of skin at low strains because they are initially stretched as the tissue is strained while the *collagen* fibers remained crimped. In addition, the *elastin* fibers are more elastic and are possible to be reversibly stretched to more than 100% (Lanir 1987).

Epidermis and dermis are networked by the *collagen* fibers to a subcutaneous fatty tissue called *hypodermis*, which resides in the third layer of the skin. The *hypodermis* is connected to fascia that directly surrounds the muscle bundles. It is in this subcutaneous region where the skin slides with internal soft tissues. On the other hand, the upper layers are impervious to protect from injuries.

2.3. Facial Tissue Structure

Knowledge in facial anatomy and biophysics is crucial for biomechanical modeling of biological structure. Soft tissues are fundamentally composed of fibrous protein called *collagen*. Fung reported that the collagen constitutes 75% of skin dry weight, 4% for the *elastin* and the remaining weight is shared between *reticulin* and a *hydrophilic* gel called ground substance (Fung 1981). The mechanical properties of tissue differ depending on the organization of fibers, cells, and ground substance of a tissue structure (Fung 1981). As depicted in **Figure 2.5**, the tendon is organized in hierarchical bundles of fibers arranged in a parallel-fibered structure in a selection of defined direction. A closer analysis at the fiber network proves that the parallel arrangement is more irregular and distributed in various directions for ligaments than for tendons (Fung 1981).

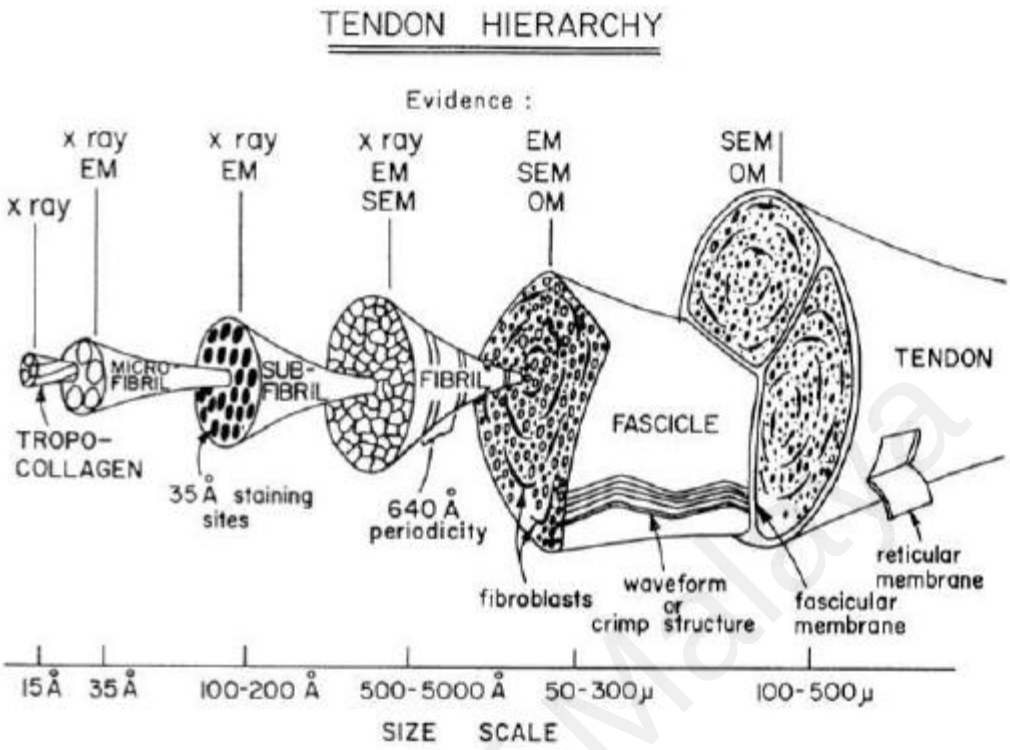

Figure 2.5: The organization of fibrous structures in tendon (source: Fung 1981)

2.4. Biomechanics and Soft Tissue Properties

Biomechanics is signified as the study of engineering mechanics applied to the field of biology and physiology. It is closely coupled with the analysis of dynamical and mechanical systems of the human body. In common practices, the engineering methods and classical mathematical models are incorporated during the biomechanical study of living tissues. However, being the creation of God, the living tissues have different properties than typical engineering problems. For instance, the living tissues encompasses unique properties such as self-adapting and self-repairing where under a given tolerable load, the tissue would return to its normal state and in general, under the condition of healing, soft tissues are capable of regenerating new tissues.

From an engineering point of view, the human body is considered a load-transmitting mechanism. Thus, springs the exploration and development of experimental research for the soft tissue mechanics. A number of experiments such as (Ahmadian et al. 2005, Kenedi et al. 1975, Maciel et al. 2003, Liu et al. 2004, Han et al. 2002) have been carried out to understand the physical behavior of soft tissue in the view of biomechanics. Based on these experiments, the mechanical properties of soft tissues are basically described as *viscoelastic*, *inhomogeneous*, *hysteresis*, *anisotropic* and have *non-linear* force characteristics (Fung 1981). The subsequent subsection details the properties definition.

2.4.1. Non-linear elasticity

The major characteristic of soft tissue is outlined as *nonlinear elasticity*. The stress-strain relationship termed as constitutive equation shown in **Figure 2.6** determines the linearity response of soft tissue. At the initial stage, the response of soft tissue is linear under low strain denoting low modulus region. This is when usual tissue normally functions. Subsequently, during the intermediate region in the average strain, the collagen fibers begin to straighten and tissue stiffness increases proportionally with the modulus. The largest region where all fibers are straight at increasing high strain computes maximum linear modulus that remains relatively constant until the yielding point is reached. A yield point indicates the moment at which the material destruction occurs. Thus, at the final region of larger strain, the modulus decreases before complete tissue ruptures happen. The stress-strain relationship highly varies from person to person. According to Kwan and Woo, "*The low modulus region is attributed to the removal of the undulations of collagen fibrils that normally exist in a relaxed tissue. As the fibrils become taut and loaded, the tissue modulus*

reaches a maximum value, and thereafter, the tensile stress increases linearly with increasing strain. With further loading, groups of fibrils begin to fail, causing the decrease in modulus until complete tissue rupture occurs." (Kwan and Woo 1989)

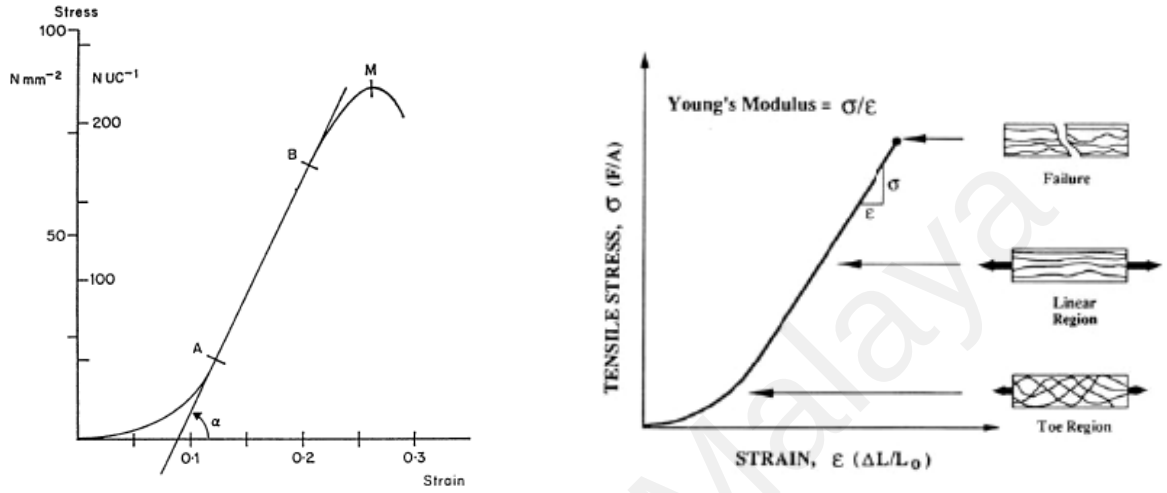

(a) (b)

Figure 2.6: (a): Load elongation curve (source: Viidik 1980), (b): Soft tissue stress-strain curve (source: Maciel, Boulic and Thalmann 2003)

2.4.2. Non-homogeneous, anisotropy

Soft tissues are composed of various types of materials containing cells, fibrous and microscopical structures. Spatial distribution of the material stiffness is important for soft tissue modeling. Each of these materials has specific preferential orientation in the skin. *Non-homogeneity* is described as the coordinate dependence along the same spatial direction throughout the skin. A material is defined *isotropic* if all of its property is the same in all directions. Conversely, the soft tissue which falls under the *anisotropy* category consists of property that varies in arbitrary directions. The facial tissue has the characteristics of *non-homogeneous* and *anisotropy*.

2.4.3. Plasticity

The deformation of a normal functional tissue under the range of small strain is reversible. The process of load given to and unload from the tissue through strain called loading and unloading is referred as *hysteresis* such as shown in **Figure 2.7** shows the *hysteresis* curve of a typical tissue. This is in accordance to various engineering material where soft tissue demonstrates plastic behavior within a limited strain. However, large deformation on the tissue leads to irreversible material rupture. This deformation labeled plastic differs from the reversible elastic deformations. In spite of the material destruction, living tissue is known for its self-repairing ability. After a certain period of destruction, the tissue repairing mechanism would generate new tissues conveyed as the process of reversing destructive alterations. Evidently, the time factor plays a major role in determining the suitable mathematical formulation for soft tissue modeling. Unfortunately, at the moment, the plasticity theory for soft tissue is comparatively limited to approximate its significance for soft tissue modeling.

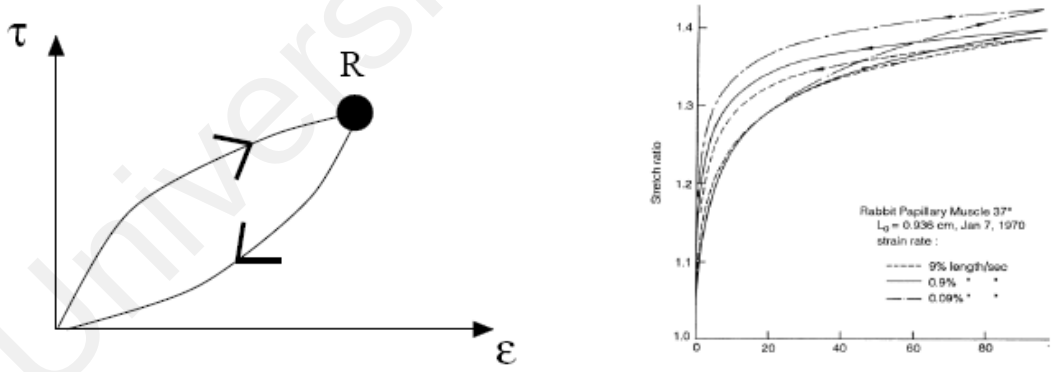

(a) (b)

Figure 2.7: The *hysteresis* behavior of soft tissue: (a): *Hysteresis* loop (source: Delingette 1998), (b): *Hysteresis* curve (source: Fung 1981)

2.4.4. Viscoelasticity

The stress-strain relationship of non-linear material property is an example of equilibrium between the interactions of stress and strain. However, when equilibrium is not reached, a history-dependent mechanical behavior of living tissue exists (Fung 1981). Experiments have shown that given the same strain value, the stress values appeared higher than the one at equilibrium as depicted in **Figure 2.8**. Experiments have also revealed that stress gradually decreases against time when tissue is abruptly extended and maintained at the new length. This characteristic is called *stress relaxation* as posed in **Figure 2.9**. If a tissue is given a constant load, against time the lengthening velocity would decrease until equilibrium is reached. This fact, shown in **Figure 2.10** is expressed as *creep*. These behaviors which behave relying on time and history of the deformation are termed *viscoelasticity* (Fung 1981).

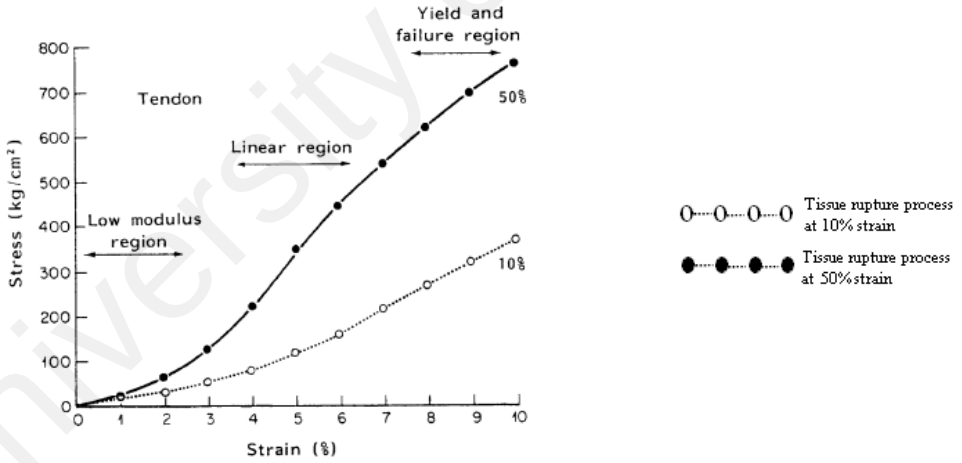

Figure 2.8: The effect of equilibrium towards stress-strain curve (source: Birk et al. 1991)

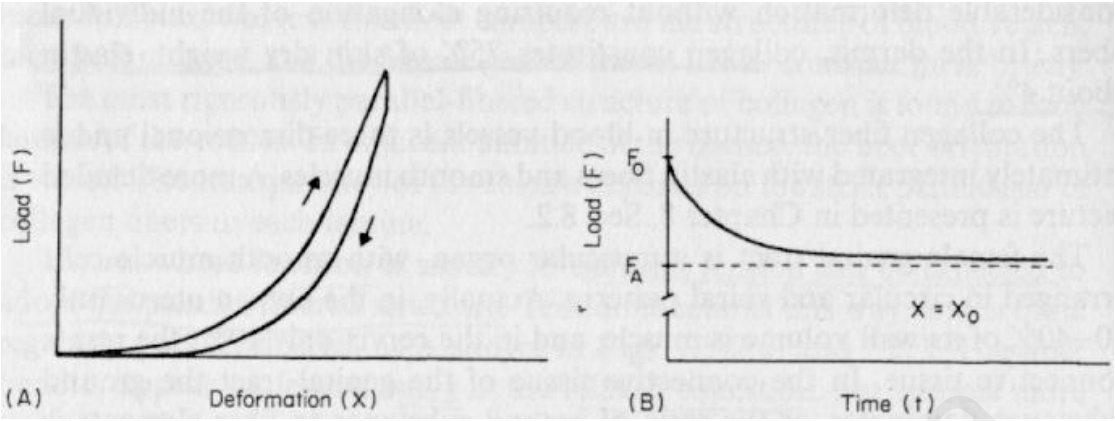

Figure 2.9: Stress relaxation of a ligament specimen. (a): Load-elongation and relaxation curve, (b): Specimen was stretched until F_0, then maintained its length where the load relaxes at a limiting value F_A (source: Fung 1981)

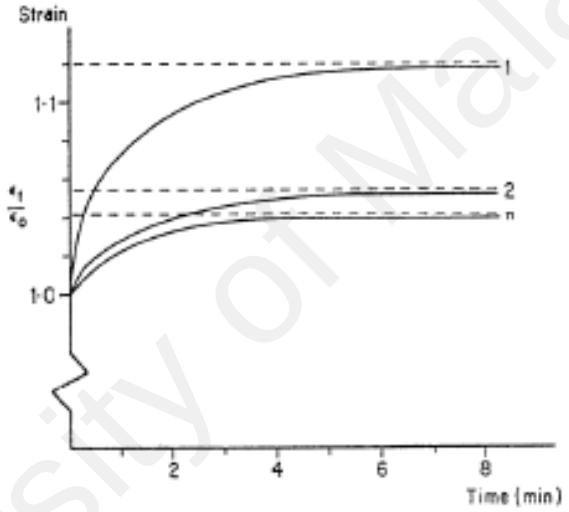

Figure 2.10: *Creep* phenomena of a soft tissue (source: Viidik 1980)

2.4.5. Other Properties

The compressibility of soft tissue is still in debate. A number of researches assume soft tissues as compressible (Kenedi et al. 1965, Veronda and Westmann 1970) while others (Fung 1967, Blatz et al. 1969, Hilderbrandt et al. 1969) believed soft tissues are sensibly incompressible. A material is considered incompressible if the volume remains unaltered by deformation. Tissue with high water proportion such as the brain is usually modeled as incompressible materials while tissues with low water proportion are assumed quasi incompressible (Gladilin 2003).

As demonstrated in **Figure 2.11(a)**, the stress-strain curve of the constitutive equation graph is progressively shifted to the right if the loading-unloading cycles are repeatedly applied to a tissue at the same stress level. However, after a number of cycles, the mechanical response of the tissue reaches a stable iteration stage. The initial phase of material behavior common to major living tissues at which they are used former to experimentation is termed *preconditioning* (Viidik 1987). The load-elongation curve is illustrated in **Figure 2.11(b)**.

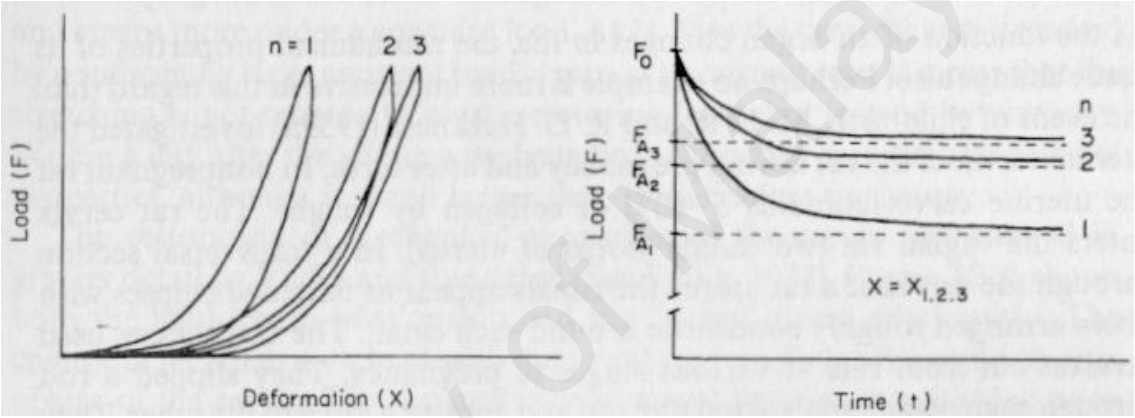

Figure 2.11: Preconditioning of a ligament specimen in (a) and the equivalent load-elongation and relaxation curve in (b) (source: Fung1981)

2.5. Caucasians Bone vs. Asians

In general, Caucasians have larger bone frame in comparison to Asians. This is caused by many reasons which among a few are environmental, genetic, cultural background, lifestyle and nutritional. For example, individual body proportions differ between different race or ethnic group where Asians have longer trunks and shorter legs than Caucasians (Seeman 1998). (Wang et al. 2002) reported that the buckling ratio which relatively estimates cortical thickness is higher in Caucasian woman than Asian women. This explains the reason of longer, wider and stronger femoral neck in Caucasian women than Asian woman who posses moderately thicker cortices in a narrower femoral neck. (Karlamangla et al.

2002) revealed that the Japanese have greater measures of bending, impact and compressive strength compared with Caucasians.

The size differences between the race ethnic groups is another factor contributes to the diverse bone mineral density. A study to determine the occlusal status in Asian male adults was performed by (Soh et al. 2005). The research was performed to observe the degree of normalized facial appearance in terms of occlusal status in three ethnic groups; Malay, Chinese and Indian. The main findings found out from the research was: 1) Asians have lower occurrence in crooked tooth *(Malocclusion Class I)* than Caucasians showed in (Ingervall et al. 1978, Salonen et al. 1992, Tod and Taverne 1997); 2) Asians are more prone to having lower teeth that are further ahead of the upper teeth *(Malocclusion Class III)*, termed as *underbite* in comparison to Caucasians. Both Chinese and Malay ethnics commonly encounter the *underbite* problem. Another research performed by (Woon et al. 1989) found no difference in the poor positioning of the teeth between Chinese and Malay ethnic groups; 3) Indian males are four times more possible to having upper teeth further ahead of the lower teeth *(Malocclusion Class II)*, termed as *overbite* than Asian Chinese and Malay males but lowest occurrence for the *underbite* among the three ethnic groups. **Figure 2.12** shows the three malocclusion classes and the normal teeth positioning.

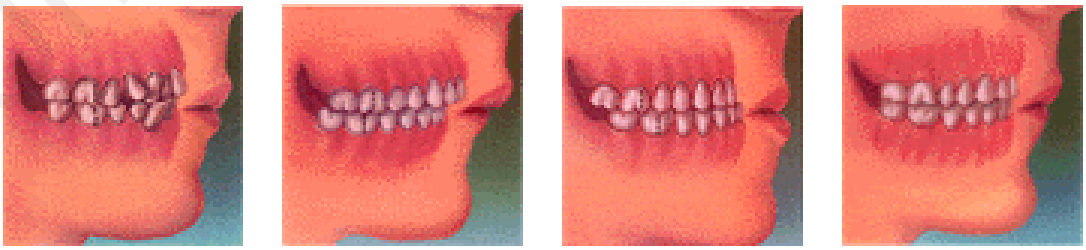

(a) (b) (c) (d)

Figure 2.12: Various malocclusion classes and proper occlusion. (a): Class I, (b): Class II(*overbite*), (c): Class III(*underbite*), (d): Normal jaw (source : Bracesinfo 1999)

Majority of the current and previous researches in the virtual orthognathic surgery planning and simulation for the facial soft tissue prediction were carried out by using Caucasian data (Koch et al. 1996, Zachow et al. 2000, Gladilin et al. 2004). A few researches focus on the Chinese (Xia et al. 1995, Horace et al. 2000, Shen et al. 2000) and Japanase (Alcalde et al. 1998, Terai et al. 1999, Watanabe et al., 2005) ethnicity predominantly from China and Japan. The biggest ethnic in Malaysia is the Malay. Until the time of writing, the author has not found any research study, whether local or abroad, on the computer aided orthognathic surgery planning and simulation using the finite element method particularly for the Malay ethnicity in the Asian region or Malaysia in precise. Therefore, this work is undertaken to initiate the study of postoperative facial soft tissue prediction for the Malay ethnic from Malaysia.

2.6. Three-Dimensional Medical Imaging

Three-dimensional (3D) medical imaging is a tool that allows clinicians to view 3D representation of anatomic structures on a computer screen promising enhanced visual representation, diagnosis and treatment planning for various physical disorders in medicine including orthognathic surgery and orthodontic treatment in dentistry. Several types of modalities such as conventional tomography (Maue-Dickson et al. 1979, Shirkhoda et al. 1984), computer tomography (CT) (Kawamata et al. 2000), (Hemmy et al. 1983), magnetic resonance imaging (MRI) (Daniel et al. 1998), (Nastri et al. 2004), and ultrasound (Delcker and Diener 1994) are available in the 3D medical imaging by producing a set of sequential cross-sectional slice images of the human body. CT is the best modality for hard tissue structure while MRI produces excellent soft tissue representation. **Figure 2.13** shows the

reconstruction of 3D images based on slice image data generated by CT and MRI. Section 2.6.1: *Digital Medical Imaging* will further explain about the CT and MRI imaging modalities.

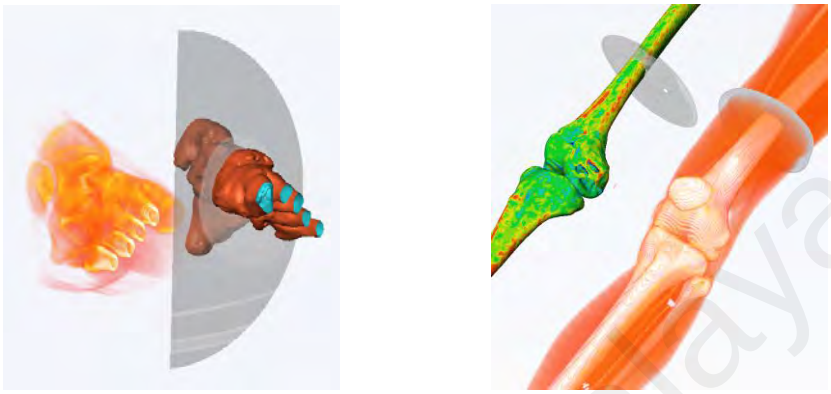

(a) (b)

Figure 2.13: Original slice image and the reconstructed 3D images. (a): 3D foot from MRI(left) and CT(right) and (b): 3D leg from MRI(right) and CT(left) (source: Amira demo 1999)

2.6.1. Principles of Three-Dimensional Imaging Modalities

A two-dimensional (2D) digital image is constructed by an array of finite numbers of discrete picture elements called *pixels* arranged on a rectangular grid as illustrated in **Figure 2.14(a)**. Every pixel has a gray value information which corresponds to the CT number in the *Houndsfield* unit. The information determines color in the 2D image. In 3D imaging, the individual *pixel* elements are termed *voxels*. A 3D image is usually composed of *voxels* piled up in layers shown in **Figure 2.14(b)**. The number of layers or data slices which could range from a few layers to hundreds of layers is determined by the type of tissue to be constructed. In addition, the total numbers of data slices varies depending on the type of imaging method, the size of tissue to be extracted and scanning factor among a few other reasons. Thus, various 3D imaging techniques are available for visualization where different types of information can be extracted relying on the specific tissue of

interest. **Figure 2-15** shows an example of the 3D reconstruction of a vessel for the cardiovascular blood flow derived from MRI data slices.

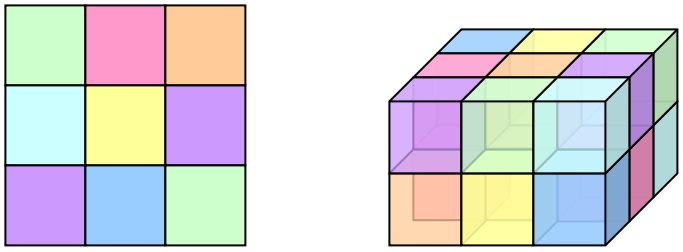

(a) (b)

Figure 2.14: (a): *Pixels* used to create image and (b): *Voxels* used to construct 3D model

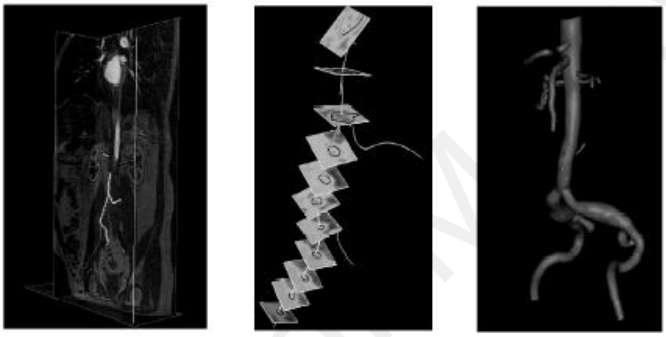

(a) (b) (c)

Figure 2.15: Vessel for cardiovascular blood flow. (a): Vessel path obtained from MRI data, (b): Stacked of 2D slices along the selected tissue and (c): 3D reconstructed model of the vessel (source: Müller et al. 2005)

2.6.1.1. MRI

MR imaging uses two main principles to produce an image (Brooks 2001). First, the MRI technique takes into consideration of the time required for diverse tissue properties to give up radiofrequency (RF) energy to the system during a scanning process. Second, MRI exploits the density differences of hydrogen protons in a variety of tissues to obtain the desired tissue image. Hydrogen is used mainly because it is massively available in the body tissue due to water and fat consumed through food. The hydrogen is bounded with various types of molecules thus results to different tissue composition displayed in numerous gray scale images (Brooks 2001). The MR imaging technique is commonly used in soft-tissue musculoskeletal and vascular imaging. A number of applications for example, in the area of

breast disease (Daniel 1998), cardiovascular blood flow (Müller et al. 2005) and brain segmentation (Snell et al. 1994) have been developed by utilizing the MRI technique.

The MR image, besides ultrasound and laser-scanned image is a type of 3D imaging approach without exposure to radiation. Hence, this technique is a safe procedure although it uses strong static magnetic fields, time-varying gradient fields and pulsed RF fields (Brooks 2001). However, MRI is prohibited for patients with cardiac pacemaker implants or metallic implants because of the effect of strong magnetic field on either magnetically sensitive equipment or ferromagnetic objects in the patient's body (Bhachu 2000, Boutin 1994). **Figure 2-16** shows a few examples of defected MR images due to artifacts.

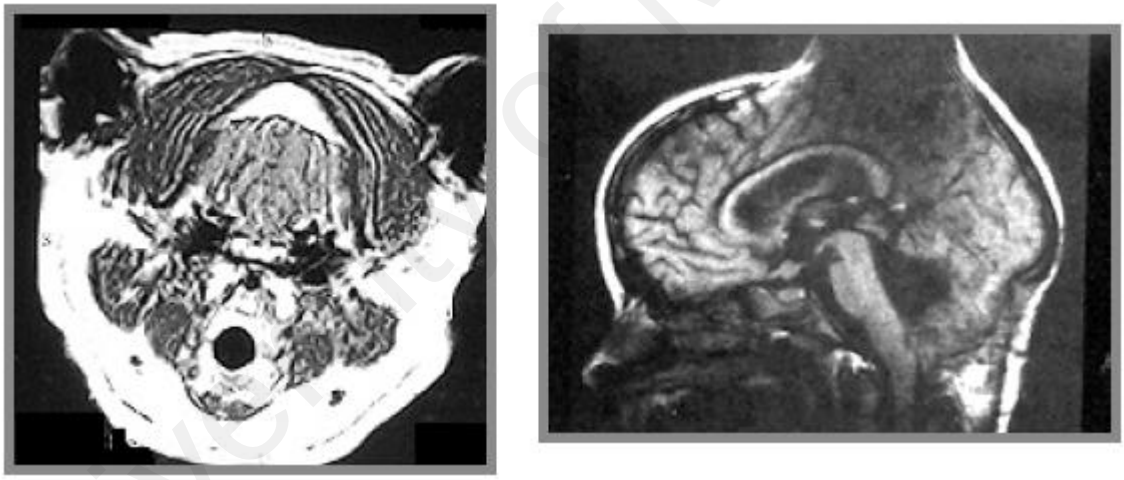

(a) (b)

Figure 2.16: Examples of defected MR image caused by (a): Motion artifact due to movement and (b): Metallic artifact due hair clip worn during scanning (source: Introduction to Magnetic Resonance Imaging 2005)

2.6.1.2. CT Images

CT is the most commonly used imaging technique in dentistry due to the request for mainly bony structures. CT images are achieved by direct but minimal x-ray radiation to the body part of concern by a few scanning components comprised of a detector array, an x-ray source, a patient support couch and a computer featured with suitable operating console.

The currently available CT techniques are determined by several types of scanner for which they are the translate-rotate scanner, rotate-rotate scanner and rotate-only scanner. The scanners determine the scanning procedure. A few examples of these scanners are respectively fan-shaped beam and linear detector array, fan-shaped beam and curvilinear detector array and helical CT. The characteristics of CT images are different from the conventional film because the image receptor is not film but a direct digital sensor in which better exposure is attained due to the impact of image density and contrast. Extreme densities between tissues are not visible in film based image.

In every scan, the CT images are acquired in axial plane. These images referred as slices are taken in sequential order. The manipulation of these slices would produce coronal and sagittal images thus permit the generation of 3D images. **Figure 2.17** shows an example of these slices in their relevant planes.

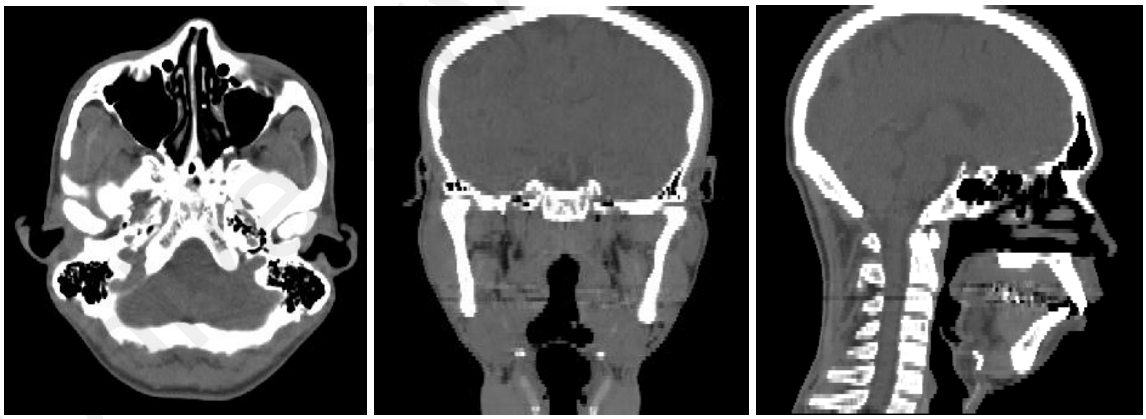

(a) (b) (c)

Figure 2.17: Human head CT slices at different planes. (a): Axial view, (b): Coronal view and (c): Sagittal view

A thresholding process separates diverse tissues such as bone, teeth and skin for improved visualization for the tissue structure of interest. A specific range of gray values which differs these tissues are defined accordingly. This task is easy due to the reason that the

gray values corresponds to CT numbers within the range of -1000 and +3000. **Table 2.1** lists the general range for a few types of tissues.

Table 2.1: Threshold range for various material types (source: Parks 2001)

Material type	CT numbers
Air	-1000
Lung	-200
Water	0
Cerebrospinal fluid (CSF)	15
Blood	20
Gray matter	40
White matter	45
Muscle	50
Medullary bone	300
Cortical bone	1000

The types of tissues considered for this work are the outer skin layer, maxilla and mandibular bone. The respective CT numbers for these facial models are given under *section 3.3.1: Image Segmentation*. Therefore, the use of CT imaging is of greater advantage than MR imaging as the region of interest are easily selected, viewed and constructed with different density parameters for the same data set.

2.7. Surgery Planning

Various medical applications have been developed in the beginning of 1970's since the invention of CT by Hounsfield in 1972 (Hounsfield and Ambrose 1973). Among the common applications are hip or knee replacement in *orthopaedic* surgery (Soyama et al. 1989, Sarni et al. 2004, Maciel et al. 2002), treatment of brain lesions such as tumors

(Joedicke et al. 1998, Black et al. 1997, Hata et al. 1998) in brain surgery not leaving the prediction of postoperative facial appearance in craniofacial and maxillofacial surgery.

A patient whose face needed surgical correction due to facial deformity would have to undergo numerous discussions with craniofacial surgeons. Should a corrective surgery proceeds, the generally performed conventional method rely on a surgeon's experience and judgment on the prediction of a patient specific facial appearance. The common technique for this approach is usually realized via sketches on two-dimensional lateral x-ray images known as *cephalogram* to forecast the soft tissue changes before operation, requiring certain amount of knowledge from a skilled medical artist thus consequences to time consuming and tedious task.

Conversely, the computer aided surgery planning for orthognathic reconstructive surgery permits perpetual planning for the respective patient almost instantaneously. Moreover, precise planning is achievable hence reduces planning time and improves postoperative outcome. The accuracy required for such operations is within millimeters. Deviations can be responsible for success or failure of an operation. The planning procedures require a realistic simulation of the geometry alteration of a particular bone structure of a face. The geometrical information is attained from CT images. Thus, with the intervention of surgeons involved during the surgery, a reliable surgery planning methodology is possible. Applying a number of re-planning enables the surgeon to choose the most optimal surgical procedure before the actual surgery is performed.

In order to achieve sufficient flexibility in reshaping the face, a surgical procedure necessitates a craniofacial surgeon to determine the best location for bone cutting and

repositioning. Each bone fragment should be moved in directions such as right-left, up-down or forward-backward specified in millimeters depending on the corrective scheme. These procedures will be taken as a blueprint for the surgeon to execute as precise as possible during the real surgery in the operation theater.

The availability of surgery planning embedded in the computer assisted surgery applications are not meant to replace the existing methods. However, these applications serves as further enhanced techniques that could complement, definitely adds value to the current methodology. Thus, significantly contributes towards a safer, harmless, risk minimal treatment and most importantly reduce or at an advantage eliminate traumatic side effects of therapeutical procedures.

2.8. Surgery Simulation

An incredibly experienced and highly skilled craniofacial surgeon is able to estimate and mentally visualize a fair facial outlook of a patient even before the operation is accomplished. Surgeons do not have a proper method to put on view the prediction of the patient's face so that the patient is able to visualize how they will look like during the consulting in advance of the surgery. The surgeon's assumption may differ from the patient's thoughts. Additionally, the patient may disregard the idea of surgery which could result to worse scenario if the facial deformation is critical. Also, if a surgery is performed without careful planning, the patient will suffer from trauma of pain during the recovery process or it could even be worse if the surgery failed to produce an acceptable patient's facial anatomy. The current postoperative prediction on lateral *cephalograms* does not

present much trust from the patient. Therefore, a method to provide better visualization between patient and surgeon is crucial. Hence, surgery simulation is often opted together with the computer aided surgery planning application.

The surgery simulation in the context of reconstructive surgery and soft tissue prediction for orthognathic surgery involves rendering and animation of the predicted patient specific postoperative appearance from the actual facial features. As a result to this technique, surgeons and patient benefited from higher degree of confidence towards the surgery and of course more precise surgery procedures.

The best tool to understand three-dimensional structures is by rendering whereby the viewer gets an impression of visualizing an actual organ of study. The two major types of rendering are surface rendering and volume rendering. Detailed explanations are described in section 2.8.1: *Surface Rendering* and section 2.8.2: *Volume Rendering* below.

2.8.1. Surface Rendering

Surface rendering is a technique for visualizing a geometrical representation of a surface from an actual three dimensional volume data or in other words, defined as two-dimensional surfaces at different planes embedded in a three-dimensional space. A surface rendering is achieved through *isosurface* termed by a surface formed from a cross connection of data points within a volume of equal value or density (Roberts 1993). The surface appears as a continuous representation of surface primitives such as triangulations between contours constructed based on contouring lines over data points. Two main data

representation (Roberts 1993) for contoured surfaces are 1) structured planar representation as seen in **Figure 2.18** where contours are easily created from sorted data points in planes and 2) unstructured random data points where data points are in a random arrangement as illustrated in **Figure 2.19**.

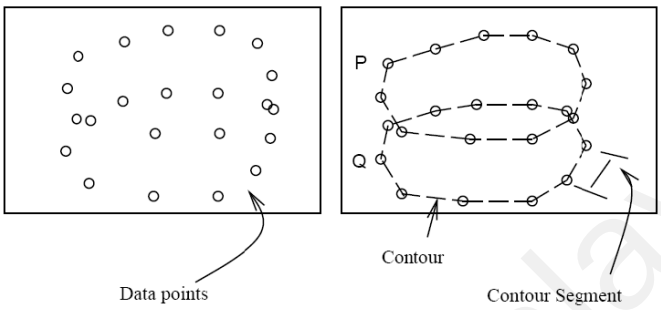

Figure 2.18: Structured data points (source: Roberts 1993)

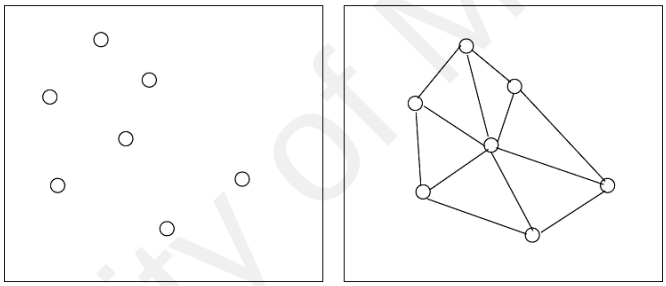

Figure 2.19: Unstructured data points (source: Roberts 1993)

These data points whether structured or unstructured can be connected by triangles through various selections of algorithms. The process of producing surfaces from the three-dimensional data set is referred to as triangulation.

2.8.2. Volume Rendering

In contrast to surface rendering, volume rendering is formally defined as a direct visualization of the actual three-dimensional volume data set without incorporating intermediate geometric representations for *isosurfaces*. Instead, the three-dimensional computer model is acquired by ray casting technique where rays are cast directly to the

object of interest from the viewing plane. Transparency, opacity and color information are calculated for each cell. The rays are cast until an opaque object is 'hit' or the ray exits the volume object (Roberts 1993). A research by Carnegie-Mellon on (Volume Rendering 2000) as shown in **Figure 2.20(b)** displays an example of a reconstructed volumetric structure. Although better image quality is achieved through volume rendering, the current technology has not yet to achieve excellent rendering for this option. The rendering speed is often slower than surface renderings.

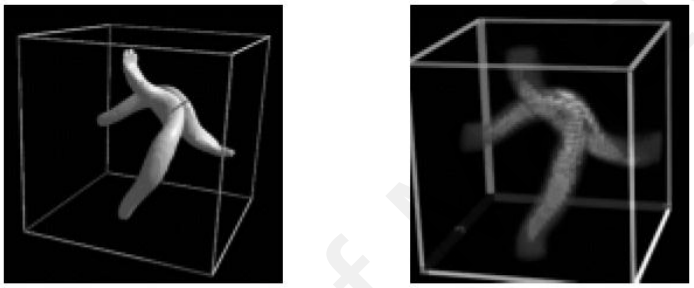

(a) (b)

Figure 2.20: Direct volume rendering for a structure. (a): Ray traced *isosurface*. (b): Volumetric rendering of structure in (a) (source : Volume Rendering 2000)

2.9. Tissue Simulation Techniques

Several approaches are available for the modeling and simulation of soft tissue deformation. The two major physically based techniques commonly used for the computation methods are described below.

2.9.1. Mass-spring Systems

The mass-spring is the classical deformable approach used for modeling deformable objects. A mass-spring model consists of a collection of point masses or nodes connected

by springs in a lattice structure. When a mass is displaced from the current position, the springs connecting point masses apply forces on its neighboring points.

The mass-spring systems have been frequently used in facial animation including muscle deformation. (Terzopoulos and Waters 1990) used three mass-point mesh layers to respectively represent the dermis, subcutaneous tissue and muscle of the facial tissue. (Lee and Terzopoulos 1995) improved the approach by employing constraints to prevent penetrations between soft tissues and bone. Simulation of muscle deformations were performed by (Nedel and Thalmann 1998) where muscle shapes were changed in its form by utilizing the mass-spring mesh. (Bourguignon and Cani 2000) in their effort, offered control over isotropy or anisotropy of elastic material. Besides the human facial anatomy modeling, mass-spring systems have also been applied for cloth motion (Baraff and Witkin 1998) and surgical simulation (Brown et al. 2001). The cloth simulation is of major importance in 3D animation because it allows for realistic modeling of dressed humans. Among the applications for which cloth simulation is applied lies in the category of textile CAD, video games and interactive web assistants. Cloth simulation in CAD softs decreases productivity as a method for direct visualization of cloth appearance exists. Furthermore, cloth simulation in the multimedia community adds realistism to dressed moving characters.

Among the advantages of mass-spring systems are easy to construct for interactive and real time simulation and simulation is easily solved within a short period of time on a typical desktop systems. This is because, mass-spring systems uses less complex mathematical formulation of Newton's motion equation (Keeve 1996a) for which each node is given a differential equation of second degree depending on the mass, damping and sum of all

spring forces influencing the system (Waters and Frisbie 1995). Therefore, less computation is required for a completion of a successful analysis. The mass-spring systems are also capable of handling large displacements and large deformation. However, mass-springs systems have a few disadvantages. The mass-springs technique is less reliable in modeling the exact physical properties of human tissue. Due to the reason that mass-spring models are handled in terms of spring constants, values and constraints to be assigned to these constants are not easily distributed. Another known problem appeared when spring constants are large. Large constants are used to model rigid or non-penetrable models. Therefore, deformations results are difficult to achieve if small time steps for numerical computation resulted in slow simulation (Gibson and Mirtich 1997) are not applied.

2.9.2. Finite Element Methods

The finite element is a more accurate method as compared to the mass-spring systems. This has been proven by researches in their publications (Keeve et al. 1996, Keeve et al. 1998, Keeve and Kikinis 1999, Delingette 1998, Roth et. al 1998, Maciel et al. 2003). In the finite element method, an object is considered a continuum, meaning a solid body with mass and energies distributed throughout the object in consideration. The continuum is divided into a finite number of elements joined at node points. In order to obtain deformation of the object, a combined function that solves the equilibrium equation found for each element is solved.

The finite element method is used in (Liu et al. 2004) to model non linear mechanical behavior of breast tissue under large indentation deformation. Material parameters such as *Young's modulus* and *Poisson's ratio* pertinent to the soft tissue are incorporated to

compute the tissue deformation. In order to achieve faster mathematical computation, a method for reducing the solution time is crucial. Therefore, the condensation technique is presented by (Bro-Nielsen and Cotin 1996) to accommodate the computation time. This technique reduces the computing time by considering solution for only meshes on the surface of a volumetric model.

The major advantage of finite element method is the precise modeling of physical soft tissue properties. Realistic simulation is ensured in contrast to the mass-spring systems. However, the computation duration required to solve biological materials are time consuming because this type of material deforms in large proportion unlike most engineering materials. For example, metal is assumed to have small deformation which can be easily solved using linear elastic theory. Therefore, the finite element computations are rarely done interactively on common workstations.

2.10. Finite Element Method

The finite element method (FEM) is a powerful engineering analysis tool suited to the digital computers to accommodate the need of solving problems in solid mechanics, fluid mechanics, heat transfer and vibrations. A fundamental idea of FEM explains that by dividing a system into a large number of small elements, they mimic the physical reality by which cell interactions even on large distances, result from a large number of localized interactions between adjacent units (Kolston 2000). Therefore, finite element techniques are suitable to be applied to various biological organs including the soft tissue prediction of facial appearance due to deformities. The behavior of organs when presented with particular stimuli such as force or pressure can be predicted by simulation using this

technology (Kolston 2000). This section introduces the basic of FEM for the simulation of elastic materials. The readers are referred to (Burnett 1987, Bickford 1989, Zienkiewics and Taylor 1989, Cook and Malkus 1989, Chandrupatla and Belegundu 1997) for a more detailed description. A simple idea of the simulation of FEM is illustrated in **Figure 2.21**.

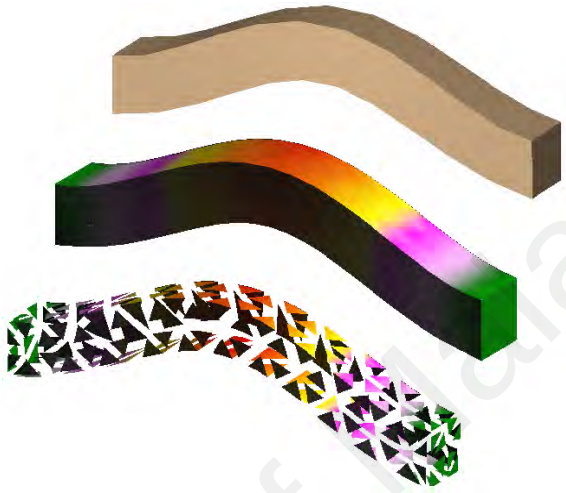

Figure 2.21: An example of the finite element analysis simulation of a tissue block

2.11. Finite Element Analysis

The finite element analysis (FEA) is a computer based numerical procedure used to determine approximate solutions such as stresses, strains and deflection of structures too complex for manual mathematical hand calculation or have no theoretical solution. In FEA, a structure is divided into finite number of simple elements. Depending on the dimensions, elements types range from line or curve for beam elements; two or three sided surface for shell elements; triangular or quadrilateral for two dimensions elements to tetrahedral and hexahedral for solid elements. **Figure 2.22** illustrates these types of elements.

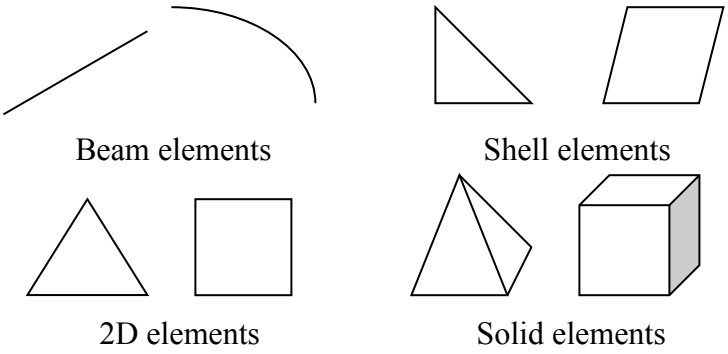

Figure 2.22: Types of elements

Each of these single elements is connected at points called nodes. For example, a line has two nodes while a triangle has 3 nodes. These nodes are referenced for the algebraic equation to determine the motion and deformation of the structure studied. Section 2.11.2: *Mathematical Models for Finite Element Analysis* details the numerical process of FEA for a problem.

2.11.1. Solution Procedures

FEA has now been widely applied in software package with user friendly interface. Careful solution planning has to be carried out before meaningful information can be obtained. The general steps involved behind the numerical solution of finite element analysis in most of the software programs are summarized below (Nikishkov 2004):

1. **Discretize the continuum**

   The structure or input data is first divided into a finite number of small elements. This process also known as meshing or discretization is normally generated by a preprocessor program. Information of these nodal coordinates and element connectivities are arranged in several arrays or matrices.

2. Select interpolation functions

Each mechanical behavior of an element composed in the matrices is defined by a set of differential equations of interpolation functions. Polynomials often selected as the interpolation function determines its degree depending on the number of nodes assigned to the element. The differential equations are converted into algebraic equation before matrix equations are derived.

3. Define element properties

The matrix equations are established so that the nodal values of the unknown work well with other parameters defined by the user. The material properties parameters pertinent to this work are *Young's modulus* and *Poisson's ratio*. Various approaches can be used for this task. The two most convenient are the variational approach and the *Galerkin* method.

4. Assemble the element equations

All elements equations are assembled to find the global equation system solution for the entire discretized region. The element connectivities are employed for the reason of assembly process. Proper load and boundary conditions supplied by user are integrated to the structural matrix before the solution process begins. Each individual element matrix equation are assembled in a combined global equation of the form

$$\{F\}=[k]\{u\}$$

where {F} = column matrix of the externally applied loads; [k] = stiffness matrix of the structure which is always a symmetric matrix and {u} = column matrix

representing the deflection of all the node points, that results when the load {F} is applied.

5. **Solve the global equations**

   The global equation system is normally assigned sparse, symmetric and positive definite. Direct and iterative methods are two options available for the structural matrix solution. The deflections of all nodes known as nodal displacements are calculated by interpolation of nodes in the element. A node shared by a number of elements share the same deflection throughout the sharing elements.

6. **Compute additional results**

   Depending on the results of interest, further additional parameters can be calculated. For example in mechanical problems, besides displacements, stress and strains are also of interest to the user.

2.11.2. Mathematical Models for Finite Element Analysis

In this section, the following 6 steps elucidate various mathematical models for the analysis solution giving attention to nonlinear problems. These explanations (Nikishkov 2004, MSC.Software 1999) detailed from the previous section 2.11.1: *Solution Procedures* remained fundamental. Thus, the readers are referred to more detailed concepts in a few technical references cited (Rao 1989, Reddy 1992, Ottosen and Petersson 1992, Akin 1994).

Step 1: Shape Functions

The shape functions, *N(x)* is used by FEM over the domain of element, Ω^e to express the unknown field, *u(x)* in terms of the nodal point unknowns, a^e as

$$u(x) = N(x)a^e \tag{2.2}$$

In the *Galerkin* differential method, the shape function, N_i for a linear two dimensional isoparametric finite element defined in local coordinates ξ, η ($-1 \le \xi, \eta \le 1$) as depicted in **Figure 2.23** is obtained through

$$N_i = \frac{1}{4}(1+\xi_o)(1+\eta_o) \tag{2.3}$$

where ξ_o and η_o are local coordinates of the elements in which the interpolation of displacements and coordinates are

$$u = \Sigma N_i u_i, \qquad v = \Sigma N_i v_i$$

$$x = \Sigma N_i x_i, \qquad y = \Sigma N_i y_i \tag{2.4}$$

where u and v are displacement components at point in local coordinates of (ξ,η); u_i and v_i are displacement values at the nodes of the finite element; x and y are point coordinates and x_i and y_i are coordinates of element nodes.

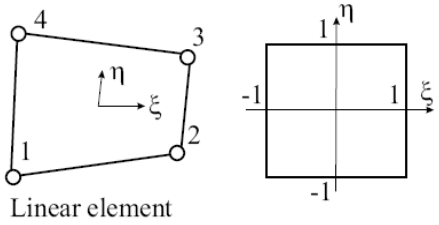

Figure 2.23: Linear quadrilateral element (left) and representation in the local coordinate system (right) (source: Nikishkov 2004)

The matrix of the relations in (2.4) is

$$\{u\} = [N]\{q\}$$

$$\{u\} = \{u\ v\}$$

$$\{q\} = \{u_1\ v_1\ u_2\ v_2 \ldots\} \tag{2.5}$$

$$\{x\} = [N]\{x^e\}$$

$$\{x\} = \{x\ y\}$$

$$\{x^e\} = \{x_1\ y_1\ x_2\ y_2 \ldots\} \tag{2.6}$$

where the interpolation matrix for nodal values is

$$[N] = \begin{bmatrix} N_1 & 0 & N_2 & 0 & \ldots \\ 0 & N_1 & 0 & N_2 & \ldots \end{bmatrix} \tag{2.7}$$

Step 2: Material Loop

Once the interpolation matrix composed of nodal values is attained, the subsequent step would be the derivation of dependent flux fields such as strain or stress flux in terms of the nodal points unknowns. The strain, ε within the element expressed in terms of the element nodal displacements is expressed as

$$\varepsilon(x) = Ba \tag{2.8}$$

where B is the strain displacement matrix achieved via

$$[B] = [\mathrm{B}_1\ \mathrm{B}_2 \ldots]$$

$$[B_i] = \begin{bmatrix} \frac{\delta N_i}{\delta x} & 0 \\ 0 & \frac{\delta N_i}{\delta y} \\ \frac{\delta N_i}{\delta y} & \frac{\delta N_i}{\delta x} \end{bmatrix} \tag{2.9}$$

As defined by the Hooke's Law (Huebner 2001) stress, σ is related to the strains, ε by incorporating the *Young's modulus, E* user input, as

$$\sigma(x) = E\varepsilon(x) \tag{2.10}$$

Step 3: Element Matrices

Each element is equilibrated with the environment expressed as

$$K^e a^e + f^e = 0 \tag{2.11}$$

where the element matrices, K^e and f^e have consistently lumped all physical significance of the element at its nodes, in which

$$K^e = \int_{\Omega^e} B^T EB dV \tag{2.12}$$

represents the physical property such as stiffness matrix while

$$-f^e = \int_{\Omega^e} N(x)^T b dV + \int_{\Gamma^e} N(x)^T t dS + F \tag{2.13}$$

represents the force vector or loads experienced by the element, *e.* These loads are composed of body loads, *b* in volume such as weight and surface loads, *t* on the surface such as pressure or concentrated loads, *F*.

For a *homogeneous* and *isotropic* material, the elasticity matrix, [*E*] defined by two *Lamé* material constants λ and μ is described as

$$[E] = \begin{bmatrix} \lambda+2\mu & \lambda & \lambda & 0 & 0 & 0 \\ \lambda & \lambda+2\mu & \lambda & 0 & 0 & 0 \\ \lambda & \lambda & \lambda+2\mu & 0 & 0 & 0 \\ 0 & 0 & 0 & \mu & 0 & 0 \\ 0 & 0 & 0 & 0 & \mu & 0 \\ 0 & 0 & 0 & 0 & 0 & \mu \end{bmatrix} \tag{2.14}$$

Through the elasticity modulus, *E* and *Poisson's* ratio, *v*

$$\lambda = \frac{vE}{(1+v)(1-2v)}$$

$$\mu = \frac{E}{2(1+v)} \tag{2.15}$$

Step 4: Assembly

All elements are assembled to form the global equation system in such a manner to ensure continuity of nodal points unknowns, $a=a^e$ and to equilibrate the structure with its environment which requires

$$K = \sum_e K^e$$

$$f = \sum_e f^e \tag{2.16}$$

Therefore, a finite number of system equations are resulted by

$$Ka + f = 0 \tag{2.17}$$

Step 5: Solve Equations

The stiffness matrix, K defined above is singular. In order to solve the global equation system, a set of constraints on the system which limit the number of degrees of freedom is needed, sufficiently for only one solution to exist. Interpreted geometrically, a finite element body would float in the space thus occupies infinite positions without any constraints defined. Only one possible position is allowed for the success of a solution. Therefore, a number of nodes of the mesh are fixed to a predetermined position before the system is solved. These constraints are called boundary conditions also known as *displacements*.

The boundary conditions of the nodal point values are specified on the boundary of the body and the system equations are partitioned as

$$\begin{bmatrix} K_{uu} & K_{us} \\ K_{su} & K_{ss} \end{bmatrix} \begin{bmatrix} a_u \\ a_s \end{bmatrix} = -\begin{bmatrix} f_a \\ f_r \end{bmatrix} \tag{2.18}$$

where a_u are the unknown nodal values, a_s are the specified nodal values, f_a are the applied nodal loads and f_r are the nodal point reactions. Therefore, the solution becomes

$$a_u = -K_{uu}^{-1}(f_a + K_{us}a_s)$$

$$f_r = -(K_{su}a_u + K_{ss}a_s) \tag{2.19}$$

Step 6: Recover

The dependent flux fields such as strain and stress are recovered by substituting the unknown nodal values, a_u found in Step 5 back into Step 2.

2.11.3. Advantage of Finite Element Method

A number of the advantages of finite element method among various others are:

1. Capable of handling complex problems which varies in geometries, analysis, loading and constraints.
2. Allows for close to reality model setup comprised of diverse material properties values for the elements in consideration if the exact material values are known.
3. Geometric effects such as large displacements and contact condition are possible in most of the finite element analysis software packages.
4. Competent of solving problems not solvable using the conventional method of hand mathematical calculation or without any theoretical solution.
5. Infinite behavior of a complicated structure can be visualized and analyzed based on various combinations of possible loads and boundary conditions.

2.11.4. Disadvantage of Finite Element Method

The disadvantages of finite element method are:

1. Careful consideration on experience and judgment must be accounted for the tedious preparation of a reasonable input data before analysis proceeds. In addition, large output data are difficult to interpret.
2. The input data are prone to modeling error by the user such as poor selection of element type, distorted elements and inadequate geometrical models.
3. The finite element method is an approximation of an actual system. Therefore, the exact results to the real problem will never be achieved due to numerical problems such as round offs and error accumulation. The main error is due to the discretization procedure and approximation differences of values at discretized points. Round offs problem is due to computer representation.
4. Powerful computer and reliable finite element package are necessary to ensure computation time within acceptable length of period for the problem of concern.
5. A particular analysis only produces a specific numerical result once a finite element analysis succeeds.

2.12. Previous Works

In all modeling problem, it is necessary to do choices, to put hypotheses of simplification, and to define the important points in comparison with a given application (Chabanas 2002). The two main choices for modeling surgery simulation are by building physical models and utilizing medical imaging and computer graphics techniques. The physical models are generated from computer tomography data using *stereolithography* and milling machines

for which the *stereolithography* machine build life-like models from a block of *polyurethane* while the milling machine builds the models slice by slice in a basin filled with liquid called photosensitive resin (Teschner et al. 1999). On the other hand, the use of medical imaging techniques in conjunction with computer graphics methods generates anatomy models on computer. The computer models are more accurate because tissue properties are possible to be represented by mathematical models.

The growth of surgical procedure based on computer models accelerated since the development of three-dimensional visualization techniques of tomographic data in the late 1980's. (Lorensen and Cline 1987) produced the Marching Cube Algorithm which capacitates the generation of surface triangle meshes from volumetric medical data sets. This algorithm was utilized to cater for methods of the bone structure reconstruction in (Yasuda et al. 1990), (Keeve et al.1996) and (Teschner et al. 2000).

In 1984, (Barr 1984) produced first results on deformable object modeling followed by (Larrabee 1986) who presented skin deformation using the finite element models in 1986. (Deng 1988) proposed an analysis of plastic surgery by utilizing the finite element method in her PhD thesis. (Vannier et al. 1983) initiated the idea of combining bone structure models together with the soft tissue models to predict soft tissue changes resultant to bone realignment. The first craniofacial surgery systems were produced in 1990 and 1991 respectively by (Yasuda et al. 1990) and (Pieper 1991). These systems are capable of presenting simple simulations thus approximately predict the soft tissue changes. Pieper simulated the postoperative facial appearance of plastic surgery by means of finite element modeling employed as part of the surgical procedures planning. He concentrated on the cutting and stretching of skin rather than the underlying bones repositioning. His approach

was deficient in suitable resolution for a reliable simulation of facial appearance changes. In the subsequent years, the craniofacial surgery simulation systems increased exponentially. Further approaches were discovered by (Kikinis et al.1992) trailed by (Girod et al. 1993, Delingette et al. 1994, Bohner et al. 1996, Koch et al. 1996) and (Bro-Nielsen 1998). In the following millennium, more researches such as (Zachow et al. 2000, Gladilin 2003) and (Schmidt et al. 2004) contributed their techniques for enhancement for the facial reconstruction surgery planning and simulation systems.

2.12.1. Previous Research Based on Finite Element Method

The following describe the basic ideas of the major researches who contributed to the field of 3D orthognathic surgery planning and simulation systems. Their work is in relation to finite element modeling.

Keeve et al

In their research, (Keeve et al. 1996, 1997, 1998, 1999) produced a system which allows preoperative simulation of the patient's facial soft tissue changes for a craniofacial surgery. The surgery was simulated using the actual patient data comprised of skull and skin layer respectively derived by CT data through the *Marching Cubes* algorithm and 3D laser scanner. The skin surface and skull structure were registered together before biomechanical properties of the tissues were assigned and computed by either mass spring or finite element tissue model.

Their fundamental idea used for the simulation through finite element model is by dividing the facial skin into a mesh of a finite number of six node prism elements as displayed in **Figure 2.24**. Displacement-based finite element modeling approach was employed where displacements were given for a number of nodes. During computation, these displacements resulted to strains for which the stress could be calculated through Hooke's law, which finally creates internal forces that moves the bone towards the skin. In the project, the finite element model had been integrated into a computer-aided surgical planning system. A few cases studies had been used to test the system functionality. The impact of underlying bone realignment transferred to the facial skin resulted from the simulation were presented. This system allows for numerous procedural attempts for the surgical planning and simulation. The simulation ran on SGI High Impact workstation. The simulated results had been verified with the actual postoperative results.

A number of disadvantages arose from their research are: 1) generic facial mesh was used to map the general anatomical structures to the individual patient data, 2) the utilized non-linear material properties were not comprehensive to accommodate modeling of tissue properties such as *viscoelasticity* and *anisotropy*, 3) the noninvasive in-vivo measurement techniques were required in order to determine patient specific elastic tissue properties. **Figure 2.25** illustrates the work presented by Keeve et al.

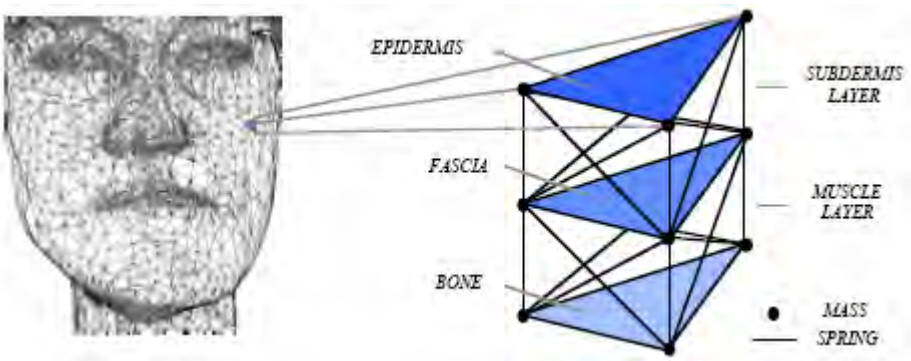

Figure 2.24: Facial tissue representation (source : Keeve et al. 1996)

Figure 2.25: Initial and simulated surgery results (source : Keeve et al. 1996)

Koch et al

(Koch et al. 1996, 2000, 2002) started their work with predicting post surgical appearance by the surface based models before they presented a framework for facial surgery simulation based on volumetric finite element modeling. A patient was accompanied throughout the process of planning, medical treatment and simulation.

CT scanner and laser scanner were used to capture the facial skull and skin data. The skin surface extracted from laser scanner was then registered to the facial surface obtained from the CT scanner by using landmarks. The conjugate directions method was utilized to

minimize error on the surface differences. The facial tissue was then tiled with a modified prism shaped elements shown in **Figure 2.26**, followed by the segmentation of different regions in order to derive tissues such as skin, fat, muscle and bones. Subsequently, each of the tissue type was assigned material parameters which are the *Young's modulus*, *E* to define elasticity and *Poisson's ratio, v* to describe compressibility. The surgical planning was carried out using the Alias^{TM} modeling system. Proper boundary conditions were assigned before the finite element formulation was introduced for surgery simulation.

The work by Koch et al was restricted to the linear elasticity solution due to the reason that in comparison to car crash, the displacements and deformations in most craniofacial surgeons are relatively small in the engineering and FEM point of view. Their approach of solution was motivated by the demand to obey the rules of physics and to cater the need for visually appealing facial surfaces. Therefore the prismatic function of C^1-continuity was used for the facial surface while C^0-continuous was employed to represent the skull surface. The simulated results were qualitatively and quantitatively validated with the postoperative data obtained from laser range scanner. Quantitative validation was done by registering the results to the post surgical facial surface and the differences were presented by means of color map as shown in **Figure 2.27**.

In their work on the surface based models, a few features were insufficient. They were : 1)the separation of facial tissue into a surface and a volumetric component requires explicit definition of their material parameter, 2) this approach was lacked of biophysical information, 3) volumetric behavior requires additional external forces obtained through the surface based approach, 4) non-linear approach was not employed for the surface based model solution.

The extended volumetric approach produced better results with enhanced non-linear analysis. More advanced techniques were needed to model the improved geometry representation of soft tissue and non-linear constraints. However, the utilized data were not at sufficient resolution. Their current geometrical models were based on polygons. Therefore, information lost happened during the data conversion between the FEM and *Alias* software packages. Furthermore, their future research was to achieve a surgery planning and simulation system that could accommodate the wrinkles problem aside from performing more case studies with patients of different ages, gender and ethics origins.

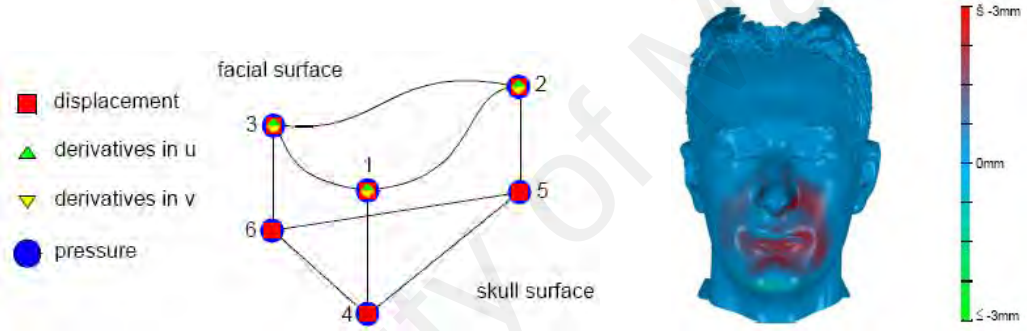

Figure 2.26: The proposed prism element (left) (source: Koch et al. 2002)
Figure 2.27: Error measurement and color map between simulated and real post surgical surface (right)

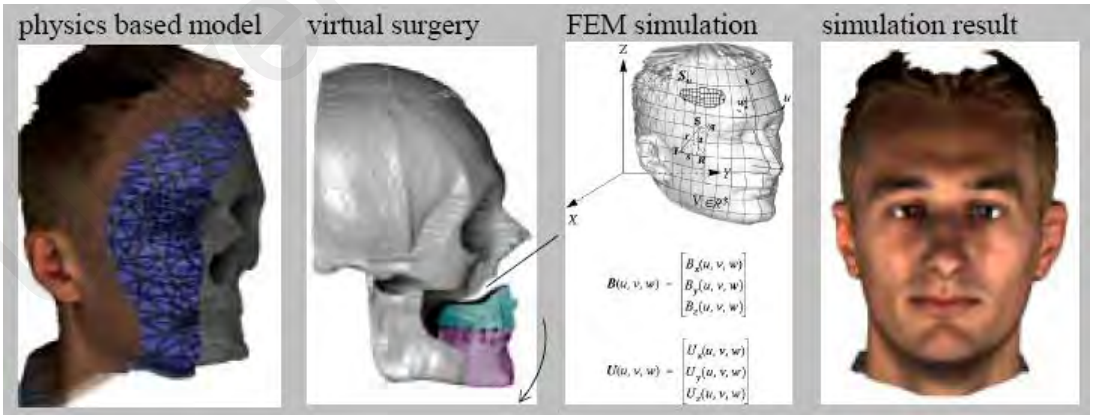

Figure 2.28: Surgery simulation procedure (source: Koch et al. 2002)

Zachow et al

The work presented by (Zachow et al. 2000) focused on the simulation and behavior of facial soft tissue deformation with regard to natural jaw movement, surgical bone realignment and muscle based mimics of maxillofacial surgery.

The volumetric grid or tetrahedral grids were employed for the finite element analysis. The grids which represented various tissue regions were generated from segmentation of patient specific CT data. Their work was based on visualization system Amira and Kaskade FE toolkit, which were developed at their Zuse-Institute Berlin (ZIB) institute (Stalling et al. 1999, Deuflhard et al. 1989).

The fundamental approach for preparing the data for finite element analysis was similar to majority of the previous works. CT data was filtered for noise before segmentation of various tissue regions continues. A closed surface model was subsequently generated and optimized prior to the generation of tetrahedral grid. Finally, the volumetric grid was once again optimized in advance to the finite element computation and simulation. The model was solved under the linear stress-strain relationship by using the Hookean elastic solid formulation. Calculations were performed on SGI Onyx II workstation.

Their work differs with the previous in terms of surgery planning. Most of the prior researches presented planar cuts on the geometrical models as shown in **Figure 2.29** and **Figure 2.30**. Zachow et al. found out this approach was not necessary, thus they presented bone or parts separation done in accordance to surgical guidelines that suits the need of functional rehabilitation and symmetry jaw results. Therefore, the separated parts for

correct bone realignment were influenced by the rotational and translational parameters under the supervision of craniofacial surgeons. Furthermore, quantitative assessment of the simulation resultant to the predicted facial tissue by comparison with postoperative CT data was evaluated in (Zachow et al. 2004). **Figure 2.31** illustrates their facial soft tissue prediction results based on the actual clinical case.

The drawback of their work is the lack of sufficient material models of biological tissue although experiments which defined tissue as *homogeneous* and *inhomogeneous* had been performed in (Zachow et al. 2004). In addition, their future works focus on the simulation of muscle based mimics and simulation of sliding contact between bone and soft tissue.

(Zachow et al. 2006) presented the importance of computer-aided surgery planning system for the cranio-maxillofacial surgery giving attention on the facial anatomy reconstruction for harmonious facial appearance. Comparisons in between the manual approach and the enhanced surgery planning methodology for precise soft tissue prediction were highlighted in their most recent work.

Figure 2.29: Simulation of mandibular distraction and soft tissue prediction (source : Zachow et al. 2000)

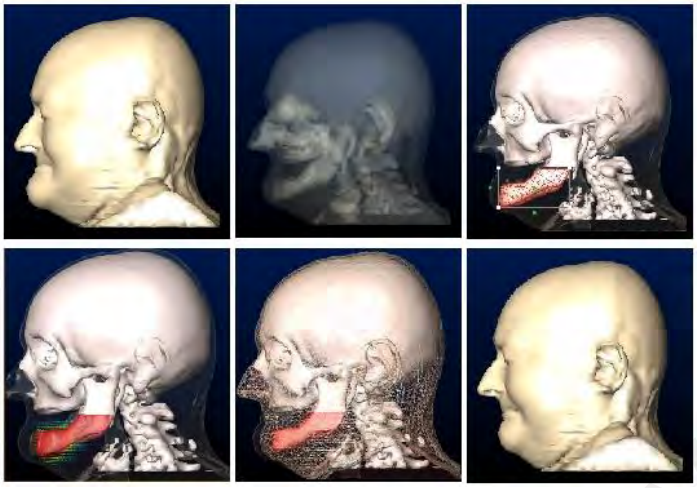

Figure 2.30: *Osteotomy* and soft tissue prediction (source: ZIB 2006)

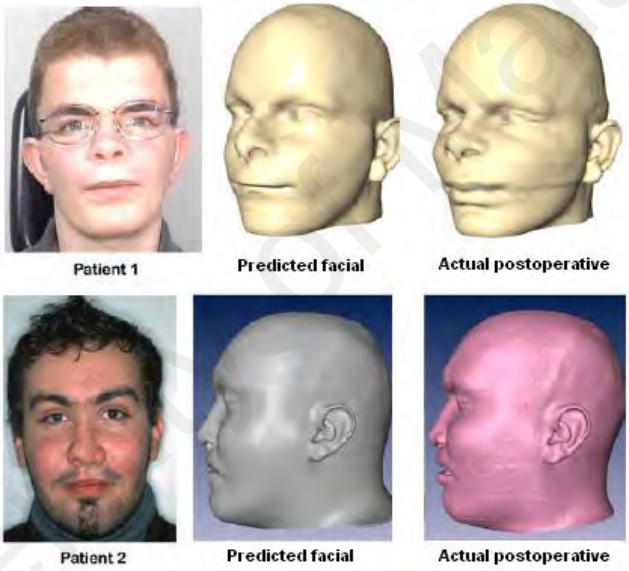

Figure 2.31: Comparison of the predicted and actual postoperative results (source: Zachow et al. 2004)

Gladilin et al

(Gladilin et al. 2001a), also from ZIB, is a team member of Zachow et al working on the same research project. Their primary concern was to realistically predict and simulate facial soft tissue or a patient's postoperative appearance for a craniofacial surgery as resulted in **Figure 2.32**. The facial geometrical modeling reconstructed from CT data was performed with the visualization and modeling system, Amira. The finite element physically based

modeling approach was adopted for the static soft tissue prediction in addition to muscle simulation.

"Small deformation" such as small elongations and small rotations was assumed for the facial tissue model. Therefore, allows for the application of *isotropic*, *homogeneous* and linear elastic continuum properties for the soft tissue. The linear elastic modeling method was first applied for the soft tissue deformation. Hence simulate and predict the patient's postoperative outlook. However, (Gladilin et al. 2002) found that "large deformation" is more applicable for long term prediction for the patient's postoperative appearance. Furthermore, (Gladilin et al. 2001c) have earlier investigated the scope of linear elastic model and the use of it revealed that the results produced substantial error in the case of large deformation. Therefore, (Gladilin et al. 2002) enhanced the work and presented results of non-linear elastic finite element model, where their primary focus was on the effects of the geometrical nonlinearity. The result of their enhanced work is seen in **Figure 2.34**.

In (Gladilin et al. 2001a and 2001b), they have also estimated the patient's facial mimics for the predicted postoperative results for the reason of patient's compliance. A vital factor for the simulation of facial mimic as illustrated in **Figure 2.33** is the realistic modeling of contracting muscle and the interaction with neighboring soft tissue. However, because muscle information was not obtainable from CT data, heuristic consideration of the muscle shape and their biomechanical functionality was applied. Their results were validated with the patient specific head model derived from CT data in (Gladilin et al. 2004).

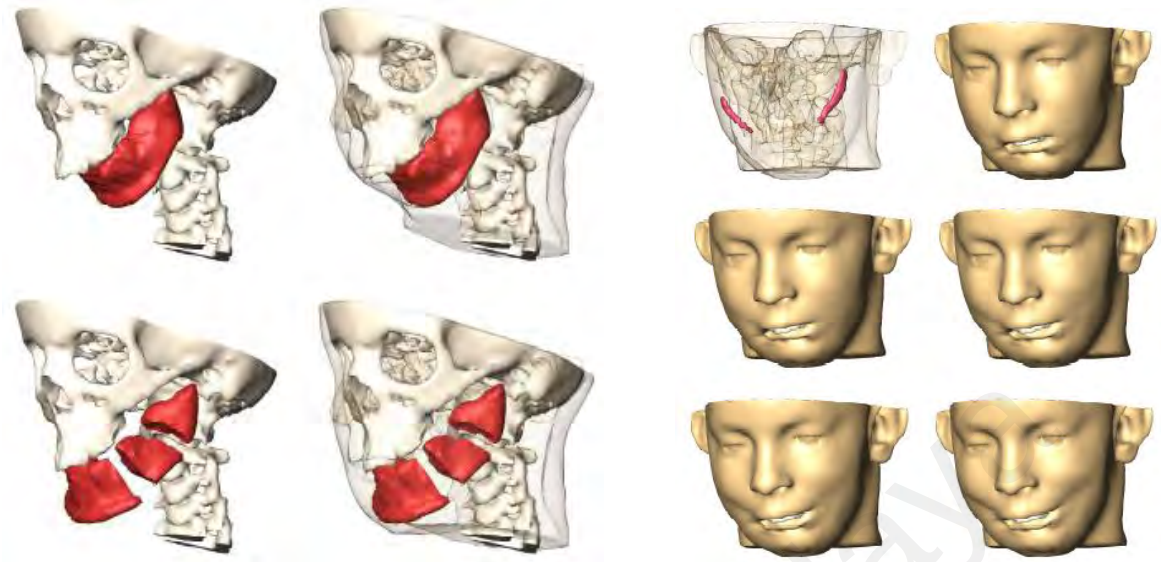

Figure 2.32: Simulation of mandibular distraction (left) (source: Gladilin et al. 2002)
Figure 2.33: Facial mimics induced by muscle contraction (right) (source: Gladilin et al. 2001b)

Figure 2.34: Comparison between facial soft tissue predicted by linear (lighter line mesh) and nonlinear (darker shaded mesh) elastic model (source: Gladilin et al. 2002)

Schmidt et al

(Schmidt et al. 2004) used a collection of loosely coupled software components to develop a system that predicts effect of the surgery on the soft tissue displacement for maxillofacial surgery simulation. The geometric head model derived from CT data was used for virtual *osteotomy* by surgeons before the model were submitted over a remote FEM application for tissue prediction and simulation.

Their work focused on the medical grid computing where advanced simulation were made possible to the high performance platform by transparent and secure access to large remote computation resources. Thus, the non-technical users such as surgeons do not need to face and view the back end FEM computation process during their surgery planning and simulation. Hence, the solution task appeared as if the system runs the computation autonomously. Their system provided two solution options for which they are linear and non-linear FEM solution. The FEBINA solver was applied for the computation solution. Surgery planning was performed by specifying points on the skull represented by a surface mesh as depicted in **Figure 2.35**. After the cuts have been applied, the bones are then converted into 3D volumes. The result is presented in **Figure 2.36**.

A number of disadvantages arose in their work are: 1) support for automatic fitting of cut lines to skull surface geometry, removal nor reduction of metal artifacts were incorporated, 3) muscle tissue and other soft tissue details were not included as part of planning and simulation.

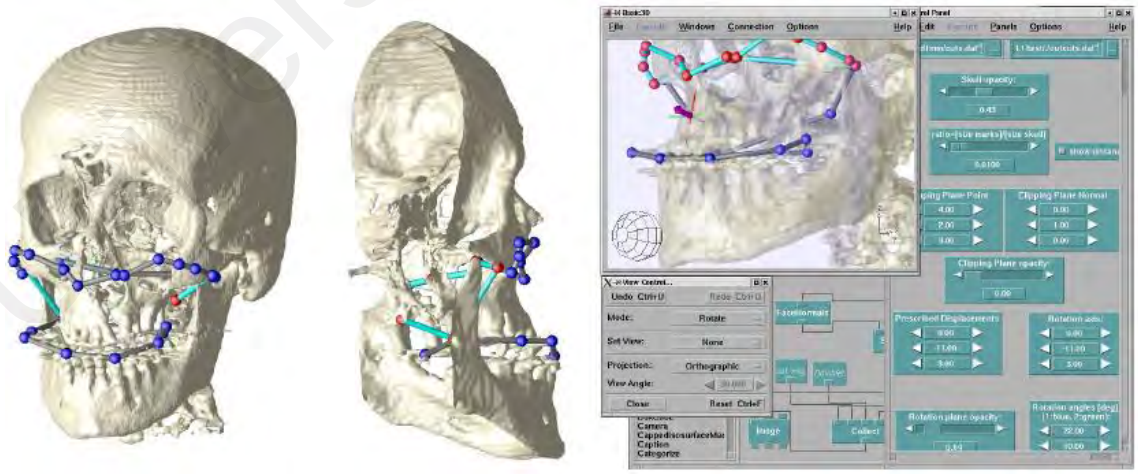

Figure 2.35: The surgery planning tool used to specify points to cut on the skull (source: Schmidt et al. 2004)

Figure 2.36: Preoperative (left) and simulated postoperative (right) patient appearance (source: Schmidt et al. 2004)

3

METHODOLOGY

3.1. Overview

This chapter details on the procedural aspects of the entire system development. Explanation begins with brief description on the process of data acquisition. Geometrical anatomy modeling based on the acquired data is described giving attention on image processing techniques such as segmentation, triangulation and mesh generation. The modal improvement criteria are also detailed. This chapter continues with the surgical planning procedure involving bone cutting and repositioning. Subsequently, the computation surgery which explains the model setup in more detail is presented and finally, the finite element analysis setup particular for the problem matter is described.

3.2. Acquisition of Computer Tomography Images

A volume data set for the facial models is needed to cater for two purposes. First, volume segmentation is required to obtain the material parameters as a platform to construct FEM mesh and second for the generation of skull geometry to carry out virtual surgery. The two available approaches to attain these models are computer tomographies (CT) and magnetic resonance imaging tomographies (MRI). The MRI provides better extraction for soft tissues. On the other hand, hard tissues such as the bone are best extracted from CT data by

image segmentation operations explained in subsequent sections. Due to the reason that the muscular anatomy is not taken into consideration for this work, the soft tissue segmentation is insignificant. Hence, the CT based volume data is preferred because of enhanced visibility for bone tissues and for economical reasons.

3.3. Anatomy Geometry Modeling

The goal of this research is to run a finite element analysis to determine the deformation of a facial skin. However, first of all, an important initial procedure is to produce an adequate facial model pertinent to the desired type of analysis. An example of a facial model with soft tissues is shown in **Figure 3.1**. In consideration of assumptions, the simplified facial models used are the skin, upper jaw and lower jaw as illustrated in **Figure 3.2**. Based on 2D CT images, the aforementioned 3D models are constructed. The step by step explanation below will provide basic understanding of the geometrical modeling.

Figure 3.1: Patient specific skull, tissue and skin

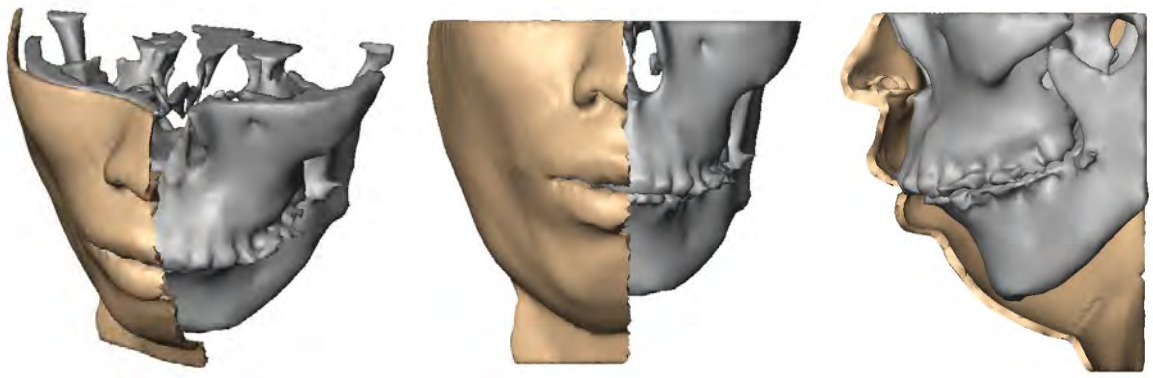

Figure 3.2: Patient specific skull and skin layer

3.3.1. Image Segmentation

The main objective of this section is to construct a triangular mesh of a preoperative CT scan which concerns the conversion of pixel-based images to a triangular mesh particular to the geometry of facial skin layer, upper jaw and lower jaw with minimal quality loss. The Materialise's Interactive Medical Image Control System (Mimics) (Materialise 1991) will be used to derive the geometries starting from the preoperative CT scan. Mimics is an interactive image-processing tool for visualization and segmentation of CT images, MRI images and 3D rendering objects often used for surgery planning. The steps of geometry modeling for facial surface and bone structure will be discussed in this section. In spite of the fact that these tissues reconstructions are done in two different stages, the same procedures are adopted throughout the process. A few quality parameters involved during the process have been tested and will be described in detail.

a) Thresholding

The geometries of facial skin and bone tissues were segmented by thresholding, a selection of region of interest by specifying a lower and an upper threshold value. All pixels with

values within the range will be taken as either facial skin tissue or bone tissue depending on the values assigned. The lower values used are 226 and -774 while upper values are 352 and -5, respectively for the bone and skin. The threshold values are defined by either moving the minimum and maximum sliders to fine tune the value in the threshold toolbar or by filling in a value in a specified box. These pixels are grouped in a mask. Subsequent steps as discussed below will be based on the segmented mask. **Figure 3.3** shows highlighted threshold on a slice preoperative CT image of a considered patient. Due to the different intensities between both materials, selecting an optimal threshold value is difficult. Therefore, manual segmentation is necessary in some regions as discussed in the *Mask Editing* paragraph below.

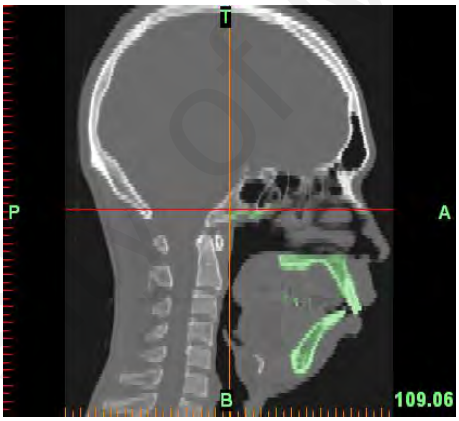

Figure 3.3: Segmented mask of selected threshold on axial CT image slice of a mandible

b) Windowing

In order to obtain better image visibility before further processing, it is recommended to adjust the contrast of the images. Windowing is done by specifying gray values on a grayscale slider. All values above the maximum value will be displayed in white while all values below the minimum are displayed in black. This contrast enhancement allows the user to view CT image slices using different ranges of density. The minimum scale selected for bone and skin are correspondingly -1018 and 1359, having 3064 and 1641 as the maximum scale.

c) Mask Editing

This research project deals with a few facial parts such as mandible, maxilla and facial skin surface. The remaining material parameters such as skull, muscle and fat are left idle. For example, in **Figure 3.7**, only bone structure in the yellow region is considered. Hence, the edit mask is a function used to split the desired parts and delete the unwanted regions. The "erase" option provides the capacity of separating the parts by erasing a few selected slices of the CT images within the segmented mask. **Table 3.1** shows the location at which the image slices are deleted to achieve the best portioned geometry. However, the current result is only visible in two dimensional images. Triangulation which in other word means construction of geometry based on a mask comprising the desired parts allocates a three dimensional visualization. This is further explained in section 3.3.2: *Triangulation of the segmented mask.*

Table 3.1: Location at which image slice is deleted

	Axial	**Coronal**	**Sagittal**
Bone	135.00	105.22	114.17
Skin	137.50	105.65	None

In a first attempt of triangulation as depicted in **Figure 3.4**, the geometry produced was surrounded by unnecessary parts even after the image separation step had been carried out. Therefore, the excessive thresholded point or better known as pixel are manually removed for every image slice using the erase option, promising a time consuming task. This procedure is repeated until smooth and clean geometry is produced. The best facial surface geometry model obtained is shown in **Figure 3.5**. However, a close up observation revealed that there exist small holes on the facial skin layer thus necessitate for further processing before FEA calculation is permitted. The small holes occurred because a few important

pixels have been unintentionally removed during the manual mask editing operation. The facial skin geometry enhancement is discussed in the section 3.4: *Model Improvement*.

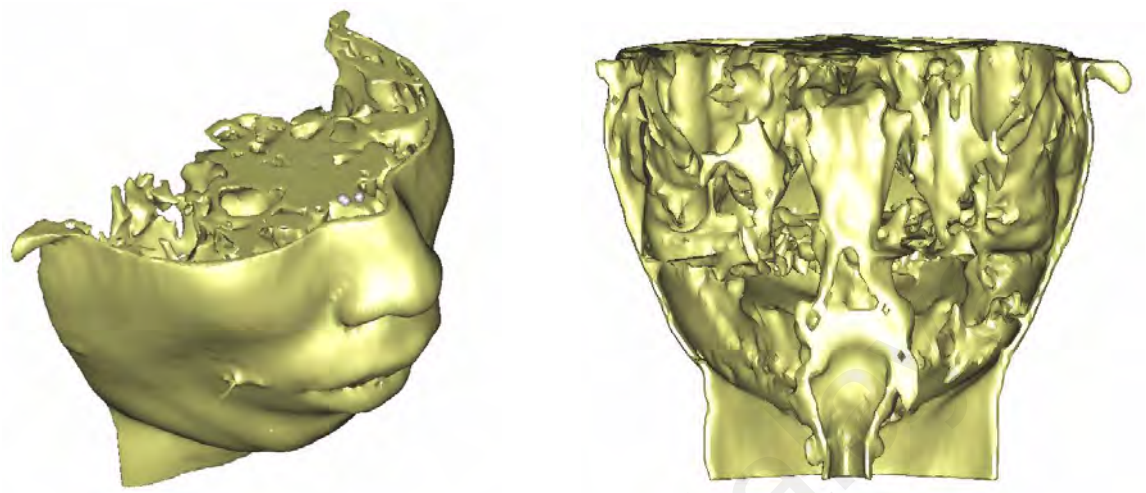

(a) (b)

Figure 3.4: Unnecessary regions on initial facial skin geometry triangulation. (a): Isometric view of defected 3D facial skin model, (b): Back view showing superfluous information in the middle region

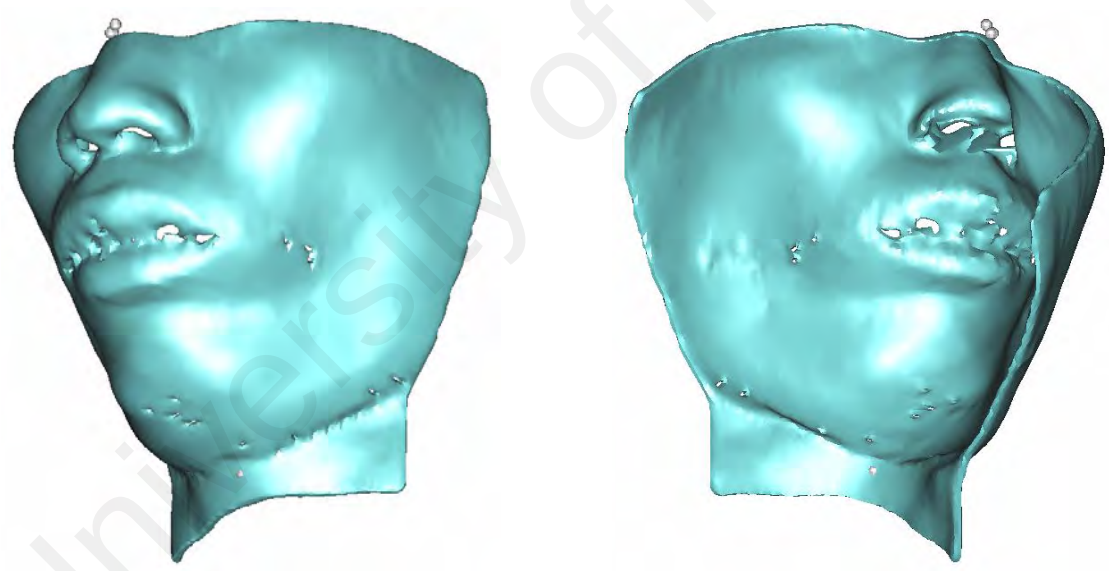

(a) (b)

Figure 3.5: Facial skin geometry after manual mask editing. (a): Front isometric view and (b): Back isometric view of the facial skin surface

Besides separating parts, the edit option is also used to eliminate artifacts recognized as metal teeth filling due to metallic object. Artifacts as shown in **Figure 3.6** resulted in defective 3D model output perceivable in **Figure 3.4(a)**.

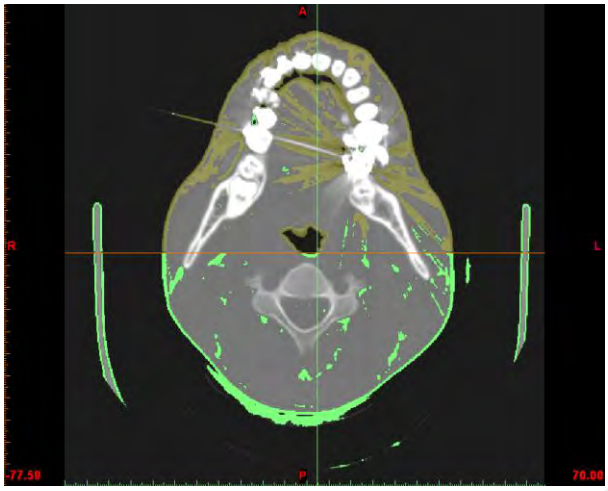

Figure 3.6: Artifact affecting the skin tissue

d) Region Growing

On completion of regions separation into separate parts on the two dimensional CT images, the structures of interest are stored in a new mask with the risk of introducing multiple parts geometry but conversely ensure the generation of closed volume. Multiple parts are caused by floating particles around the object to be generated. This problem can be avoided by recreating region growing mask. The new mask illustrated in different color keeps the selected region of interest, eliminates noise and separate unconnected structures. This procedure is carried out by selecting a point from the segmented mask known as source mask whereby all points connected to the marked point will be kept in a mask called the target mask thus explains the term, region growing. The “multiple layer” option is checked so that all image slices throughout the mask acquire the same action. In addition, the “leave original mask” option is marked to copy and paste all information in existing mask to the new mask.

3.3.2. Triangulation of the Segmented Mask

The subsequent step is the 3D model generation of the segmented tissue. On the click of "Calculate 3D" button after a selection of the yearned mask in addition to parameters estimation, Mimics processes the defined regions and displays the segmentation results. Computer Tomography Modeler (CTM) interpolates the data and interface directly to one of a few available output formats.

The chosen output format in the triangular-based approach is STL. The STL interface will generate a triangle mesh around the selected volume in which each surface pixel of the segmented CT image results in two or six triangles. The numbers of triangles determine the quality of reconstruction meaning more triangles gives higher quality model. However, the drawback is that more triangles certainly require more memory for the entire process. This should be concerned about when employing STL files as an output.

Figure 3.7: Patient specific geometry model

3.3.2.1. 3D Generation Parameters

The 3D visualization is performed by means of triangulation of a segmented 3D region on the mask. Mimics (Materialise 1991) with inbuilt Magics RP provides a number of parameters that permits manipulation for the 3D model generation. These parameters need to be adequately estimated to compromise between computer time and the quality of the STL file. In spite of offering chances of minimizing the number of triangles in the model, the parameters options in use will always decrease the part quality and surface resolution.

a) Quality

The quality of the STL file is determined by the parameter settings. All related quality aspects are grouped in the predefined settings Low, Medium and High. The Custom setting utilized for this research project is user defined. It is in these abovementioned settings where the choice of various parameter values ascertains the quality of the generated 3D model. The quality checks rely on the manipulation of these parameters. Customization of various parameter values determines the quality of generated 3D model. Until the right combination is achieved, various attempts of tests had been carried out. These quality checks will be further discussed in section 3.4: *Model Improvement*.

b) Method of Interpolation

There are two options available for image interpolation and 3D triangular mesh generation; grey value and contour interpolation. Principally, contour interpolation is a 2D interpolation in the plane of the images smoothly expanded in the third dimension. On the other hand, grey value interpolation is a real 3D interpolation and thus more accurate. This means, during an interpolation, the grey value of the previous and following image is considered. The grey value interpolation takes into account on the partial volume effect where it gives

attention to the details in correct dimensions and positioning. However, unnecessary details are produced due to the noise within the images. **Figure 3.8(d)** shows an example of grey value interpolation with continuity matrix reduction preference. It is important to realize that grey value interpolation does not always produce good results. A resulting mesh gives a noisy surface when a slice distance of the scan considerably deviates from the slice thickness. Grey value interpolation works best only if the slice thickness and slice distance are the same. This condition is fulfilled during the data acquisition or scanning process.

The contour interpolation uses grey value interpolation within the slices. Based on the evidence above in addition to several tests performed, as illustrated in **Figure 3.8**, it is concluded that the contour interpolation method gives smoother 3D results with reduced gaps and is therefore recommended for medical CT applications (Materialise 1991).

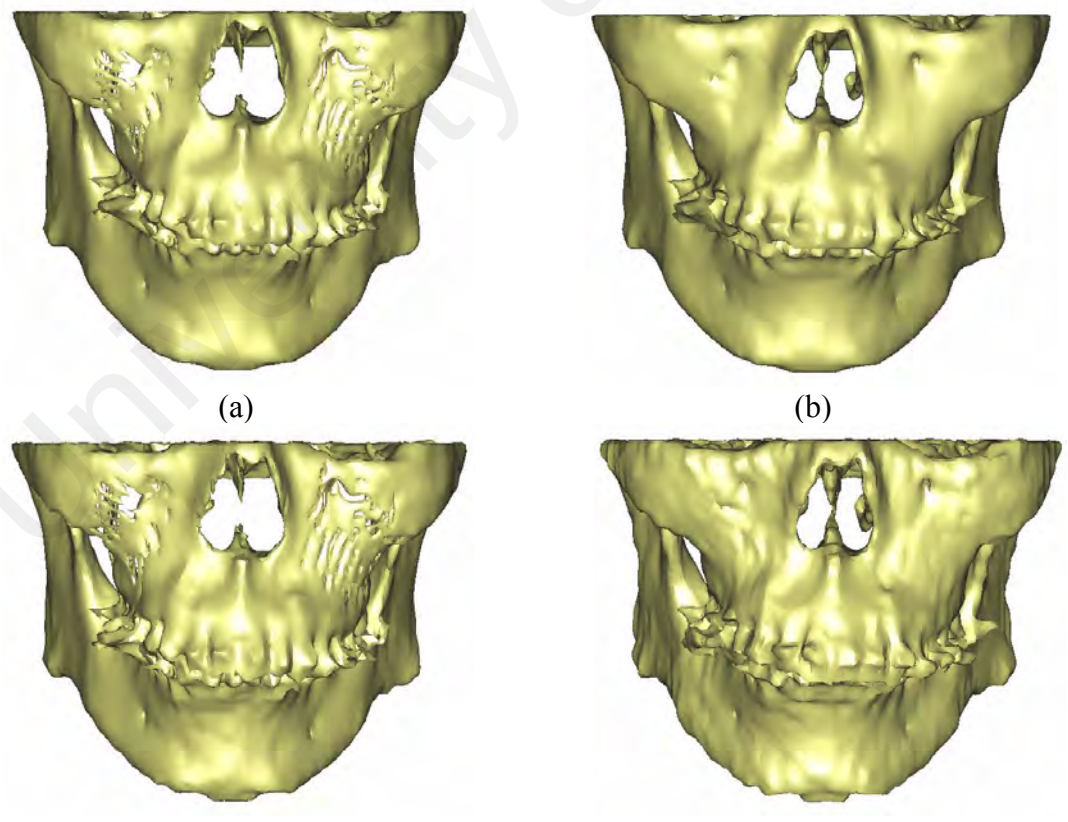

Figure 3.8: Differences of the interpolation method. (a): Contour and accuracy, (b): Contour and continuity, (c): Grey value and accuracy, (d): Grey value and continuity

c) Matrix Reduction

The matrix reduction option allows the grouping of *voxels* for triangulation. The XY resolution and Z resolution relatively decides the number of *voxels* grouped in the XY plane and the Z direction. Reduction is made on the count of numbers of *voxels* in X plane, Y plane and Z direction respectively.

The X and Y planes refer to the size of pixel while the Z direction for the height. Larger number assigned for each size and height of a pixel indicates excessive reduced information which will lead to loss of information for small models when using grey value interpolation although artificial texture and correct dimensions are achieved. **Figure 3.8(d)** shows the material texture artificially presented on the generated model. Conversely, contour interpolation leads to incorrect dimensions which results to inaccurate measurement because the generated model appears too large compared to the original volume.

During research, it is proved that the process of triangulation is rather time-consuming when each resolution is assigned the value 1 which means no matrix reduction allocated. An XY resolution of 4 is acceptable whereas the Z resolution remains 1. Two available matrix reduction algorithm options are accuracy and continuity. Accuracy algorithm as the term explains gives accurate model dimension but less nice results because gaps appear when wall thickness of the geometry is smaller than the pixel size. On the contrary, continuity algorithm generates nice results with larger 3D dimensions when bigger matrix reduction is used. Therefore, the continuity algorithm is of choice simply for the reason that medical applications demands good quality models to work on.

d) Smoothing

The smoothing option which operates like a filter for noise reduction is meant to make rough surfaces smoother. The "iteration parameter" and "smooth factor" determines the intensity of the smoothing algorithm. Numbers of cycles for smoothing is articulated by the "iteration parameter". Each iteration step changes the quality of triangulation. High values used for the number of iterations will result to smoother surface. However, if too high values are used, the geometry will likely shake off its shape.

The importance of local geometry is indicated by the "smooth factor". The local geometry is considered important and the smoothing is limited if the "smooth factor" ratio is close to 0. In contrast, high factor value close to 1 determines a new position by the position of other triangle points in the neighborhood. A good hint for smooth surface is to keep the numbers of iterations low when using high "smooth factor" value. **Figure 3.9** depicts the differences between rough and smoothed surface. Research has figured out that smoothing does not contribute to triangle reduction for the considered geometry. Furthermore, it is suggested to smooth a model in 3 iteration steps by a smoothing ratio of 1.0.

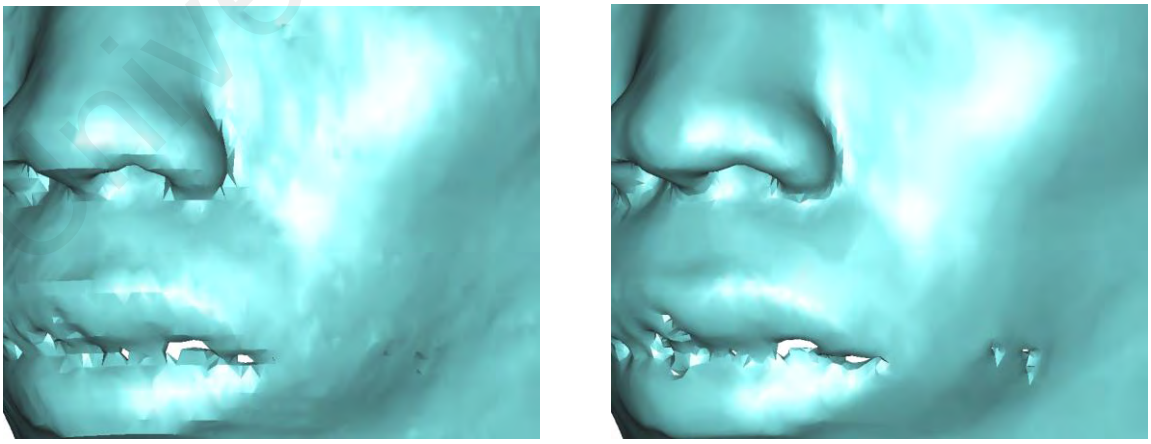

(a) (b)

Figure 3.9: Smoothing operation on facial skin geometry. (a): Rough surface and (b): Smoothed surface

e) Triangle Reduction

One of the most important options for the geometry generation is the triangle reduction. The self-explained triangle reduction reduces the number of triangles in a mesh.

Two available triangle reduction types are the “point-type” and the “edge-type”. The “point-based” mode will remove points to reduce the quantity of triangles whereas the “edge-type” will try to remove a triangle edge which consists of two vertexes together with connecting line between these two points. The “edge-type” is best used for medical application due to less noise introduced to the surface geometry. Both modes comprise of same parameters which are the “tolerance”, the “edge angle” and the “number of iterations”.

The “tolerance” signifies the maximum deviation in mm that a related triangle is allowed to have to be part of the same plane that contains the selected triangle. During tests, it appeared that the “tolerance” is a trivial factor in triangle reduction. The reduction is negligible and outweighed by the deviation at higher “tolerance” value. Therefore, 01.mm is sufficient for the “tolerance” option. In addition, it is reasonable to keep the value related to the pixel size, half the size of the pixel is sufficient.

The “numbers of iterations” defines number of cycle the algorithm should make the reduction calculation. Several iterations are necessary to allow triangle reduction in large flat areas. A stable result is achieved after approximately 15 iterations. Increasing the number of iteration is discouraged due to higher deviation in the result. Hence the default value of 5 for the number iteration steps is maintained.

An “edge angle” is measured between the normals of a triangle. The “edge angle” decides the correct angle to determine edges of the part which cannot be removed. Removing triangles means losing information. Triangles deviating less than the selected angle will be grouped into a plane of other triangles. Once the edge is known, reduction will reduce points available along the edge but will keep the edge. The angle value determines the maximum angle which can be created during reduction where no edge exists. In other words, this means when there is an edge there will remain one; however when there is no edge, no edge will be created. In consequence, it is advised not to use reducer on very noisy objects as the scanned surfaces. This can be resolved by performing smoothing beforehand although there will be no effect on the number of triangles. Increasing the “edge angle” value will lead to less determined edges and more triangle reduction. Assigning too high angle values will cause improper deviations. Geometry preservation is more important than triangle reduction. This is the reason why it is best to set the “edge angle” value to 10 degrees which is also the default value.

3.3.3. Mesh Generation

Magics RP inbuilt in Mimics provides “remeshing” option for the generation of 3D geometry to obtain optimized file for further finite element analysis. During meshing, two important aspects which are remesh quality and geometrical implication must be considered. Fine meshing enhances the geometry quality. Conversely, irregular mesh reduces the geometry features. Therefore, the need to balance in between accuracy and quality is crucial.

The process of generating triangles is called mesh generation. A mesh is referred to *discretization* or partitioning of geometry into simple small elements such as triangles or quadrilaterals. Triangles are often used for mesh generation. This is because triangles are the most primitive shape for two-dimensional (2D) elements. A triangle consists of three sides for which the analysis computation for this time of element is less complex than other advanced elements such as tetrahedrals. Therefore, there is a trade off between the elements shape and the computational resources in that elements with more sides and complex shapes requires more computational time to achieve a solution during an analysis. In considering the use of typical personal computer in this research, employing the triangular elements are sufficient for acceptable computation time of an analysis. The application requirements decide how a mesh should be constructed. Judgment of a good mesh relies on the requirement of either small elements for details, large elements for efficiency or/and nicely shaped elements for accuracy. More geometrically regular triangles guarantee better and more reliable results for the finite element analysis calculations.

3.3.3.1. Mesh Quality Control

The quality of a mesh is related to the form of triangles they are composed. Measurements for the quality are based on properties that describe a triangle which among a few are base, length and height. Magics RP provides many options for triangles quality measurement. The appearance and values of a histogram varies depending on the user defined quality measurement parameters.

To check for quality measurement, the height/base parameter is used where the ratio between the height and base of a triangle is measured and normalized. Out of two available

height/base parameter options respectively absolute and normalized, the normalized is utilized for *remeshing* because unlike the absolute type, the values for calculation rely on a limited scale. In other words, this means low quality triangles are reflected by left horizontal axis while the high quality triangles are reflected by right horizontal axis. As shown in **Figure 3.10**, distribution of the triangles based on their quality is presented on the quality histogram.

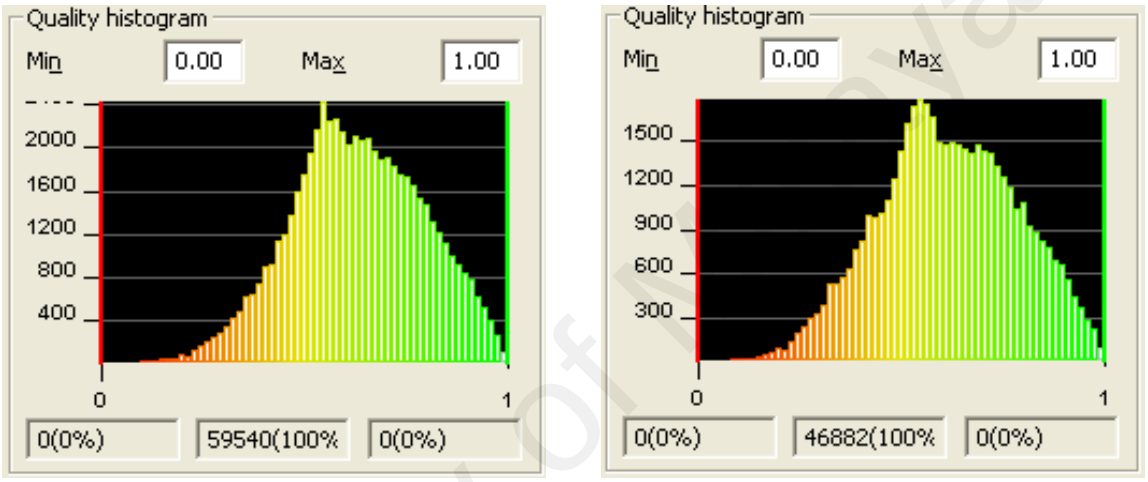

(a) (b)

Figure 3.10: Triangles distribution in quality histogram for (a): Facial bone and (b): Facial skin surface

Good quality triangles are signified by value 1. On the opposed side, bad quality triangles are indicated by value 0. The goal of the height/base quality measurement is to accomplish ideal equilateral triangles in which every side of the triangle has the same length where each angle is 60 degrees. In order to do so, badly shaped triangles resultant to triangles below the threshold value indicated by the red color on the left of the histogram must be eliminated. This is realized by first assigning a suitable threshold value in the maximum text box or by dragging the green slider on the right side of the histogram. Value 0.30 is selected based on the rule of thumb, a decision made by experience. Higher value would reduce the number of good quality triangles while lower value keeps the goal unsolved. The three values under the histogram from left to right correspondingly defines the amount of

triangles below the minimum quality threshold, between the minimum and maximum threshold and higher threshold together with the percentage of the total numbers of triangles they constitute.

The following paragraphs discuss about the quality measurements and triangle enhancements of the generated 3D geometry. Each paragraph below represents same procedures for both bone and skin tissue. Therefore, explanation is done simultaneously for each step involved. At the end of this section, the results of the generated mesh are presented in **Figure 3.15** and **Figure 3.16**.

The initial minimum threshold value once the generated geometry tissues shown in **Figure 3.11(a)** and **Figure 3.12(a)** is imported into the FEA module of Magics RP given threshold value of 0.3 is 0. This is an indication that there were no low quality triangles in the geometry. Majority of the triangles categorized as medium quality triangles resides in the second value. The number of triangles for the bone is 1288 whereas the skin tissue had 1506 triangles. The main target is to increase the quality of these triangles which then reflects to higher number of triangles in the third value. There are 58252 high quality triangles in the bone tissue and 45376 in the skin tissue. Further explanation is in the *Remeshing Protocol* paragraph. It is emphasized that these values could change subject to the numbers of triangle composed in the geometry. The numbers of triangles varies during the process of geometry generation.

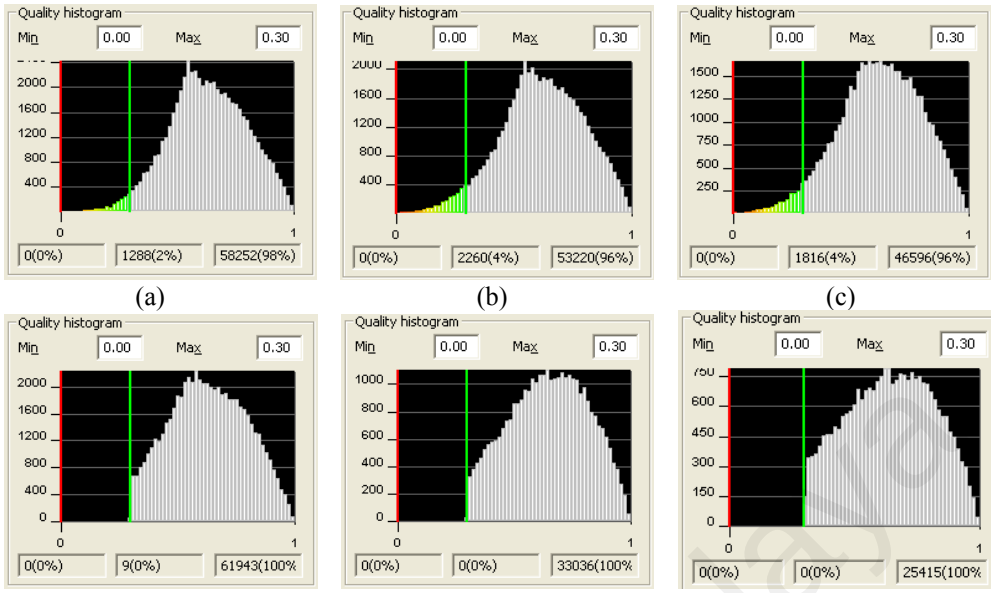

(a) (b) (c)

(d) (e) (f)

Figure 3.11: Triangles quality improvement for bone structure

(a) After allocation of threshold
(b) Point based normal triangle reduction
(c) Edge based normal triangle reduction
(d) Split based automatic remeshing
(e) After 7 times quality preserving triangle reduction
(f) After 10 times quality preserving triangle reduction

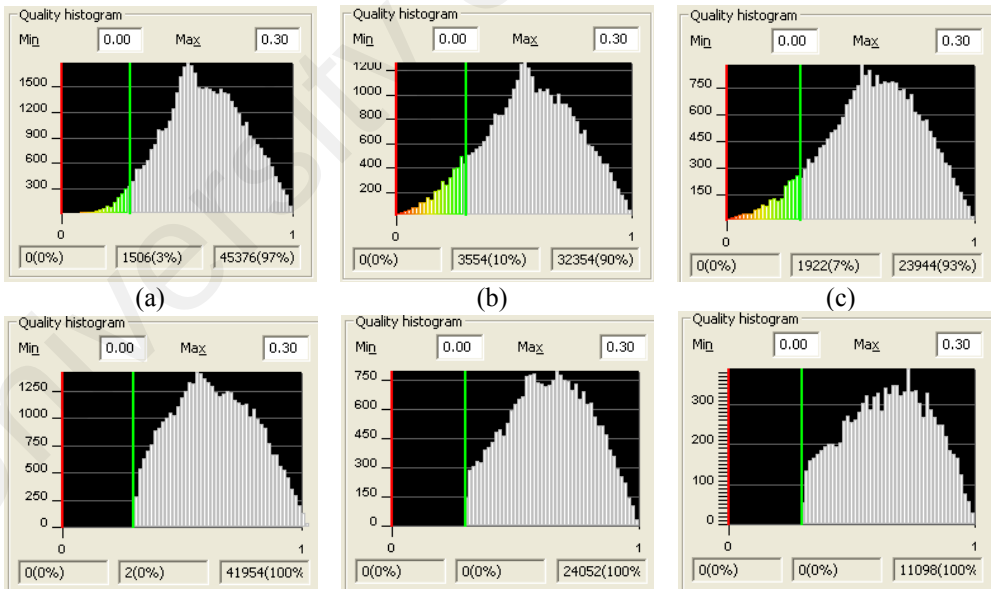

(a) (b) (c)

(d) (e) (f)

Figure 3.12: Triangles quality improvement for facial skin geometry

(a) After allocation of threshold
(b) Point based normal triangle reduction
(c) Edge based normal triangle reduction
(d) Split based automatic remeshing
(e) After 7 times quality preserving triangle reduction
(f) After 10 times quality preserving triangle reduction

3.3.3.2. Remeshing Protocol

The next step after triangles quality observation is *remeshing*. A number of procedures (Materialise 1991) are suggested by Magics RP to ensure optimum mesh for FEA calculation is achieved. The three main procedures for *remeshing* are reducing the number of triangles, improving the quality of the triangles and reducing the number of triangles of the geometry again with respect to the quality of triangles. There are 3 types of triangle reduction introduced in the remeshing protocol. The available options are "normal triangle reduction", "split-based method" and "quality preservation method". The steps discussed below are applied for both facial skin and bone tissue.

a) Normal Triangle Reduction

In order to produce equilateral triangles, the first procedure involved is reducing the numbers of existing triangles. The "normal triangle reduction" option is similar to the triangle reduction of the 3D generation parameters previously explained. They differ in that the latter is used before a 3D geometry is calculated whereas the option discussed in this paragraph is used after the geometry is generated. Although these options have the same set of parameters, a few of the parameters convey different meaning.

The reduce mode consists of "point-type" and "edge-type" reductions have been explained in the *Triangle reduction* paragraph. Each of these types is used once while the normal triangle reduction is done twice. Two neighboring small triangles could present scattered around the geometry. If these two triangles are replaced by one large triangle, there is a possibility that little deviation in position is introduced. Therefore, the tolerance parameters which indicates the maximum deviation allowed between the original triangles and the newly created triangle is important to ensure the new triangle does not differ much in its

size of two merged small triangles. So a small tolerance value of 0.05 is employed. The number of iterations parameter is assigned 5. This value is sufficient because having to do triangle reduction twice with the same number of iterations value gives equivalent results as doing it once with the value doubled. After all, the normal triangle reduction option is needed to run twice. The angle value is defined 30 degrees because 60 degrees value would produce larger elements thus improper for the analysis. It is good to note that important information could be eliminated if both of the tolerance and angle values are large enough.

Figure 3.11(b) and **Figure 3.12(b)** illustrate the point based normal triangle reduction for each type of facial skin layer and bone tissues. Based on analysis on differences between the two histograms, it is concluded that the facial skin layer has more medium quality triangles as compared to the bone. The amount of medium triangles in the bone is 2260 and the skin has 3554 triangles. However, the bone tissue encompasses 6% more high quality triangles by 20866. The same conclusion as above applies for the edge based normal triangle reduction depicted in **Figure 3.11(c)** and **Figure 3.12(c)**. At this time, the histograms have been further reduced. These reductions can be clearly seen in the left indicator next to the red slider of each histogram where the values are lower in contrast to the previous histograms. There are 1816 medium quality triangles in the bone tissue while the total numbers of triangles in the skin tissue are 1922. Higher quality triangles in the bone are 46596 but almost half of this number exists in the skin geometry.

b) Improve Mesh Quality Using Split-based Method

On completion of normal triangle reductions operation, the "split based automatic remeshing" is used to reshape the triangles with a quality below the indicated maximal

threshold so that all resulting triangles have a quality value above the maximum threshold value. Throughout the meshing process, the algorithm will try to enhance triangles that have a quality above the maximum threshold value earlier set as 0.30. The maximum geometry error is the maximum deviation allowed between the initial triangle and the new enhanced triangles after automatic *remeshing* is carried out. The values should not be large. Therefore, 0.05 is adequate to detect the differences also known as *geometric error*. Moving further, the minimal edge length defines a limit of the length of triangles edges during *remeshing*. A small value of 0.01 is assigned so that the triangles shape is within requirement. The number of iteration employed to generate triangles of better quality is 10. In addition, the maximum edge length is used to limit the longest edge of the produced triangles at the value of 8. Finally, the "preserve initial mesh quality" is checked to store the original mesh belonged to the geometry.

The split based method histograms in **Figure 3.11(d)** and **Figure 3.12(d)** shows massive triangle reduction from prior histograms. There are less than 10 medium quality triangles in each skin and bone because the remaining had been improved and grouped in the high quality category. In total, the bone tissue had 61943 triangles while skin tissue had 41954 triangles.

c) Improve Parameters Quality Using Quality Preserving Triangle Reduction

As can be seen in **Figure 3.13**, the mesh model is far from uniform. This can be seen where *mesh cobwebs* still contains a lot of small triangles shown by dark spots on the geometry. These small triangles are removed by several calls to the "quality preserving triangle reduction" option with increasing *geometric error*. To produce optimal geometry, the numbers of calls for the bone tissue is 10 times while the skin requires only 3 calls in

increase of 0.5 for each call. The initial geometric error is 0.5. Except for the numbers of iteration assigned 5, the remaining parameters comprised of quality threshold, maximum geometry error and maximum edge length are kept the same value as discussed above throughout the quality preserving triangle reduction. The "skip bad edges" parameter is ticked so that the algorithm ignores bad edges thus speeds up the reducing process. However, on completion of the calls there still exist a few numbers of low quality triangles which could not be eliminated using more geometric error calls. The numbers of geometric error calls depends on the visual appearance of the mesh. This iterating procedure is stopped once the mesh looks uniform and the total amount of medium quality triangles is relatively small. Therefore, manual editing is performed to eliminate the low quality triangles.

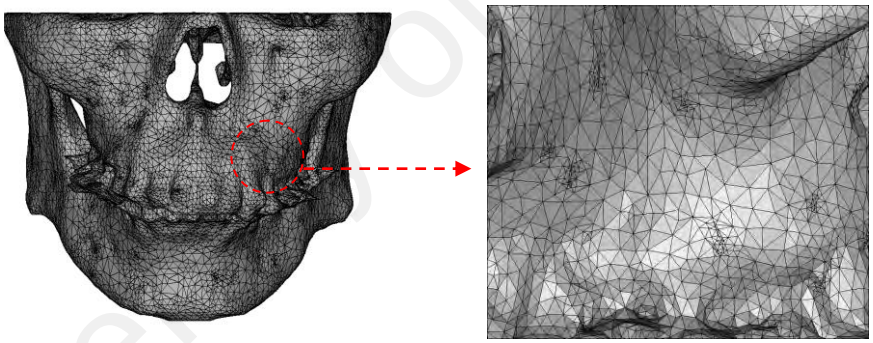

Figure 3.13: Mesh cobwebs

In order to achieve 0 medium quality triangles, 7 calls for the "quality preservation triangle reduction" were made for the bone geometry while 3 calls for skin geometry were adequate. Although, results of this procedure assured high quality triangles for the remaining triangles, the geometry does not visually indicate an ideal model which should consists of equilateral triangles. Therefore, further geometric error calls were made in increase of 0.5 for each call until the ideal geometry is acquired. The last quality preservation triangle reduction call for both geometries was 0.5. Hence, and altogether 10

calls were made throughout the quality improvement step. The differences between the results of each histogram can be seen in **Figure 3.11(e,f)** and **Figure 3.12(e,f)**.

d) Call for Intersection Tests

In order to detect for the location of the intersecting triangles, the "intersection tests" is governed. Once the location is found, the obstacle is fixed by deleting the involved triangles before the resulting hole is filled by creating new triangles. The test is once again carried out to ensure no intersecting triangles exist. Otherwise, the FEA will not accept the geometry for further analysis. An example of intersecting triangles is shown in **Figure 3.14**.

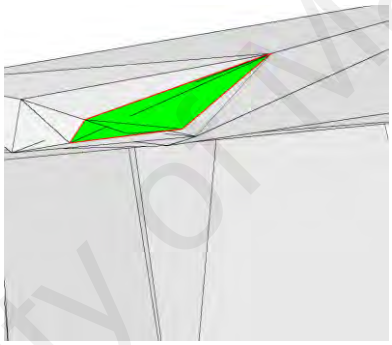

Figure 3.14: Highlighted intersecting triangle

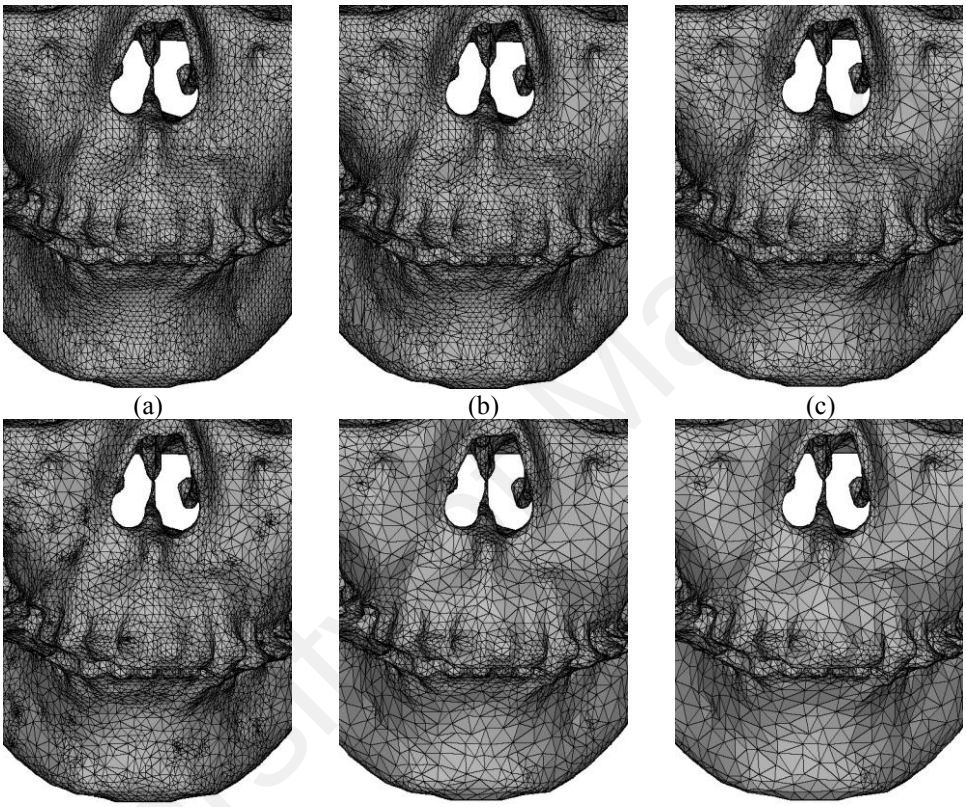

Figure 3.15: Mesh after each reduction on bone surface data
(a) Initial data after triangulation
(b) Point based triangle reduction
(c) Edge based triangle reduction
(d) Mesh improvement with split-based method
(e) After 7 geometric error calls with quality preserving triangle reduction
(f) After 10 geometric error calls with quality preserving triangle reduction

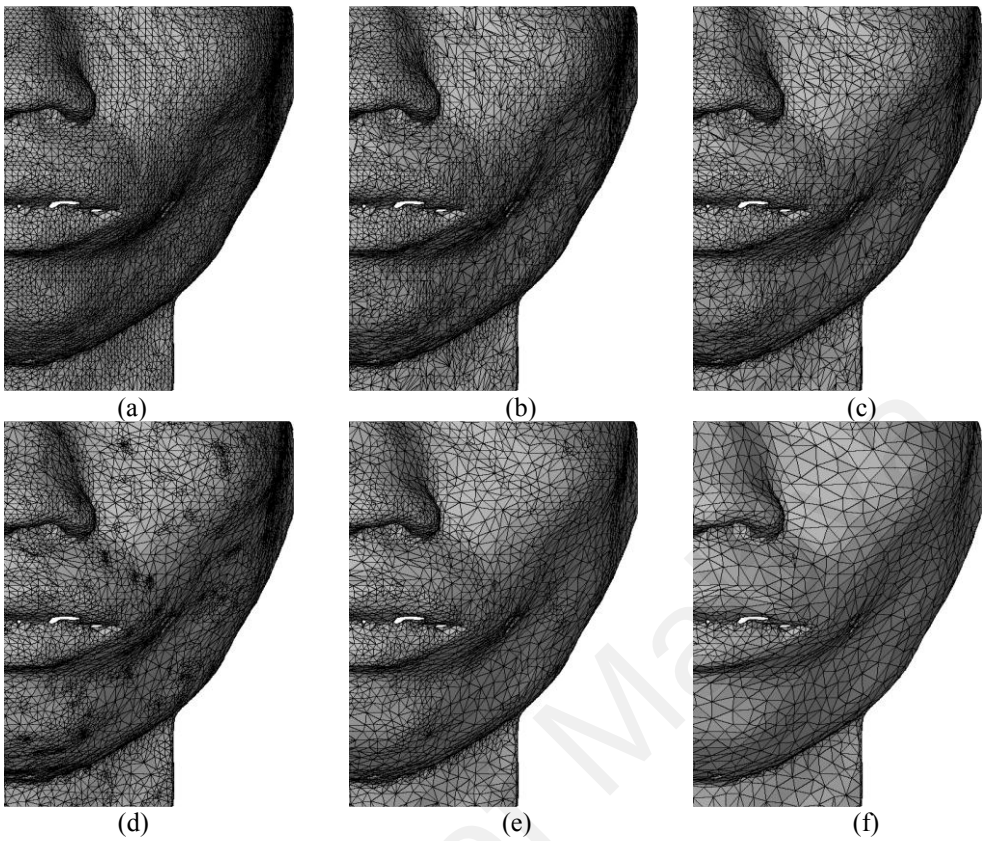

Figure 3.16: Mesh after each reduction on facial surface data
(a) Initial data after triangulation
(b) Point based triangle reduction
(c) Edge based triangle reduction
(d) Mesh improvement with split-based method
(e) After 7 geometric error calls with quality preserving triangle reduction
(f) After 10 geometric error calls with quality preserving triangle reduction

3.4. Model Improvement

Up until this point, the generated models are considered ideal because they composed of optimized meshes. However, these models could not be successfully calculated during the FEA processing due to excessive numbers of triangles. Therefore, further model preprocessing using CAD software package is mandatory. The STL file interfaces between Mimics and the CAD software. In spite of producing smooth surfaces due to elements recreation, the models no longer contain optimized equilateral triangles. Hence, these models need to be remeshed in subsequent FEA software package.

3.4.1. Bone Model Improvement

The scope of this research gives more attention on the lower jaw. But, the currently generated bone model consists of upper and lower jaw. Therefore, these two parts must be separated. The trick is to delete the triangles of the upper jaw and resave or save the STL file by giving another filename. During the process of removing the unwanted triangles, there will appear holes in the working area. These holes are patched using the "fill" option. As can be seen in **Figure 3.15**, there are rough surfaces in between mandible and maxilla appeared because of the teeth structure. The utilized FEA software among majority of the packages does not tolerate with small details on the surface of a model. This is because sharp regions such as sharp teeth area seen in **Figure 3.17(a)** are not easily remeshed. Thus, the rough surfaces must be smoothed by deleting and recreating triangular elements by selecting a portion of the rough surfaces and delete them using the "delete" option available in a CAD software before a new set of triangular meshes are created using the "fill" option of the same software package. The final result achieved is shown in **Figure 3.17(b)**.

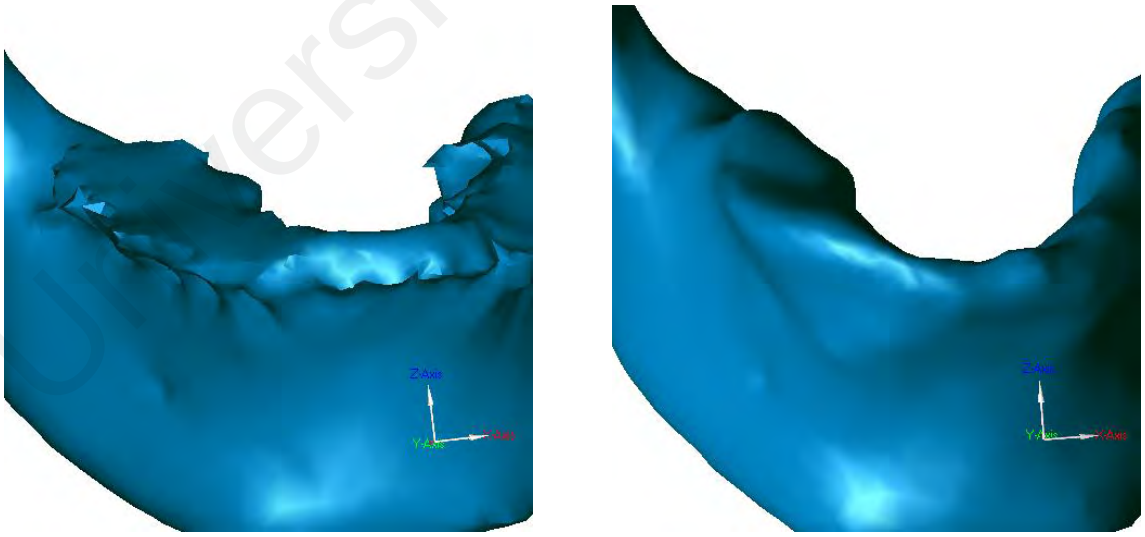

(a) (b)

Figure 3.17: Improved mandible structure. (a): Rough surface mandible and (b): Smoothed surface mandible

3.4.2. Skin Model Improvement

Illustration on **Figure 3.5** showed holes in the improved model after unwanted information had been extracted by manual editing. Furthermore, in **Figure 3.9**, the holes in between the lower and upper lips appeared clutched by excessive triangular elements during the 3D model generation. In these cases the holes must be patched while the unnecessary triangles must be eliminated. The same procedure used for the bone improvement is pursued. Firstly, elements around the hole is selected then removed resulting to gaps around the considered region. After that, the "fill" option is used to automatically create new triangles to patch the unfilled gaps. The holes which have been patched by now, consist of many spike triangles. This is resolved by running the relax operation twice. On completion of these steps, the intersection triangle test from the CAD software is once again executed. If there exists any intersecting triangles, the same procedures beginning from triangles selection are repeated until no more intersecting triangles is detected. The **Figure 3.18** below shows the steps involved during the skin geometry improvement process.

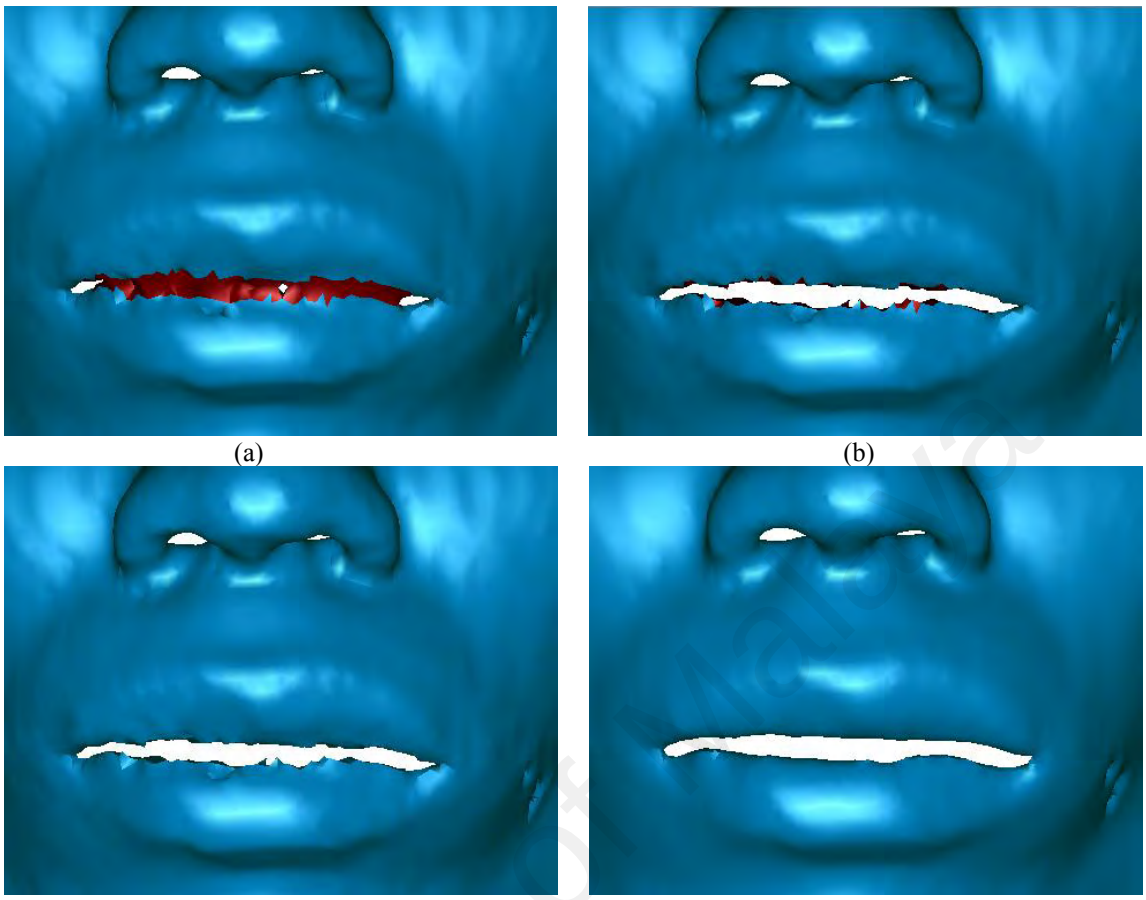

Figure 3.18: Excessive triangles removal
(a) Selection on unwanted triangle elements
(b) Spikes appeared on the closed model highlighted in red color at the lips region
(c) Filled gaps with new triangular elements
(d) Smoothed lips boundary after the relax operation

3.5. Repositioning of Bones

With the help of craniofacial surgeons, the surgical bone cuts known as *osteotomy* and advancement of the mandible are modeled to simulate the surgery procedure. The 3D reconstructed facial models comprised of skin surface; mandible and maxilla are used for the surgery planning. This research project gives focus on *osteotomy* on the mandible or lower jaw. The considered patient had a *bimaxilliary protrusion, long face and left lateral scissor* bite problem, a condition where the upper and lower teeth disproportionately did not meet at the incisor point of the mandible and maxilla. The mandibular *osteotomy* is crucial

to correct the deformity in regards to the mandible. In the following subsection, the advantages and drawbacks arising from the simplification will be discussed. The medical aspects of orthognathic surgery treatment are first described followed by the definition of mandibular advancement *osteotomy*. Subsequently, the *osteotomy* planning and remodeling data preparation is discussed before moving on to the next chapter on finite element analysis to acquire the post surgical results.

3.5.1. Medical Preliminaries

If a person suffers from problems concerning the masticatory system such as malpositioned mandible, upper jaw or lower, he or she is deemed to be given medical attention. If there is no orthodontics treatment available for the problem in consideration, an orthognathic surgery would be the best choice to treat the malformation. Such treatment includes large displacement in between the jaws. The exact description of the surgical procedure is beyond the scope of this report; however the main ideas are described here.

First, the surgeon performed local anesthetic for the tissues around the mandible. The so called *Blair's body osteotomy* or *right body osteotomy* shown in **Figure 3.19(b)** is done on the mandible. The 5mm gaps between the bones which have been cut are filled with bone chips and connected with plates. The *DalPont's modification of sagittal osteotomy* or *left unilateral sagittal split* on the left mandible as illustrated in **Figure 3.19(a)**, **Figure 3.20** and **Figure 3.21** is subsequently performed followed by the placement plates to join the separated bone parts. The surgeon repositions the lower law relative to the upper jaw to

maximize aesthetic objectives (Harris and Reynolds 1991). Surgery was performed carefully to ensure blood circulation in the mandible.

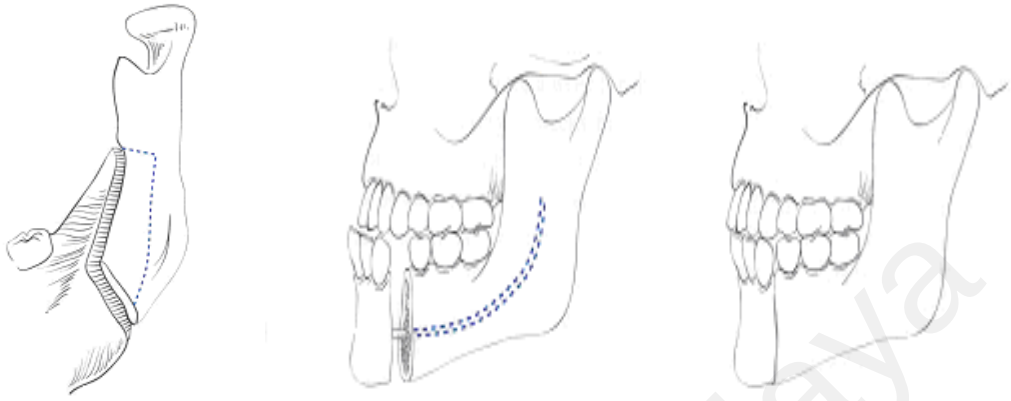

(a) (b)

Figure 3.19: (a): DalPont's mandibular modification of the sagittal *osteotomy* (b): Blair's body *osteotomy* (source: Miloro et al. 2004)

Figure 3.20: The procedure for exposing the body and ramus of the mandible (source: Richter et al. 1998)

Figure 3.21: DalPont modification of the sagittal *osteotomy* (source: Richter et al. 1998)

3.5.2. Definition of *Osteotomies*

A lot of works have been produced for interactive *osteotomy* modeling. A number of the available examples are sketches of *osteotomies* on the lateral x-ray images, definition of twist and depth of the surgical device (Schutsyer et al. 1999) and surgery planning which defines regions for bone cuts on 3 dimensional models. These techniques usually require specialized *osteotomy* surgery software. Since the concern of this research is to produce post surgical aesthetic and acceptable looking facial appearance, the exact replication of real world surgery on the computer was not given detailed consideration.

The surgery planning approach employed for *osteotomy* in this work is by defining cuts on the mandible and repositions the bone slices using Mimics. In addition to model reconstruction from CT images, the commercial modeling software capacitates precise preoperative surgery planning concerning *osteotomies* for orthognatic surgery. The skull and facial skin are first constructed using the *Marching Cube* algorithm (Lorensen and Cline 1987). After mandible and maxilla are separated from the skull and further improvement is made by applying the use of CAD software, the mandible is ready for *osteotomy*. **Figure 3.22(b)** and **Figure 3.22(c,d)** respectively shows the bone cut and positioning of the new bone slices. **Figure 3.23** shows the differences of the forwarded mandible and the actual mandible with the skull.

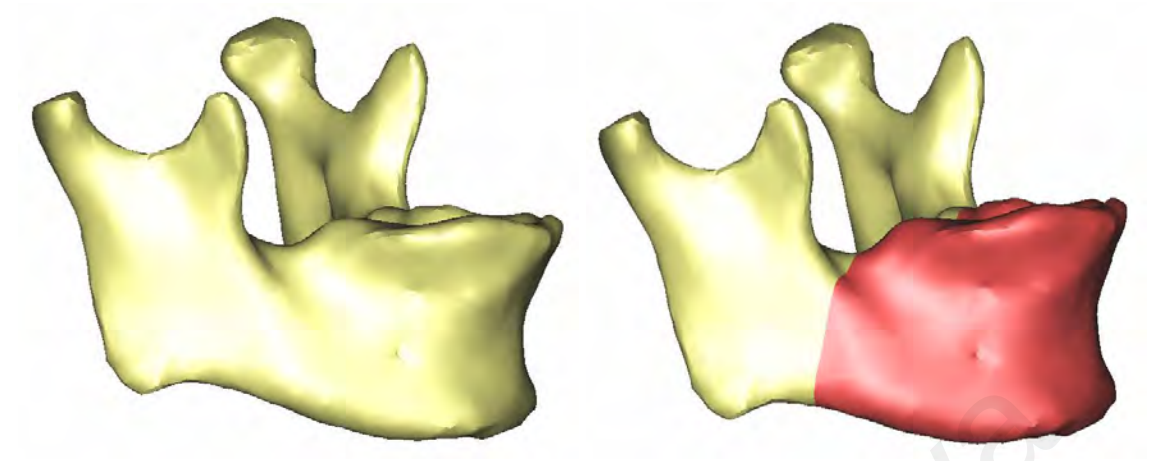

(a) (b)

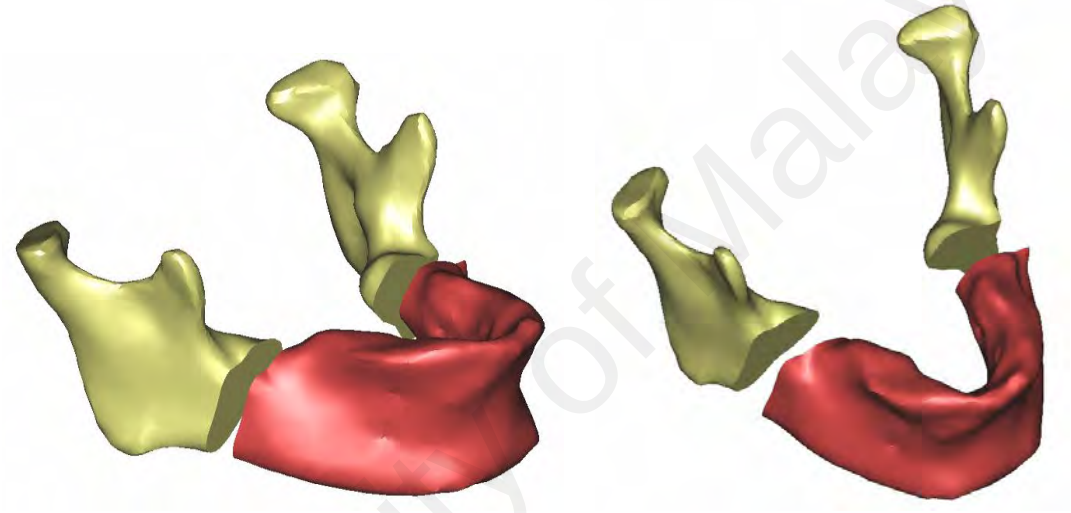

(c) (d)

Figure 3.22: Mandible cuts and bone slices repositioning. (a): Original mandible, (b): Cut mandible, (c): Side view of repositioned front bone slice and (d): Isometric view of front bone slice

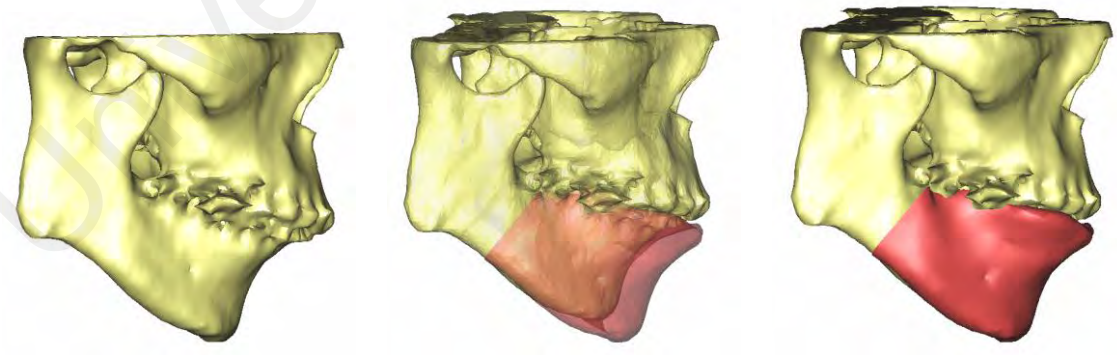

(a) (b) (c)

Figure 3.23: Skull before and after *osteotomy*. (a) : Original skull, (b): Repositioned mandible in semi-transparent surface and (c): Repositioned mandible in solid surface

3.5.3. Modeling the Surgical Treatment

In order to produce a reliable post surgical results based on finite element analysis that will be explained in subsequent section, movement of the bone regions have to be modeled as exact as possible to avoid prediction errors arising from differences between surgery planning in Mimics (Materialise 1991) and finite element analysis in MSC.AFEA (MSC.Software Corporation 1999). Thus, the exact amount of translation and rotation of the front bone regions are changed during the surgery planning was recorded so as to be applied in the finite element analysis to achieve the predicted post surgical appearance. These values are taken as input for the analysis to compute displacement vector of each node that is moved during surgery. **Table 3.2** shows the planning table for the patient specific orthognathic surgery to correct the patient specific *deep bite* syndrome.

Table 3.2: Surgical planning using reference points

Region	Osteotomy	Reference point	Movements	Directions
Lower jaw	Sagittal split	Incisor	-2.4	Lateral
Lower jaw	Sagittal split	Incisor	-8.88	Anterior/post
Lower jaw	Sagittal split	Incisor	7.61	Vertical

The accurate modeling of the *osteotomies* such as depth and twist of the cut is less important but the exact transformation and rotation are substantial for quality of the predicted results. Nevertheless, the differences of the actual surgery and simulated surgery performed on the patient are unavoidable and will be taken into consideration for evaluation purposes in section 5.3.3: *Medical sources*.

3.6. Numerical Model

In this section, the previously discussed facial model is employed to virtually predict the post surgical appearance after a treatment. Therefore, an overview of the system used for the surgery simulation is given. First, the simplified models utilized for the finite element analysis is highlighted before meshes constructing the models are explained. Subsequently, the quadrilaterals mesh generation followed by parameters for model validation before the analysis runs are detailed. Finally, the material properties assignments together with boundary conditions which consist of displacement and contact definition are discussed.

3.6.1. Simplified Numerical Model of Facial Tissue

The physics based models created by applying the techniques described in the previous section are capable for the maxillofacial surgery simulation. The surgery planning is done in Mimics while numerical computation is carried out by MSC.Marc solver through MSC.AFEA (MSC.Software Corporation 1999), a finite element analysis software package used to cater the need for proper definitions of the finite element problem, the local stiffness matrix computation, the assembly and the solution of the global equation system. Moreover, the predicted result is also visualized by the software where analysis in terms of stress and strain is possible.

Accompanying simplifying assumptions, the facial models considered for this research project are the lower jaw, upper jaw and three quarter of the facial skin surface. These models will be used for subsequent virtual orthognathic surgery simulation which consists of FEA calculation to predict the post surgical appearance and surgery planning and

rendering for better visualization. Other material parameters such as muscular anatomy, fat and water were not incorporated due to lack of anatomy information, complex computation and expensive memory consumption for the completion of an analysis. The models used for FEA are skin surface and mandible. During the surgery simulation, no tissues were connected to the bone. However, the interaction between these materials is defined through contact boundary condition. This will be further explained in the section 3.6.7: *Contact Bodies Definition*. The facial models are visualized in **Figure 3.24**.

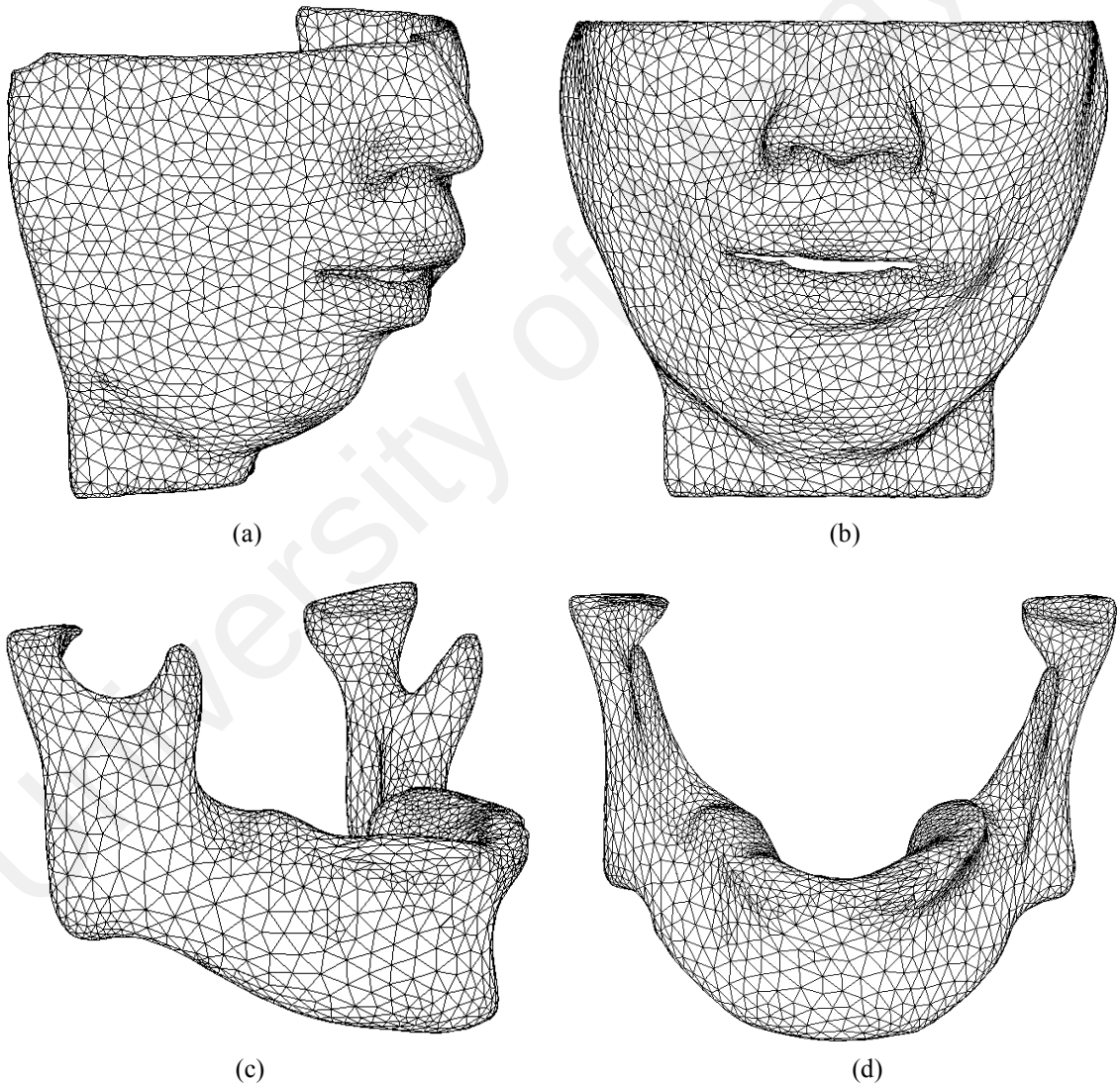

Figure 3.24: Facial models used for finite element analysis. (a): Side view and (b): Frontal view of the skin model, (c): Side view and (d): Frontal view of the mandible model

3.6.2. Initial Project Definition

Before a finite element calculation is permitted, a project is first defined by creating a database file that keeps all information regarding the model setup that includes the model information, mesh topology, model materials and properties, loads and boundary conditions definition, analysis setup and visualization results. After a filename for the database is given, a few model parameters composed of analysis code; analysis type and global model tolerance are specified. The choices of analysis code and type determine the combination of options available for analysis setup. To accommodate the purpose of numerical calculation, MSC.Marc is selected as the analysis code. The chosen analysis type is structural. The analysis type is defined structural because the goal of the problem is to determine the response of a model to a physical loading. In other words, the goal of this research project is to find out the deformation of a facial appearance given movement of the mandible in a protruding manner.

On the other hand, the global model tolerance determines the construction of a model in MSC.AFEA whether the model is built in the software or imported from a CAD software package. This tolerance parameter sets a minimum distance between separate entities such as points, curves, surfaces and solids. For example, if the distance of two points is within the tolerance value, MSC.AFEA will assume these two entities as one thus disable the creation of second point. Two available options for setting the tolerance are “based on model” and “default”. The “based on model” option calculates the tolerance value as 0.5% of the approximate maximum model dimension while “default” option uses predefined value of 0.005. Research found out that the “based on model” option ensured proper meshing and maintained congruency.

Since the scope of analysis is in regard to a prediction of a facial postoperative appearance, the models in use are imported into MSC.AFEA from the previously generated STL files on completion of enhancement and model improvement in the CAD software. A few major STL file formats are *ascii*, binary and color. The *ascii* STL format is the only type accepted by MSC.AFEA (MSC.Software Corporation 1999) version 2004. Therefore, all previous STL files generated from other software were saved as the *ascii* type.

The utilized facial models were saved as three distinct STL files whereby each of these files store a large amount of triangles needed to construct their respective model. In relative to the size of the model, the triangles are numbered from the range of minimum to maximum value. However, there lies a possibility in which these diverse files could be numbered redundantly. For that reason, each of these files must be offset whenever a file is imported into MSC.AFEA. The "define offset" option allows the user to enter an offset value suitable for the numbers of triangles in a model. An offset value is an approximation of the total numbers of triangles. For example, if a model has 1450 numbers of elements, it is best to approximate the offset value to 1500. This setting will cut down a good deal of numerical computation. In this work, the "automatic offset" option is preferred as it provides better automated estimation for the nodes and elements of the models in use. If a file is imported when there already present a model in the working database, the latter will be numbered successive to the previous. To ensure easy manipulation, each model is imported into its respective groups which vary by their group name. These groups are created before any file is imported.

3.6.3. The Importance of Good Quality Meshes

Considering the existent of up to date, high quality and efficient automeshers, developing a good mesh should not result to a big problem to deal with. It is believed that the battle is over once a model can be meshed. However, the exact opposite is often closer to the truth. Ensuring the final mesh is composed of good quality elements that converge to the desired behavior is a more difficult intention. No available finite element analysis tool is completely insensitive to poorly shaped elements thus leaving the completion of analysis impossible. As previously emphasized, an ideal model prepared for the use of finite element analysis is composed of equilateral triangular elements. The accuracy achieved by an analysis is primarily dependent on the quality of the mesh.

In section 3.4: *Model Improvement*, it is pointed out that the triangles recreated to patch holes and to smooth rough surfaces would result to quite a few badly shaped triangular elements. Hence, further quality checks are required even after the generation of a good quality mesh from the bad triangular shell mesh. This is because badly shaped triangular elements would affect the quality of new meshes and the numerical computation during the solution step. The automated mesh improvement and generation of quadrilateral mesh is the objective of this subsection.

3.6.3.1. Methods of Meshing : Finite Element Modeling in MSC.AFEA

A flow of ideas occurred during the research development. In attempt to achieve a good quality mesh, a number of approaches have been explored.

At first, it was considered to run a finite element analysis on a solid model as to resemble real life models. This option begins with the generation of STL files of the mandible and skin layer in Mimics. These surfaces derived from shell models are hollow geometrical models which are not filled with elements in the inside. The FEA *remesh module* of Mimics together with the intervention of CAD software and MSC.AFEA are used to inspect the quality and congruency of these models. During research, it was discovered that there were massive intersecting elements which overlaps with one or few neighboring elements. On completion of these quality checks and improvements, the tetrahedral mesh generation would start. However, this method is not applicable because the initiated solution of the finite element analysis failed. Therefore, it is concluded that solid models are inappropriate due to extensive memory consumption. Although the research project is performed on typical Intel Pentium 4 desktop equipped with 2Gb RAM, it is yet to cater the need of expensive computation.

Another possibility was to generate STL files in Mimics. The triangular elements needed to be improved have already been pointed out. Instead of utilizing the FEA *remesh module*, the CAD software is directly used for further model enhancement. Without the involvement of FEA *remesh module*, the models enclose excessive information. However, quad mesh generation was possible allowing for contact analysis. During development, it was observed only meshes composed of quadrilateral elements permits the desired type of analysis. Nevertheless, this method was not successful resultant to equal reason as in the first method.

The last method was in line with the research development. It is similar to the second method but ahead of the CAD software, the FEA *remesh module* is first used to solve the

problem of excessive information in the models. The finite element analysis succeeded for minimal number of triangles in every model considered. In consistent to the predefined aim, this method is the best approach for the development. The next two subsections will discuss the operating procedure of quad mesh generation using the "mesh on mesh" functionality in MSC.AFEA.

3.6.3.2. Quad Mesh Generation

A number of possible procedures were investigated during the research. As already mentioned, the goal for analysis of this work succeeds only if the models are composed of fully quadrilateral meshes. Quadrilateral is a polygon made up of four sides and four vertices. Starting from existing triangular mesh obtained from the STL files, the development of quadrilateral mesh generation will be discussed in this paragraph.

Mesh on mesh(MOM) on mandible

First of all, the generated models derived from section 3.4: *Model Improvement* is separately imported in MSC.AFEA. These models are imported as text or *ascii* STL files. Subsequently, general checks will be performed for each model. The models are equivalenced to ensure all elements are tied together with each other before duplicated elements are deleted. Once the required conditions are fulfilled, the next stage proceeds with quadrilateral mesh generation by applying the "mesh on mesh" utility. "Mesh on mesh" has the capability of creating new mesh regions to a surface defined by a finite element mesh without initial geometric definition. A new mesh of different type and density can be generated based on the existing underlying surface defined by the original shell mesh. Thus, permits for mesh refinement under selective user controls.

The parameter manipulated under the "mesh on mesh" utility is called "feature recognition" under which two available options are "edge angle" and "vertex angle". "Feature recognition" must be selected to preserve the geometry of the models on the creation of new mesh by keeping relevant features comprised of points and lines based on "feature edge angle" and "feature vertex angle". The "feature edge angle" will preserve an angle of an existing mesh if the angle between two element normals is larger than the predefined "feature edge angle" value. It would be best to set the "feature edge angle" to 0 but several tests showed that higher value is needed to ensure the success of "mesh on mesh". Thus the "feature edge angle" value is set to 60° for each model. The "feature vertex angle" will preserve a node if the vertex angle of the original mesh is less than the predefined "feature vertex angle" value. However, the "vertex angle" is insignificant in this case. Therefore, the default value of 150° is kept.

In addition to "feature recognition", the "delete elements" parameter is checked so that the original triangular mesh is removed on creation of a new quadrilateral mesh. "Existing boundary" is selected for the seed option to ensure the boundary of the input mesh is preserved. The degree of mesh refinement for a model is determined by the "global edge length" parameter. Mesh density depends on the numbers of elements a model contains, signifying smaller value results to finer mesh. Moreover, the "global edge length" parameter contributes to the approximation length of each element edge. This parameter is used to subdivide every boundary edge of the model into an integer number of elements yielding elements close to the edge value by the equation (MSC.Software 2003) below:

$$Numbers\ of\ elements = \frac{Longest\ geometry\ edge\ length}{Global\ edge\ length}$$

The default global edge angle value of 0.1 resulted to extremely dense mesh for the models in consideration. Excessive detail is not necessary for as long as sufficient geometry information is sustained. Apart from that, excessive elements will consume massive extended computation. The mesh density of 4.0 is sufficient to construct quad meshes relative to the dimensions of the models. **Figure 3.25** illustrates comparison of meshes resultant to various global edge angle values.

In **Figure 3.25(b)** a close up part of the mandible model is shown after applying "mesh on mesh" with the global edge angle set to 4.0. An interesting view emerged when the new mesh is compared with the original mesh. The quad meshes were not achieved because of mesh improvement but a totally new mesh had been created. The original mesh had only been used as a blueprint for the creation of more regular quadrilateral elements. **Table 3.3** compares the numbers of elements for the triangular and quadrilateral meshes. However, during the conversion process, the geometric forms of the model are lost. The new facial models were generated with reduced features compared to the original form. This drawback can be solved with smaller "global edge length" value than 4.0, however the analysis would never successfully complete if smaller value is used on the current platform and hardware requirements. Therefore this limitation is negligible. The quad meshes for the facial models are depicted in **Figure 3.26**.

Table 3.3: Comparison of the numbers of elements for different meshes

	Triangular elements	Quadrilateral elements
Skin model	10614	6106
Mandible model	6124	1986

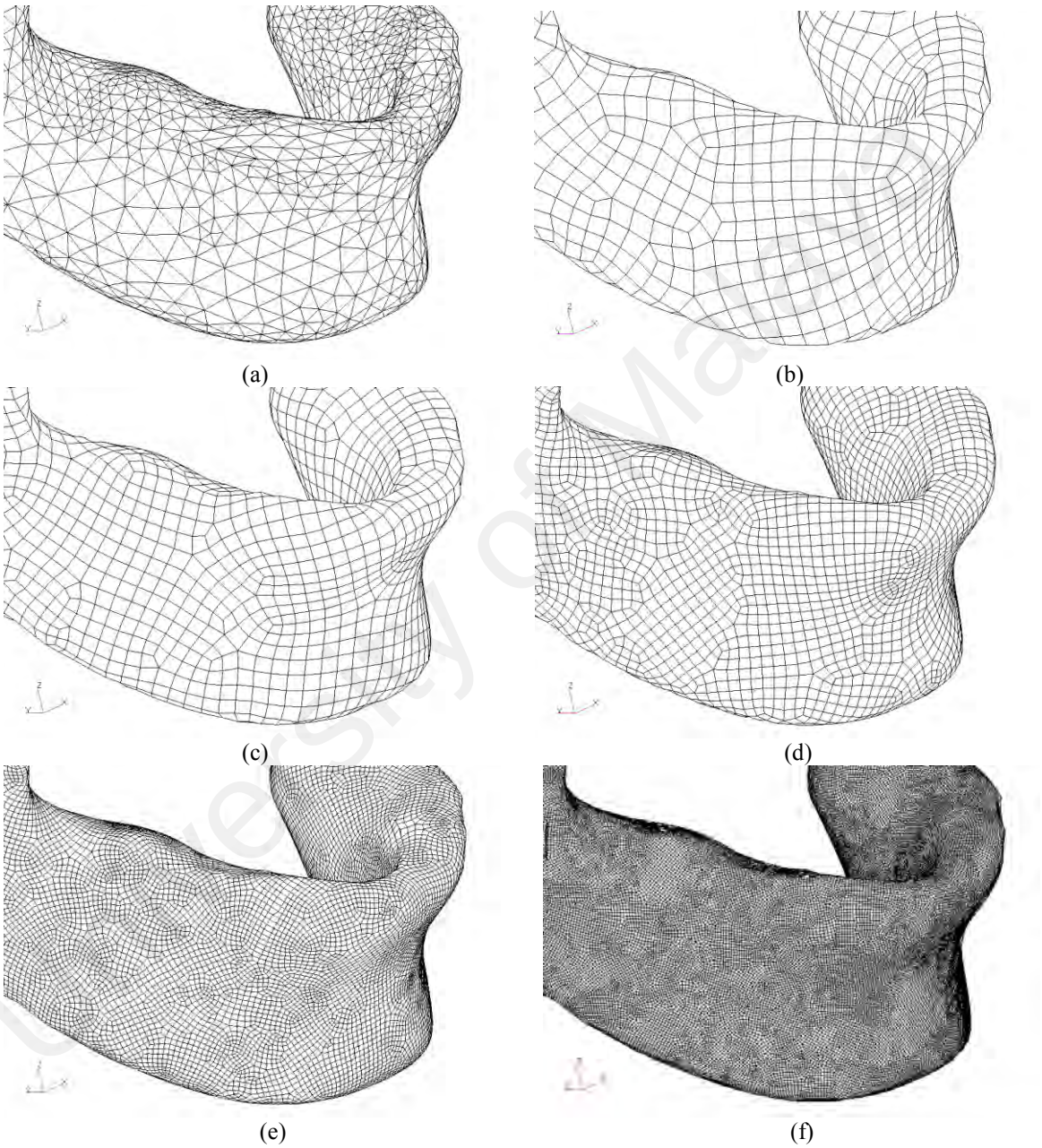

Figure 3.25: Mesh generation based on various mesh densities
(a) Original triangular mesh
(b) Quad mesh with global edge value 4.0
(c) Quad mesh with global edge value 3.0
(d) Quad mesh with global edge value 2.0
(e) Quad mesh with global edge value 1.0
(f) Quad mesh with global edge value 0.5

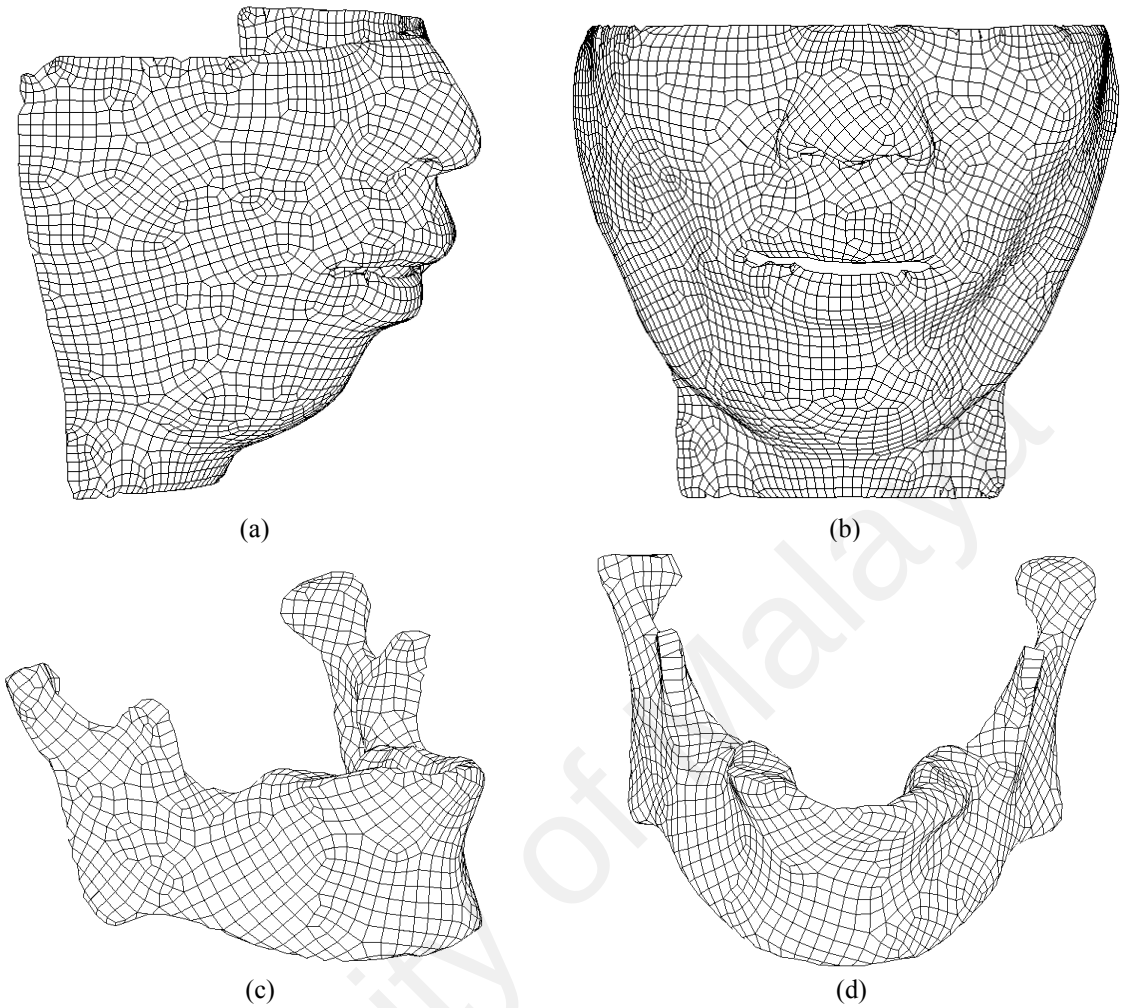

Figure 3.26 : Facial models constructed by quadrilateral meshes. (a): Side view and (b): Frontal view of the skin model, (c): Side view and (d): Frontal view of the mandible model

In spite of the automated quad elements generation, a few triangular elements from the existing mesh remained. This is because during the process of conversion from triangular mesh to quadrilateral mesh, MSC.AFEA counts the number of triangular elements around the perimeter of a surface. If an odd number is achieved, the meshing algorithm will produce one triangle for a surface within the creation of quad elements to replace existing triangular mesh. On the other hand, the total count of even element numbers will ensure only quad elements are created all over the surface.

For definite surfaces such as polygons or geometry, an option called “mesh seed” can be used to control the numbers of elements created along the perimeter. However, the indefinite structure of the anatomy model is not applicable for the “mesh seed” option. A more conventional method which is the manual quad elements creation based on the remaining triangles is applied. This is the most tedious and painful process throughout the development. During the process of manual editing, *free edges* arise. The next section 3.6.4: *Ensuring the validity of finite element model* explains the reasons behind this difficult task.

3.6.4. Ensuring the Validity of Finite Element Model

A finite element model is an approximation behavior of an actual model. The accuracy of an analysis highly depends on the elements composed in the model. It is important to ensure the validity of the finite elements to verify if the elements are connected together or whether the elements are in the inverted or reversed order. Several numbers of options are available in MSC.AFEA for verifying finite element models. The use of these capabilities in addition to the application of engineering judgments to the results of validation adds extra measure of reliability to the analysis work.

Model verification comprises of various tests which includes checks of element distortion, element duplication, model boundaries, nodal connectivity and node element ID numbering. Verification tests are performed interchangeably during the manual conversion steps of the remaining triangular mesh to quadrilateral mesh. The models for this work are quickly checked for invalid elements, poorly shaped elements and node numbering using the “verify” utility. A comprehensive visual feedback that involves color-coding or shading

is provided for these tests. The validity of finite element models determines whether or not finite element analysis can be accomplished. A final model ready for analysis is reached when results for these tests yield satisfactory results. To better improve the quality of finite element mesh would lead to more human engineering time in modifying the mesh for enhanced verification results. Three basic rules the final model should possess are 1) the model should be free from intersecting elements; 2) no hanging elements outside the model and 3) a watertight model must be achieved. The subsequent paragraphs provide details for each tests performed.

3.6.4.1. Boundaries Test

The boundaries test plots any edges of an element not shared by at least one other neighboring element. This test will display any interior or exterior crack along the geometric boundaries. These cracks are referred to "free edges" denoted by yellow edge lines. Another display type is called "free faces". Preserving the same purpose, the only difference lies in the state of visualization. The "free faces" option displays the crack in yellow in flat shaded render style.

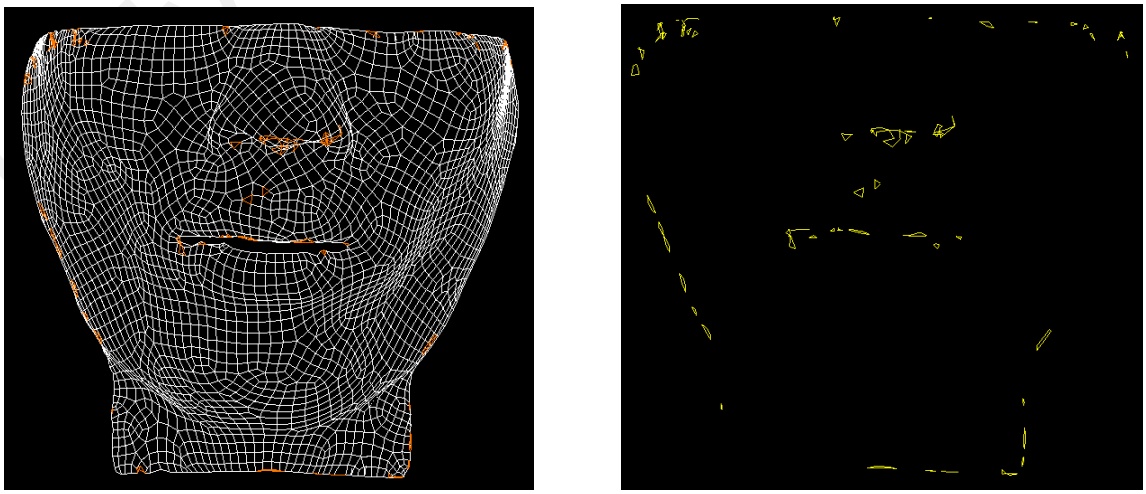

(a) (b)

Figure 3.27: Free edges on facial skin model. (a): Highlighted remaining triangular elements and (b): *Free edges* appeared on deletion of the triangular elements

A good example of *free edges* illustrated in **Figure 3.27(b)** is when triangles which reside next to neighboring quad elements are deleted. The edges of the deleted triangles are not connected to the edges of the surrounding quad elements thus leaving the model permeable. This non-watertight model is known as *non-manifold* model. More *free edges* lines indicate more cavities in the models. The only known solution to this matter is by manually creating new quad elements for the visible cavity. It is during this process difficulty noted at the end of section 3.6.3: *The importance of good quality meshes* occurred. A quad element of 4 nodes must be created from a 3 nodes triangle in taking into consideration of the surrounding quad element connected at each node, an impossible task to perform. However, by making full use of creativity, a 4 nodes quad element can be constructed if there are two neighboring triangles sharing 2 nodes. An illustration for the solution is shown in **Figure 3.28**. The creation of new quad elements are facilitated by the "tri modify" and "quad modify" options under the modify action. The "tri modify" option is used to split a triangular element into two elements which will be combined to produce a quad element. On the contrary, the "quad modify" splits the element into a pattern of 2, 4 or a user defined NxM quad elements.

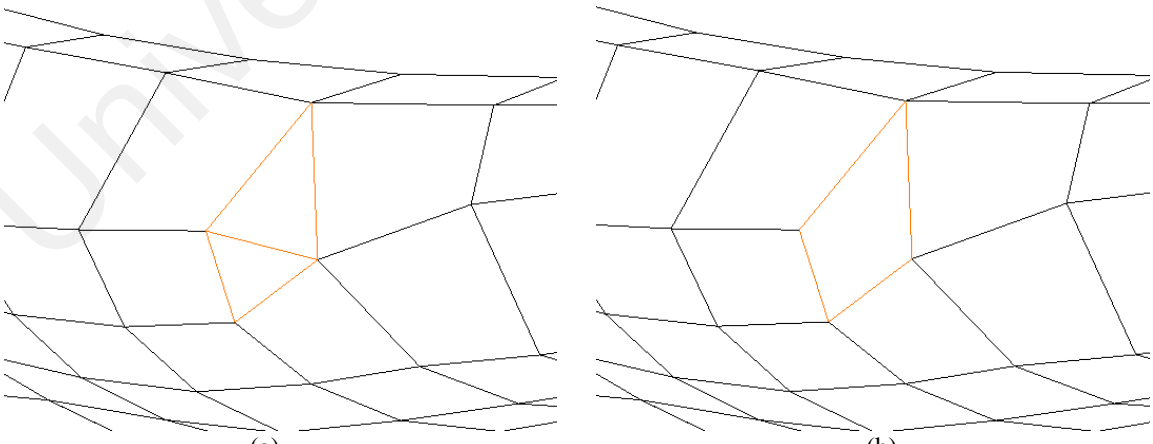

Figure 3.28: Manual editing for the creation of quadrilateral elements. (a): Two triangular elements surrounded by neighboring quadrilateral elements and (b): Combined two triangular elements creates a quadrilateral element

The worse case that could happen is when the two triangles are distant from each other leaving more manual editing process until the two are adjacent as depicted in **Figure 3.29**. The process of manual editing is completed when the entire model consist of merely quad elements in addition to no detection of free edges for every subsequent boundaries test.

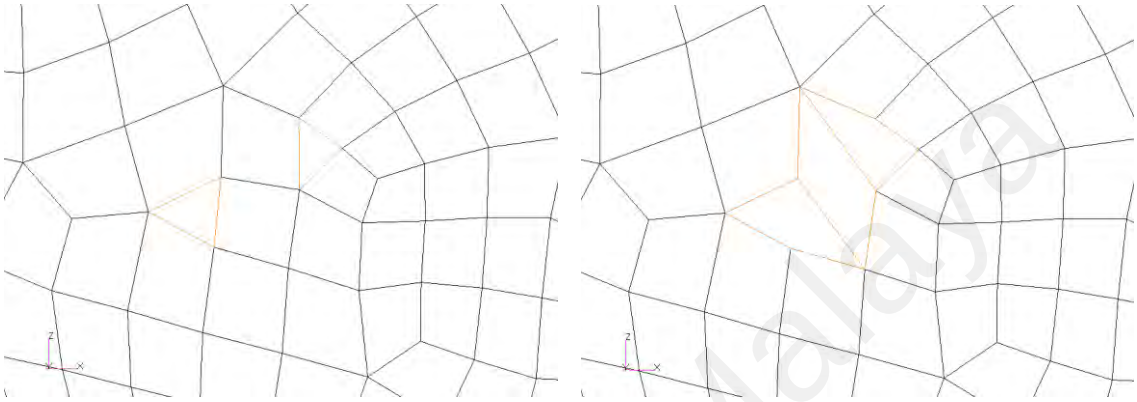

(a) (b)

Figure 3.29: Additional manual editing for the creation of quad elements. (a): Distant triangular elements and (b): New quad elements created to complete the quadrilateral mesh

3.6.4.2. Duplicates Test

Another useful verification is the duplicates test. As the term explains, the "duplicates" option, tests and highlights duplicated elements if there are two or more same elements exist on the same model. These multiple elements connected to the same nodes are detected during the duplicates test. Although they are duplicated, each element consists of one unique element ID. The display control can be toggled to automatically eliminate any duplicates discovered. These duplicates can be removed by a selection of either higher element id or lower element id. Throughout this test, the models used for this work did not detect any duplicated elements.

3.6.4.3. Normals Test

During the initial stage of successfully completed analysis, a postoperative result is imported into Amira (Mercury Computer Systems 1999), a visualization software for an enhanced graphical display. However, it had been figured out that the facial models had a few elements with different colors indicating the elements were not in their correct side, thus these colored elements needed to be inverted; turning the elements inside out. These were the few quadrilateral elements modified or recreated from triangular elements. The normals test check is compulsory for there is a manual creation of quad elements. A new element is always created in a reversed order or opposite to the normal condition of other existing elements.

Normals test displays normal directions for each element in the models. Two types of display are "color coded" and "normal vectors". The color-coded type highlights any element whose normals is reversed in red while the remaining elements are displayed in white as seen in **Figure 3.30**. The color-coding algorithm compares elements with shared edges. Therefore, it is necessary to ensure all elements are tied to each other by running an equivalence action beforehand. If the "normal vectors" display option is preferred, normal vectors and arrows pointing from the element centroid in the element normal direction is drawn for each considered element as shown in **Figure 3.31**.

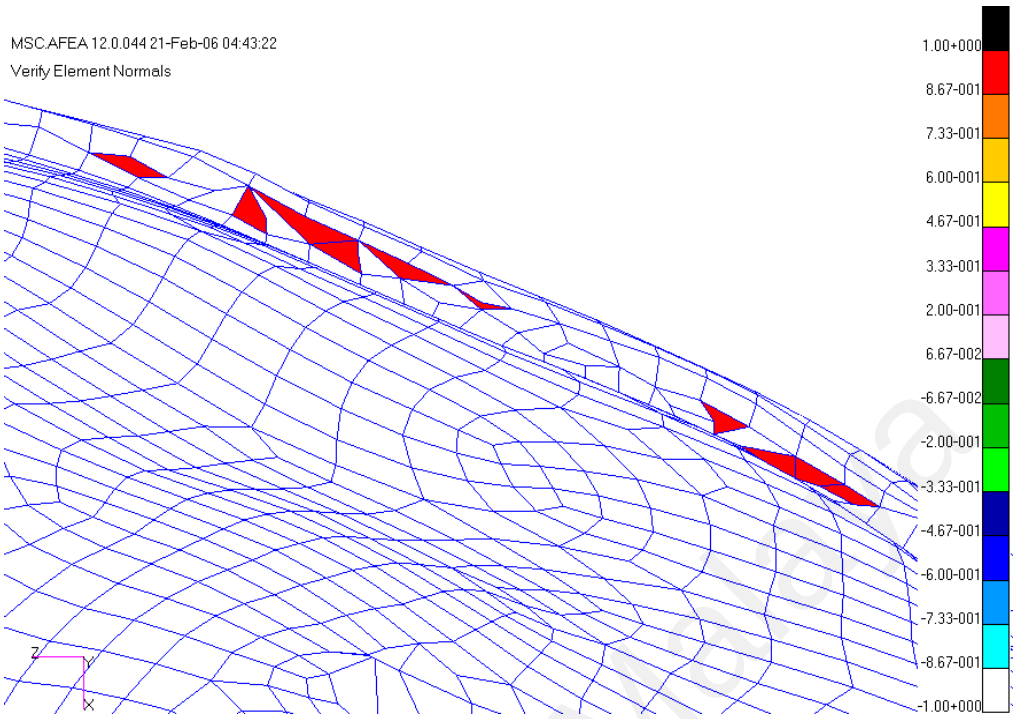

(a)

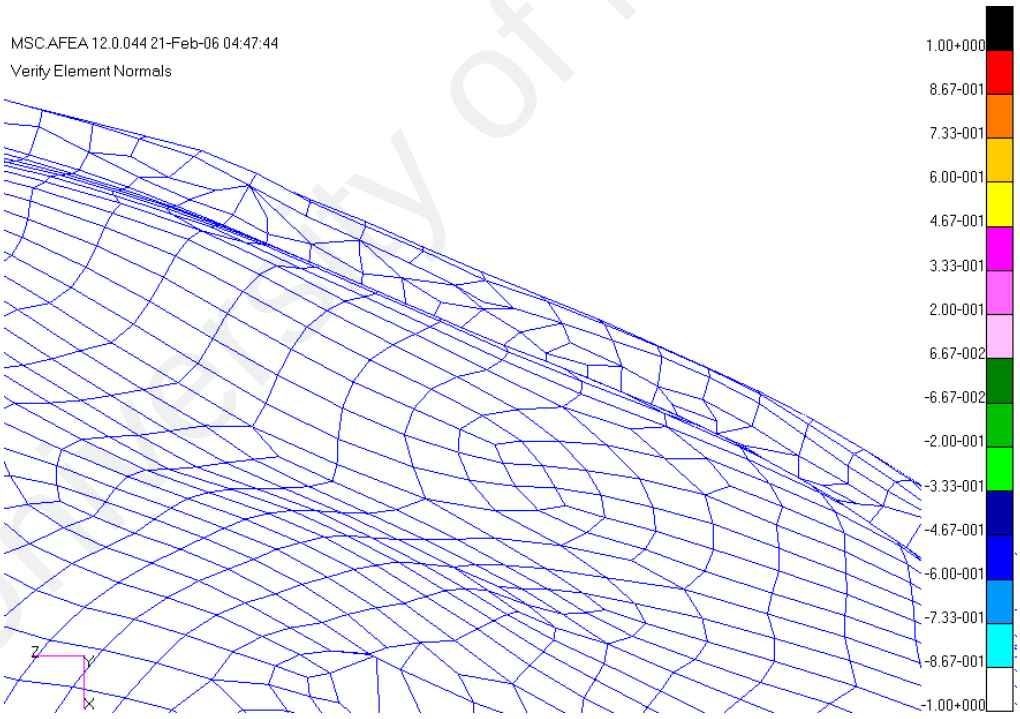

(b)

Figure 3.30: Color coded tests display the quadrilateral elements in (a): Reversed order and (b): Inverted order

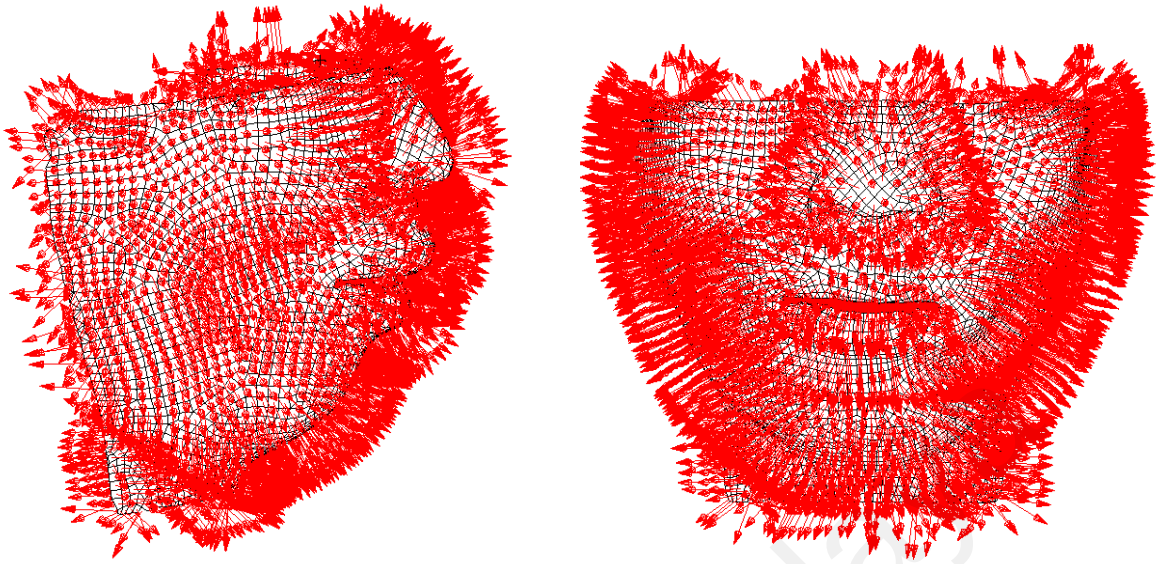

(a) (b)

Figure 3.31: Normals vectors test display in the (a): Side view and (b): Frontal view

Two options are available in order to invert the element. First, by using the reverse elements option under the verify action. Nevertheless, this option is not suitable due to the reason that all elements in the selected model will be reversed regardless to remaining elements. The goal is to invert merely appropriate elements denoted by the red color. Therefore, the reverse option under the modify action is used. To perform this action, the offending elements are made visible by displaying normal direction elements using the color code type. Then, the specific element to be inverted are selected under the modify element action. This procedure is repeated until there are no more red colored elements perceived. On completion of this task, the normals test succeeds as depicted in **Figure 3.30(b)**.

3.6.5. Material Properties Assignment

Each finite element model must be defined with material before further analysis proceeds. The material application is used to define material properties to the models applicable for

the specified analysis code. Definition of the material is made through a material model created as named groups of individual properties. These properties for example bone or soft tissue describe what the model is made of and define attributes such as stiffness, density and elasticity to the material.

The primary intention for the model setup is to accomplish contact analysis. A contact analysis is a type of finite element analysis solution in which there exist contact interactions between distinct materials. In order to achieve success for this type of analysis, MSC.Marc only necessitates assignment of material properties for deformable bodies. An analysis procedure would be unsuccessful if any rigid bodies are assigned with materials. Therefore, the skin allocated as deformable body is given material properties definition while the bone taken as rigid is left undefined. Detailed explanation regarding the contact definition is given in section 3.6.7: *Contact bodies definition*.

Section 2.4: *Biomechanics and soft tissue properties* had explained that the fundamental material properties of skin are inelastic, *hysteresis*, *creep*, *inhomogeneous*, *anisotropic* and *nonlinear*. These properties can be mathematically modeled using constitutive equations. Various other soft tissues are dictated by their specific constitutive equations also called stress-strain relationship. However, acquiring the best equations and constant values that precisely resembles a tissue is taxing. Together with that in addition to the reason of simplicity, *isotropic* and *homogeneous* properties together with the linear elastic constitutive equation are applied. The main reason other mathematical models are not employed is because the extensive requirement of various constant unattained during the period of research. In spite of this, the nonlinear finite element solution is preserved.

The elastic model has linear relationship between stresses and strain (MSC.Software 2003) and is represented by Hooke's law. As illustrated in **Figure 3.32** the stress is proportional to strain in an uniaxial tension stress. The ratio of the stress and strain produces a constant called *Young's modulus* denoted as *E* expressed in equation (3.1).

$$E = \sigma / \varepsilon \tag{3.1}$$

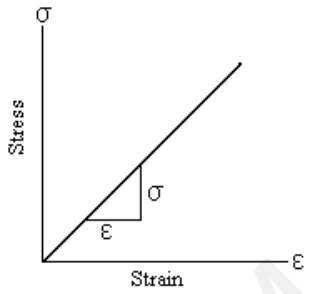

Figure 3.32: Stress-strain relationship of elastic material

Experiments had shown that the axial elongation of a structure is accompanied by lateral contraction with the ratio for linear elastic material (MSC.Software 2003) known as *Poison's ratio*, *v* stated in the form

$$v = lateral\ contraction/axial\ elongation \tag{3.2}$$

The skin material is assumed *isotropic*, a state where elastic properties are identical in all directions. An *isotropic* material has exactly two independent constants, λ and *G* called *Lamé* constants. The *Young's modulus*, *E* and *Poisson's ratio*, *v* are used to calculate these constant values. For an *isotropic* material, the *modulus of rigidity* called *shear modulus*, *G* is calculated based on equation (3.3).

$$G=E/(2(1 + v)) \tag{3.3}$$

The λ, *Lamé* constant is expressed as

$$\lambda = vE/((1+v)(1-2v)) \tag{3.4}$$

Equation (3.3) and (3.4) are used to derive the constitutive equation for an *isotropic* linear elastic material governed by

$$\sigma_{ij} = \lambda\delta_{ij}\varepsilon_{kk} + 2G\varepsilon_{ij} \quad (3.5)$$

where σ_{ij} is shear stress in $_{ij}$ plane, δ_{ij} is Kroneker delta, ε_{kk} is normal strain parallel to k^{th} axis and ε_{ij} is shear strain in $_{ij}$ plane. Readers are referred to (Fung 1981) for further explanation. The two values for *E* and *v* provided for the skin tissue are 0.5 (Gladilin 2003) and 0.3 (Gladilin 2001a).

The material definition and properties assignment are defined separately in MSC.AFEA. Properties are assigned to associate materials to the finite elements through named groups called sets. The specification of properties includes the selection of two options which are the "homogeneous" or "laminate". A "homogeneous" element means that element is made of a single material whereby laminated element implies that elements are made of a number of layers assumed to be perfectly bonded together. The "homogenous" option is preferred. The last attribute assigned for properties definition is the thickness with the value of 1.0.

3.6.6. Allocation of Displacement Boundary Conditions

Subsequent to the assignment of material properties, the facial finite element models are given *loads and boundary conditions*. The *loads or boundary conditions* associates a set of data with an analysis type and geometric and/or finite element entities of the model. In most cases, an analysis problem deals with solution pertinent to the behavior of a model in response to some actions assigned to the model. These actions such as pressure and load to name a few are regarded as *loads*. The behaviors of most of the models are constrained by certain conditions termed as *boundary conditions*. An example of a *boundary condition* in the engineering field is an end of a cantilever beam fixed to a wall. On creation of each type of *loads or boundary conditions*, they are displayed with markers which appear on the

screen as graphical symbols. The arrows and symbols provide visual feedback of the location, type, magnitude and direction of the specified loads or boundary conditions.

In this work, two types of *boundary conditions* are applied. They are *displacement* and *contacts*. No loads such as force, pressure or temperature are assigned to the models. The *displacement* is assigned to nodes to a sparse number of finite elements of the facial skin model in a structural analysis type. As mentioned in section 3.6.2: *Initial project definition*, the analysis type is defined structural because the goal of our problem is to determine the response of the facial skin model when contact occurs with the mandible model. The abovementioned boundary conditions accomplish the interaction between the two models. Therefore, the *contacts boundary condition* is given to both skin model and mandible model. The contacts option will be explained in subsequent section 3.6.7.

The *displacement* is only given to the skin layer model as depicted in **Figure 3.34** to constraint the model from flying around during the calculation of an analysis. On the other hand, the mandible model is not given any *displacement* values because motion control will be applied to the mandible. To define a boundary condition, first a new set name is given to create a group of *displacement* to keep the particular nodes of the finite elements of interest. There are three ways a *boundary condition* can be associated, for which they are "nodal", "element uniform" and "element variable". The "element uniform" defines the given boundary condition for example temperature in a uniform approach over the element face and element edges. On the other hand, the "element variable" associates the boundary condition for instance the pressure in various magnitude over the element, element face and element edge. Therefore, there exist many different values at the nodes of one element. Hence, this leads to the case where nodes that are common to adjacent elements may be

multi-valued in the *loads or boundary conditions*. However, in this work, the "nodal" type which associates *displacement* with the nodes of the elements is the only type available for the "displacement" option. Both translational *displacement* and rotational *displacement* are assigned 0 for every x, y and z direction. The value 0 indicates no translational or rotational movement for any direction in the specified nodes. As illustrated in **Figure 3.33**, the *displacements* are displayed with triple-headed arrow because both translational and rotational constraints are defined in the same direction. The translational *displacement* produces single-headed arrow while the remaining two are contributed by the rotational *displacement*. This visual representation provides a means of verification to the model through visual inspection to critically evaluate the analysis setup with an eye towards the expectation of an actual model. In addition to values assessment of the materials properties, proper verification on the *loads and boundary conditions* values helps to create an extra margin of confidence in the accuracy of the analysis simulation.

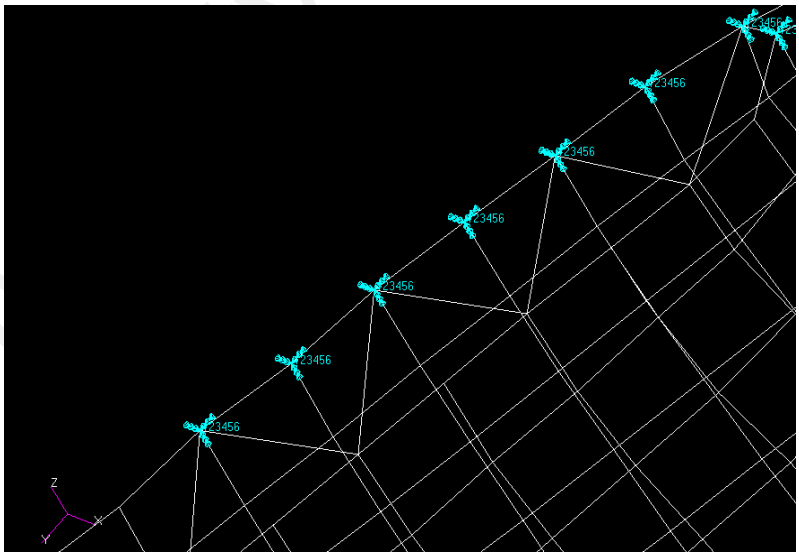

Figure 3.33: Three-headed arrow *displacement*

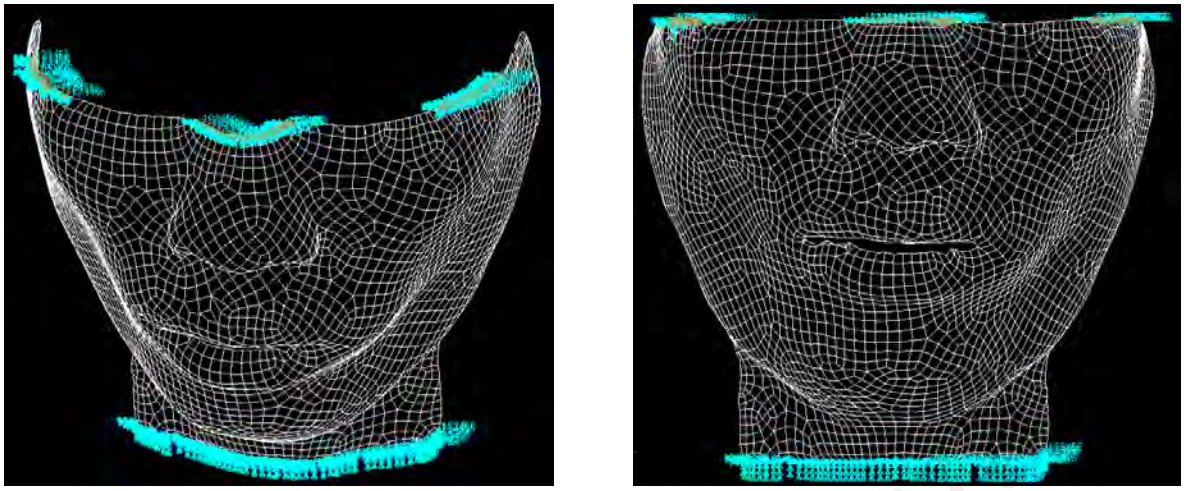

(a) (b)

Figure 3.34: *Displacement* constraint on skin model. (a): Isometric view of *displacement* on the top and neck of the facial skin surface and (b): Frontal view of the given constraint

3.6.7. Contact Bodies Definition

As previously emphasized, the models used for finite element analysis does not take into consideration the muscular anatomy. This is because MSC.AFEA could not accept excessive amount of elements for the success of an analysis. Therefore, there needed a method for the mandible to move forward thus changes the shape of the skin layer in front. This is achieved by a type of *boundary condition* called *contact*. Through a proper *contact* definition between the two models termed as bodies, an automated solution of the problem by MSC.Marc solver is assured. A *contact* can be defined by using two options, "rigid" or "deformable". It is reasonable to define the mandible as a rigid body while the skin layer is allocated a deformable body. The mandible is assigned rigid due to the nature that bone has higher degree of stiffness and density in contrast to other soft tissue materials such as skin. Relying on this fact, it has been assumed that no deformation has occurred to the mandible. However, in reality every material type will deform under the influence of a given load.

MSC.Marc (Marc Analysis Research 2005) has established a number of general rules pertaining to *contact bodies*. If these rules are violated, the possibility of unsuccessful analysis arises. A few of the related rules and important points acquired during the research are emphasized below:

i) All deformable bodies must be defined before the definition of rigid bodies.

Two bodies, respectively deformable and rigid are used for the purpose of finite element analysis in this work. The facial skin model is defined a deformable body while the mandible is modeled as rigid body. This rule cannot be violated as an unsuccessful analysis could happen if rigid bodies are defined before deformable bodies.

ii) An element and a node can only be a member of one body.

All elements and nodes of the relevant models are assigned to their particular type of bodies, either deformable or rigid. An element or a node cannot be defined in both bodies. For example, an element of the mandible which has been defined as a rigid body cannot be once again classified as a deformable body.

iii) If the considered bodies are convex and concave, the convex is first defined.

Figure 3.35 showed the skin has a convex shape. This reason intensifies the need of defining deformable body ahead of the rigid body.

iv) Assign all elements and nodes during contact definition.

At the stage of allocating either a rigid body or a deformable body, all elements and nodes relative to the models must be selected. Otherwise, an erroneous message signifying failure of analysis will be presented.

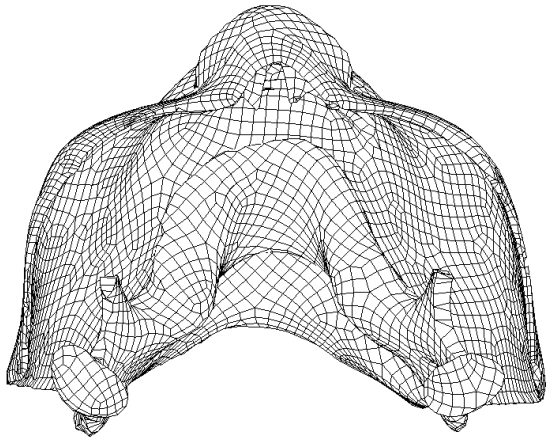

Figure 3.35: A top view of convex shaped skin model

Distributions of *contacts* for both bodies are appointed "element uniform" revealing that the *contact boundary condition* is associated throughout each element in the models. Equal to any other definition of *boundary condition*s, each creation of *contact bodies* provides a visual display. As visualized in **Figure 3.36**, the creation of rigid body displays arrows pointing inward of the meshed mandible. Quite differently, circle markers are assigned to the deformable body of the skin surface model seen in **Figure 3.37**. A vector normal of a rigid body must point in a direction away from the contacting body, in this case the deformable skin layer. Once a rigid body of the mandible is allocated, the arrows are displayed towards skin model as seen in **Figure 3.38**. In contrast to the given condition, these arrows must be reversed. A preference under the "rigid body" option called "flip contact side" is checked during the setup of rigid body for the mandible. The output is displayed in **Figure 3.39**.

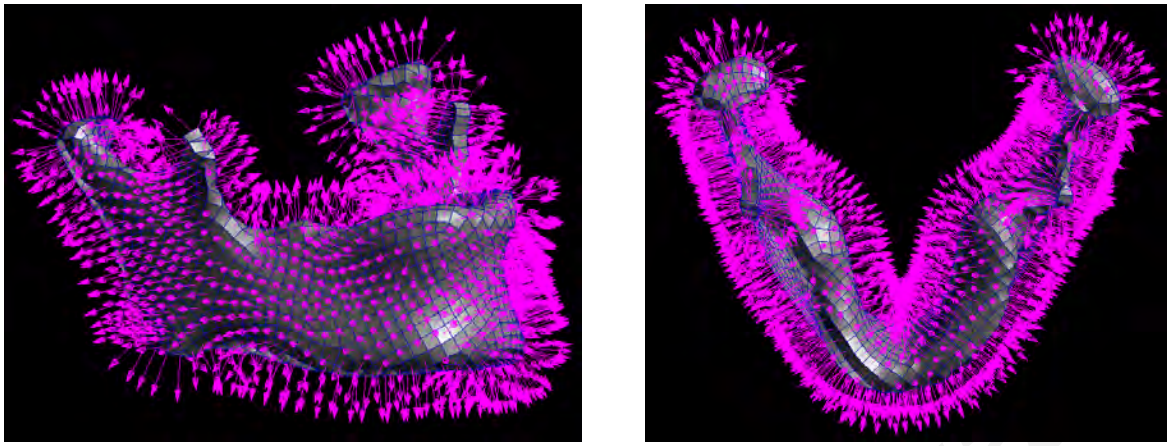

(a) (b)

Figure 3.36: Visual display of rigid mandible. (a): Side view and (b): Top view of the mandible showing arrows pointing outward

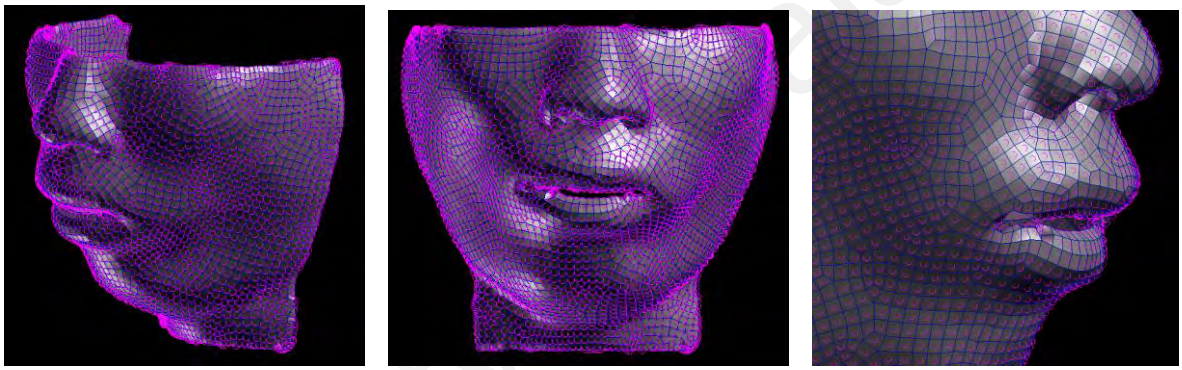

(a) (b) (c)

Figure 3.37: Visual display of deformable skin. (a): Isometric view, (b): Frontal view and (c): Upclose view of circle markers on the deformable skin

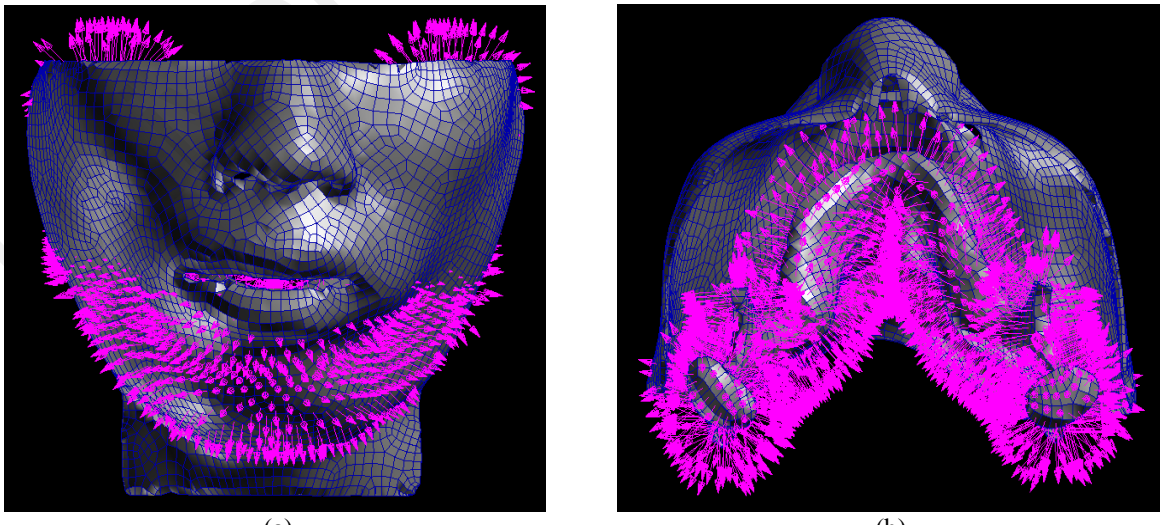

(a) (b)

Figure 3.38: Arrows from mandible pointing towards the skin layer. (a): Front view of arrows from rigid body mandible to the skin and (b): Top view of arrows from the mandible

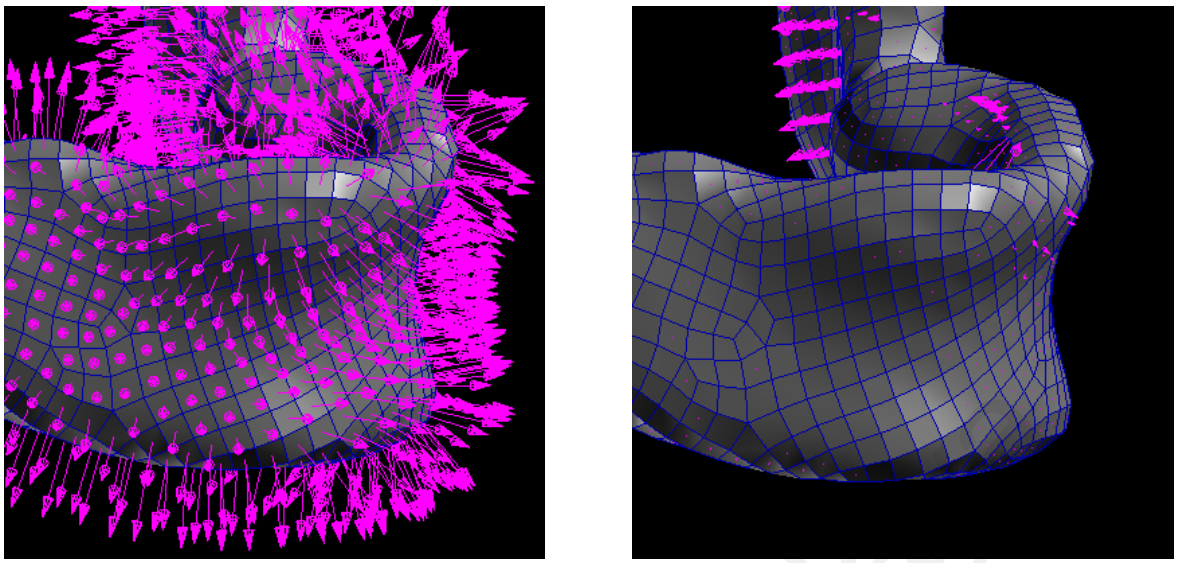

(a) (b)

Figure 3.39: Reversed arrows for rigid mandible. (a): Arrows pointing outwards before and (b): Arrows pointing inwards after flip contact option is used

Due to MSC.AFEA constraints, several parts of a model cannot be simulated at a time. Therefore, the idea of moving separated portion of the mandible bone results of *osteotomy* as explained in section 3.5.2: *Definition of osteotomies* cannot be applied for the finite element analysis simulation. However, the software capacitates motion control for the protrusion of the rigid body mandible. Hence, allows for deformation of the skin layer based on the forward motion of the mandible. The selected motion control for the rigid mandible is velocity given as -30 degrees of freedom in the y-direction on the global coordinate. The negative sign indicates that the contact from mandible acts towards the skin. Figure 3.38(a) and (b) show the contact bodies setup for which the mandible will move forward to the underlying skin layer to change the shape thus predicts the postoperative facial appearance. The remaining x- and y-directions are left zero, because the mandible is set to move in a straight and forward direction. Any value given to these directions will cause different direction to mandible movement.

The rigid and deformable *contact body* is also referred to *master-slave contact* considering rigid body as a *master* and deformable body as a *slave*. The movement of the mandible which changes the shape of the skin is achieved by mathematical calculations during the analysis solution. The *contact* algorithm will detect nodes from the mandible entering the skin nodes before appropriate constraints are generated to assure that there lays no occurrence of penetration between the bodies. The algorithm also maintains compatibility of *displacements* across touching surfaces.

Detection of *contact* in between a deformable body and a rigid body depends on the distance separating them. **Figure 3.40** delineates a graphical explanation for the *contact* procedure. The rigid body moves towards the deformable body, simply because of the reason that the deformable skin model had been given *displacement* which constraints the movement while the rigid mandible was prescribed with motion velocity. Moreover, the simulation of these procedures will display motion of the rigid body mandible towards the deformable body skin layer and then back to its original position.

During the initial model position, no *contact* at all is detected between these bodies because the *contact segment* in the mandible is not within the *contact* region. A *contact segment* is defined as nodes around the boundary of a model or an edge of either mandible or skin. Nodes comprised in the rigid mandible body will displace closer to the deformable skin body for every iteration calculated. Once the relocating nodes of the rigid body have reached the deformable skin region, the models are now considered contacting with each other. The surface region around deformable body is called *contact tolerance*. A node is considered to be in contact with the segment, if the particular node is within the *contact tolerance*. The default *contact tolerance* set by MSC.Marc is 5% of the smallest element

side or 25% of the smallest element thickness detected around the deformable model. Further contact will produce penetration within these two models. The two separated *contact bodies* are not allowed to penetrate each other during the solution. Thus they are defined as touching during the analysis setup explained in section 3.7.3: *Setting up analysis*.

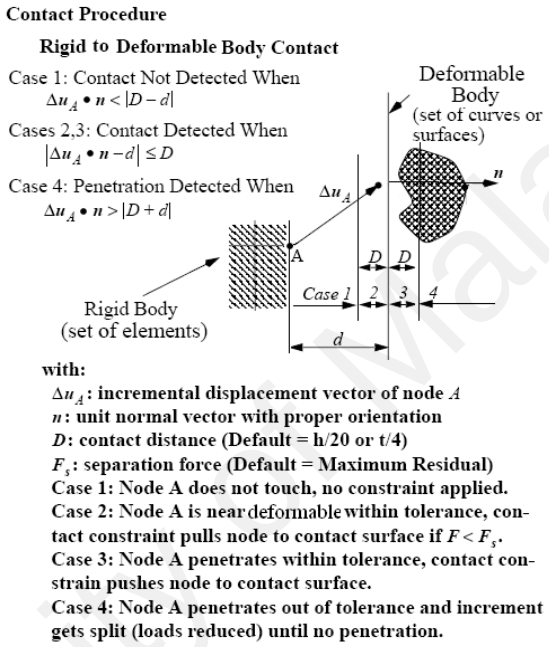

Figure 3.40: Rigid-deformable contact bodies procedure (MSC.Software 2003)

3.7. Analysis

The analysis application, links between MSC.AFEA preprocessing and post processing environment. It is through "analysis" that a model is analyzed by the specified solver to output results. Several setup steps are required before a model is submitted for an analysis:

3.7.1. Selecting Analysis Code

An analysis code signifying the type of finite element software is selected based on the objective of the analysis. Two possible analyses under the MSC analysis codes selection for finite element analysis are MSC.Patran and MSC.AFEA. Patran provides basic capabilities for linear and nonlinear analysis. On the other hand, as the name implies, MSC.Advanced FEA (AFEA) provides advanced solution for nonlinear analysis and thus is more suitable for this work.

3.7.2. Identify Solution Type

As previously mentioned, the MSC.Marc solver is selected at the beginning of the preprocessing stage to solve the submitted model. MSC.Marc acts as an interface which converts MSC.AFEA database into binary number analysis codes. After the analysis is completed, the solver reconverts to result database from the computed analysis code results files. Different solvers offer different solution types for various model behaviors. Unique sets of equations are used for each solution to achieve reliable analysis results.

3.7.3. Setting Up Analysis

A few customization in the analyze option is needed before the analysis proceeds. The analyze action and entire model object are selected for the purpose of analysis setup. Full run method requires forward translation to create an input file ahead of call upon analysis solver. A proper *jobname* is given to recognize files associated with the particular run. During the read results file selection, a results file with the same *jobname* is loaded into the

database. Figure I-1-3 in Appendix I: Schematic Solution Procedure shows the schematic diagram of the solution procedure.

The first attempt of analysis was unsuccessful because the analysis failed to converge. This matter is resolved by turning on the "non-positive definite" option in the solver option of job parameter button. The "non-positive definite" option is used whenever an analysis does not converge or the analysis stops prematurely. If this option is turned on, additional constraints are set up to remove degrees of freedom that cause a non-positive definite matrix, thus force a successful solution. The "direct sparse" solver supports most Msc.Marc solver capabilities with less memory and allows external (RAM) memory to be accessed if the solution could not cater for the memory allocated by the Msc.AFEA software. Default solver type of "direct sparse" remained. Non-linear analysis is desired for the finite element analysis particular for this work. Therefore, non-linear option is appointed in the solution parameters where static is assigned as the solution type for structural solutions. Since the prediction of postoperative appearance requires large deformation, meaning that there is considerable forward displacement of mandible during surgery, the large displacements/large strain is selected as nonlinear geometric effects which indicates the type of geometric approximation the solution needs to utilize.

In section 3.6.7: *Contact bodies definition*, the *contact boundary condition* allocated in the *load and boundary condition* option is explained. However, "touch" mode setting is assigned in the contact table during the analysis setup. The "touch" contact mode is defined for the two models; facial skin and mandible in cells of a table. Nevertheless, the rigid mandible cannot come in contact with itself; therefore the cell is left blank.

On completion of these setup, the models are finally submitted for finite element analysis to the MSC.Marc solver. The computation process took approximately 4 hours for a successful completion on a 2GB RAM of an Intel Pentium 4 desktop computer.

3.7.3.1. Monitoring Analysis

During the progress of analysis, the *jobname.dat*, *jobname.out* and *jobname.sts* files are updated for each computed iteration. The *jobname.dat* is the input file that provides information on the analysis setup. This file translated by *pat3mar* translator is submitted for the processor for further step for analysis processing. Translation is crucial so that the processor understands the input file. The *jobname.out* consists of output results in terms of numerical values. The *jobname.out* file will tell if the model was not translated or convergence was not reached and the analysis terminated. Therefore, it is through this file that users are given indication on error messages whenever an analysis does not run or ends before completion. The *jobname.sts* is the status file for which there is a tabular listing of step, increment and iteration information. The *jobname.sts* file can be checked during analysis to monitor the progress or completion of the results. All of these files are available for monitoring. A successful completion ends at exit number 3004 for the three above mentioned file types. Other values indicate unsuccessful results for this analysis. Figure II-1:1-4 of Appendix II: MSC.AFEA Results Files shows the exit number of a *.out*, *.sts*, *.log* file. Error messages will be presented, if problems appear during the analysis. This is a good remark as further approaches can be considered to achieve results at a reduced time.

3.7.3.2. Retrieving Analysis Results

Once an analysis ended, the data stored in a *.t16* file particular to the analysis *jobname* is read into MSC.AFEA using the "read results" option which indicates data is to be read in from an analysis code results file. The results file is attached to the database to ensure visible results on screen. **Chapter 4: Results and Data Analysis** will further discuss about the results obtained.

4

RESULTS & DATA ANALYSIS

In this chapter, experiment results carried out with artificial objects followed by real patient geometric models obtained from computer tomography data are presented. The general aspects of FEM considering simple artificial objects under the impact of predefined loads are obtained from the experiments which are then employed for the analysis of patient geometric facial models. Subsequently, the postoperative appearance of the patient due to bone repositioning through finite element analysis are discussed. Illustrations that represent the graphical results obtained from MSC.AFEA are used along the explanation. In addition, better visualization is perceived through the visualization software, Amira (Mercury Computer Systems 1999).

4.1. Experiments with Artificial Objects

A number of tests had been carried out before the actual geometry models were incorporated for finite element analysis. The reason these experiments are performed are : 1) to compare simulation results to the theory of FEM and 2) to validate the advanced modeling method to simple 3D geometry objects.

4.1.1. Soft Tissue Deformation

The principle theory of finite element method discussed in section 2.12: *Finite element analysis* explains that a body will deform if a load is specified to a number of nodes belonged to the body. Deformation of a model is calculated by the *displacement* of the associated nodes. The numbers of elements contained in a model determines the accuracy of deformation. However, larger amount of elements requires more numerical computation during analysis. Therefore, the total numbers of elements must be evenly balanced with the hardware capacity. **Figure 4.1** and **Table 4.1** show the degree of refinement for nodes and elements of a cube.

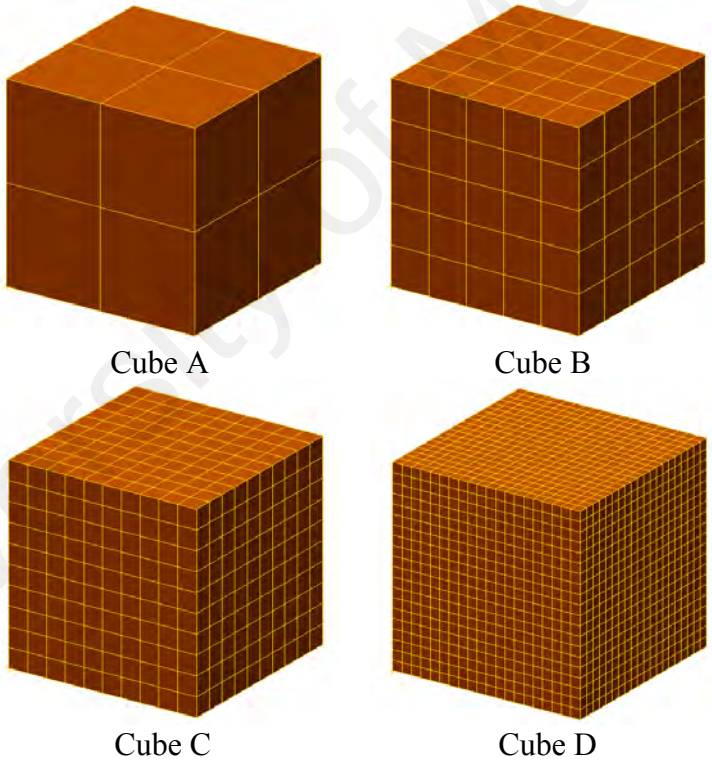

Figure 4.1: Mesh refinement of a cubic geometry

Table 4.1: Quantitative values for the degree of refinement of quadrilateral mesh

Cube	Mesh refinement	Node	Element
A	0.5	54	24
B	0.2	216	150
C	0.1	726	600
D	0.05	2646	2400

Apart from tests performed to produce an ideal mesh relative to the dimension of the models, another good practice is to experiment material properties values for the skin on geometrical objects. This procedure is important for verification between theory and hypothesis of deformable concept. **Figure 4.2** illustrates the undeformed and deformable state of the soft tissue represented in a cylindrical geometry followed by the simulation in **Figure 4.3**.

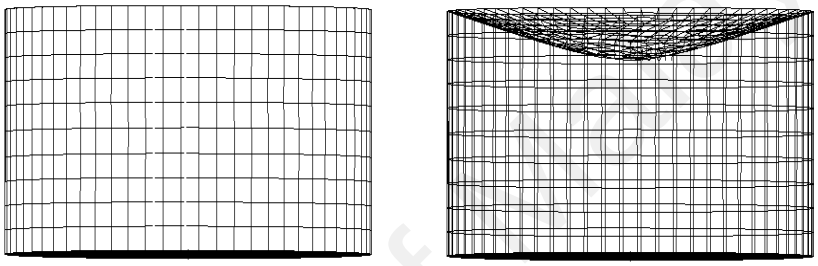

(a) (b)

Figure 4.2: The (a): Undeformed and (b): Deformed soft tissue resembled in a cylinder

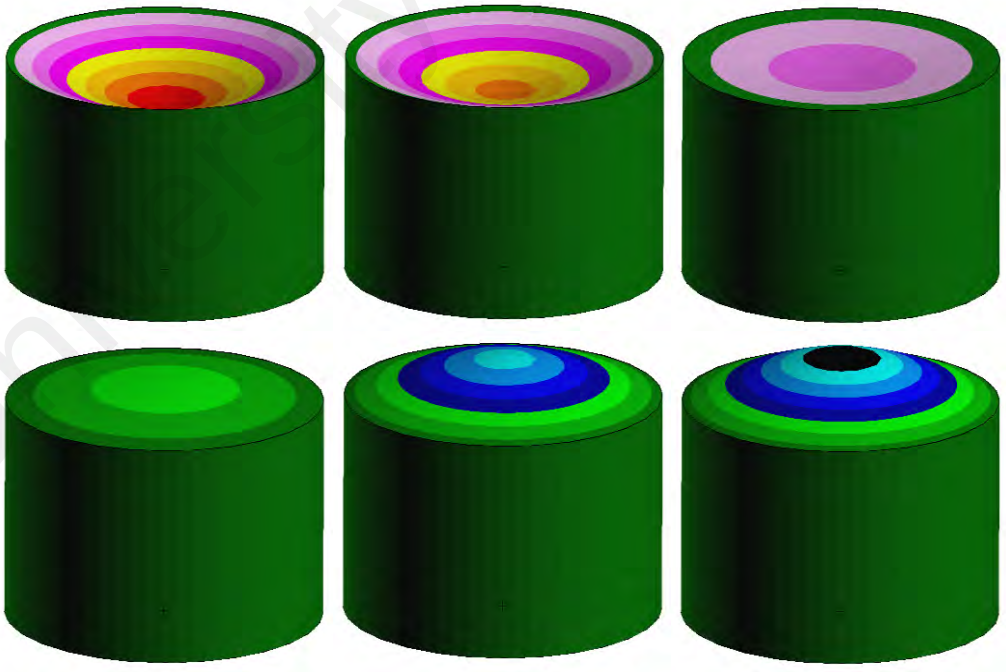

Figure 4.3: State of deformable soft tissue under linear elastic analysis

It is concluded that the *Young's modulus* value of 0.5 that characterizes the facial skin applies well to the hypothesis where deformation of an object happens when there exist any load on the nodes enclosed by the object.

4.1.2. Contact Analysis between Rigid and Deformable Bodies

Another experiment giving focus on the interaction of deformable skin layer and rigid mandible had been performed. Resultant to this test through contact analysis in MSC.AFEA, the impact of forward mandible movement towards the underlying skin is examined. Two curves which resemble deformable skin and rigid mandible were modeled to observe contact between the geometries. The deformable body is displayed as circle markers while the rigid body is displayed as tick marks pointing to opposite direction of the deformable body. Based on the results, it is concluded that a rigid body is capable of changing the shape of a deformable body consequence to the forward motion of the rigid curve. **Figure 4.4** exemplifies the procedure.

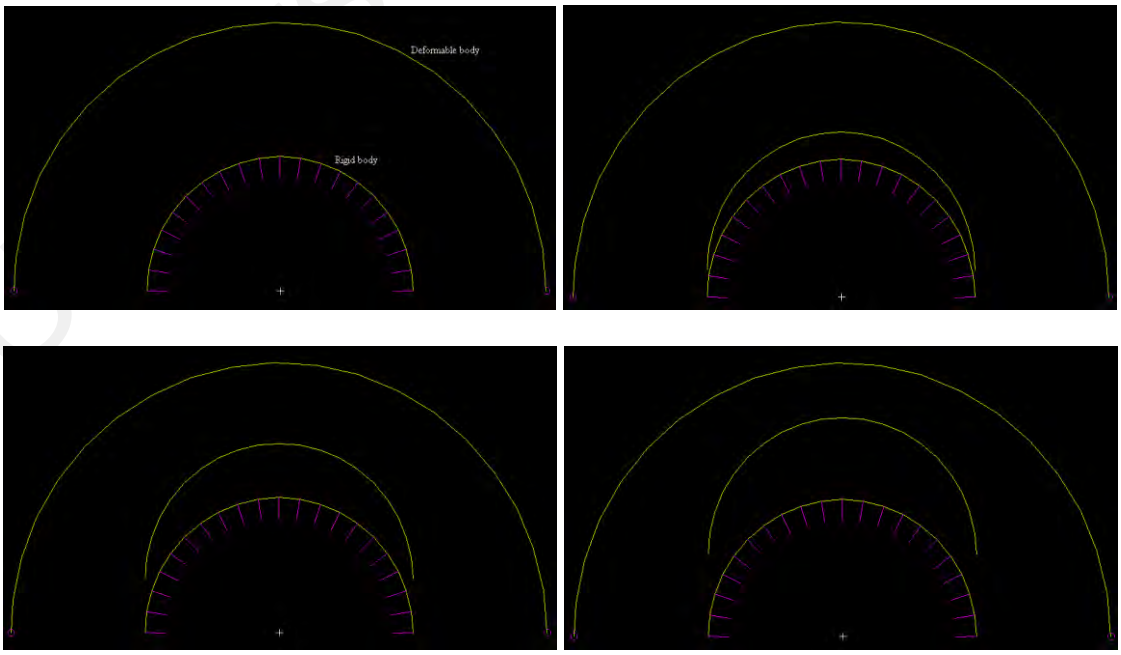

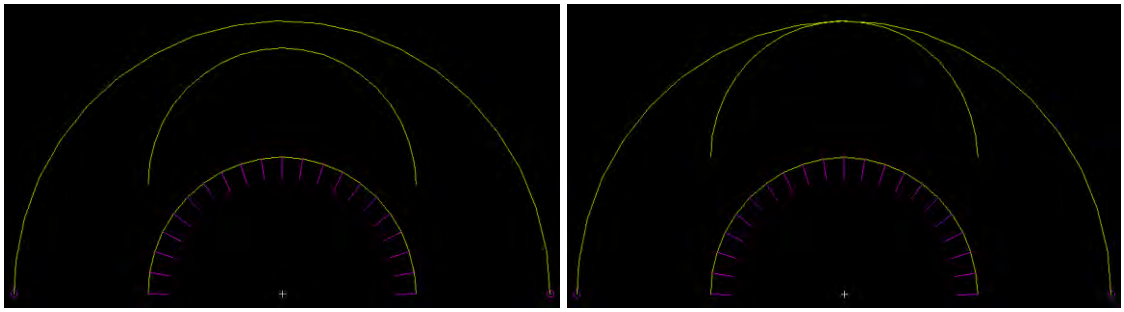

Figure 4.4: Advancement of rigid curve towards deformable curve

4.2. Preliminary Static Soft Tissue Prediction Results from MSC.AFEA

Experiments were carried out based on facial geometrical models derived from preoperative computer tomography data. Appropriate boundary conditions were assigned to selected regions to ensure the success of finite element analysis which then produced visually graphical display results. The combination of "Displacement, Translation" fringe and deformation results was selected to view the predicted postoperative facial appearance. Fringe is defined as contour plot where a range of color bands each representing a range of result values plotted onto a finite element model. A fringe result is chosen to generate a color-coded plot of the value for the results produced by the previously completed analysis. There are a number of results types available for display in that each of the results produces different graphical presentation thus gives different meaning. Among other results apart from "Displacement, Translations" are "Force, Nodal Reaction", "Strain, Total" and "Stress, Global System". Results were produced in terms of time steps for which each increment of the time within a defined range produces slight deformation in an incremental order. The best time step is chosen for the most harmony and aesthetic appearance generated by MSC.AFEA. **Figure 4.5** shows the predicted postoperative results for a number of time steps.

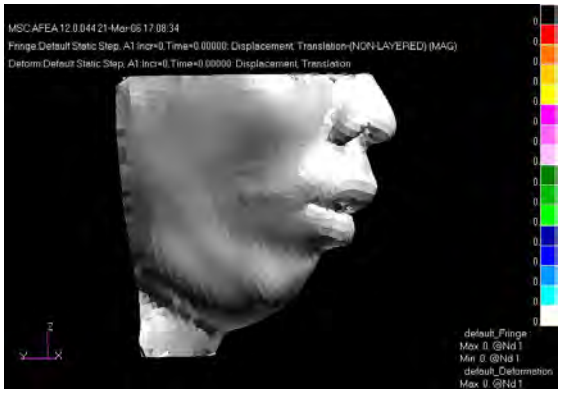
MSC.AFEA 12.0.044 21-Mar-06 17:08:34
Fringe:Default Static Step, A1:Incr=0,Time=0.00000: Displacement, Translation-(NON-LAYERED) (MAG)
Deform:Default Static Step, A1:Incr=0,Time=0.00000: Displacement, Translation
default_Fringe :
Max 0. @Nd 1
Min 0. @Nd 1
default_Deformation :
Max 0. @Nd 1

(a)

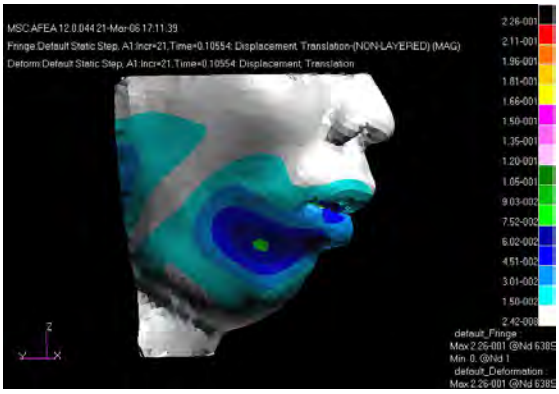
MSC.AFEA 12.0.044 21-Mar-06 17:11:39
Fringe:Default Static Step, A1:Incr=21,Time=0.10554: Displacement, Translation-(NON-LAYERED) (MAG)
Deform:Default Static Step, A1:Incr=21,Time=0.10554: Displacement, Translation
default_Fringe :
Max 2.26-001 @Nd 6385
Min 0. @Nd 1
default_Deformation :
Max 2.26-001 @Nd 6385

(b)

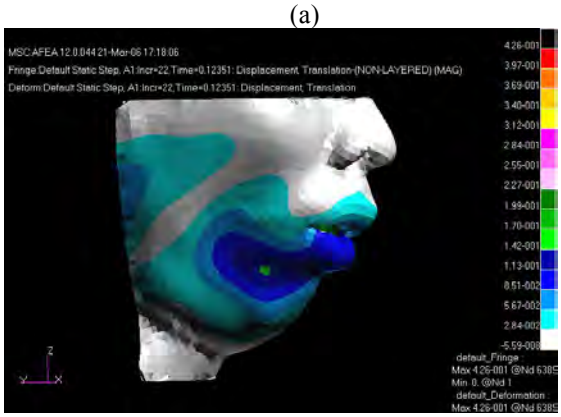
MSC.AFEA 12.0.044 21-Mar-06 17:18:06
Fringe:Default Static Step, A1:Incr=22,Time=0.12351: Displacement, Translation-(NON-LAYERED) (MAG)
Deform:Default Static Step, A1:Incr=22,Time=0.12351: Displacement, Translation
default_Fringe :
Max 4.26-001 @Nd 6385
Min 0. @Nd 1
default_Deformation :
Max 4.26-001 @Nd 6385

(c)

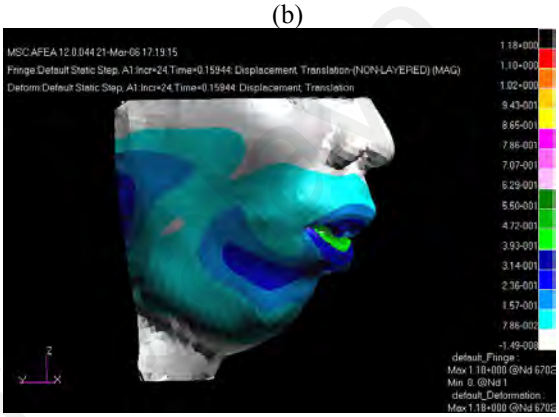
MSC.AFEA 12.0.044 21-Mar-06 17:19:15
Fringe:Default Static Step, A1:Incr=24,Time=0.15944: Displacement, Translation-(NON-LAYERED) (MAG)
Deform:Default Static Step, A1:Incr=24,Time=0.15944: Displacement, Translation
default_Fringe :
Max 1.18+000 @Nd 6705
Min 0. @Nd 1
default_Deformation :
Max 1.18+000 @Nd 6705

(d)

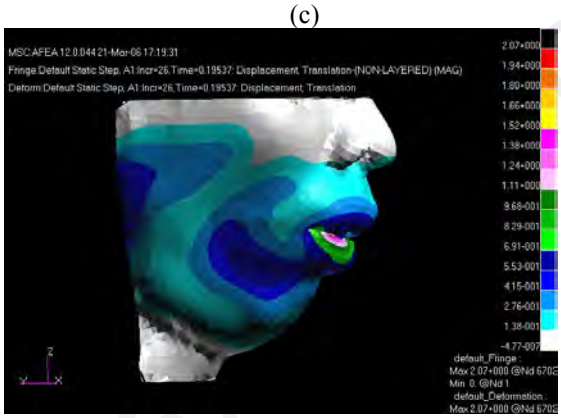
MSC.AFEA 12.0.044 21-Mar-06 17:19:31
Fringe:Default Static Step, A1:Incr=26,Time=0.19537: Displacement, Translation-(NON-LAYERED) (MAG)
Deform:Default Static Step, A1:Incr=26,Time=0.19537: Displacement, Translation
default_Fringe :
Max 2.07+000 @Nd 6702
Min 0. @Nd 1
default_Deformation :
Max 2.07+000 @Nd 6702

(e)

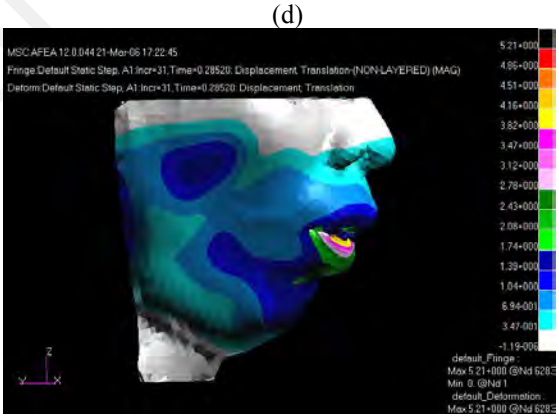
MSC.AFEA 12.0.044 21-Mar-06 17:22:45
Fringe:Default Static Step, A1:Incr=31,Time=0.28520: Displacement, Translation-(NON-LAYERED) (MAG)
Deform:Default Static Step, A1:Incr=31,Time=0.28520: Displacement, Translation
default_Fringe :
Max 5.21+000 @Nd 6285
Min 0. @Nd 1
default_Deformation :
Max 5.21+000 @Nd 6285

(f)

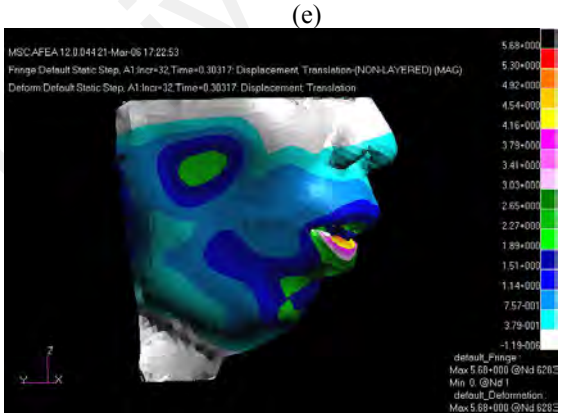
MSC.AFEA 12.0.044 21-Mar-06 17:22:53
Fringe:Default Static Step, A1:Incr=32,Time=0.30317: Displacement, Translation-(NON-LAYERED) (MAG)
Deform:Default Static Step, A1:Incr=32,Time=0.30317: Displacement, Translation
default_Fringe :
Max 5.68+000 @Nd 6283
Min 0. @Nd 1
default_Deformation :
Max 5.68+000 @Nd 6283

(g)

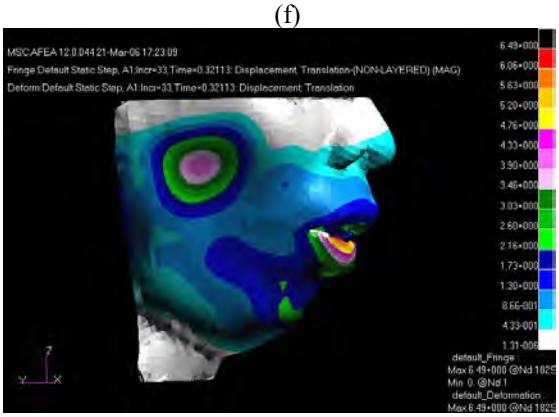
MSC.AFEA 12.0.044 21-Mar-06 17:23:09
Fringe:Default Static Step, A1:Incr=33,Time=0.32113: Displacement, Translation-(NON-LAYERED) (MAG)
Deform:Default Static Step, A1:Incr=33,Time=0.32113: Displacement, Translation
default_Fringe :
Max 6.49+000 @Nd 1825
Min 0. @Nd 1
default_Deformation :
Max 6.49+000 @Nd 1825

(h)

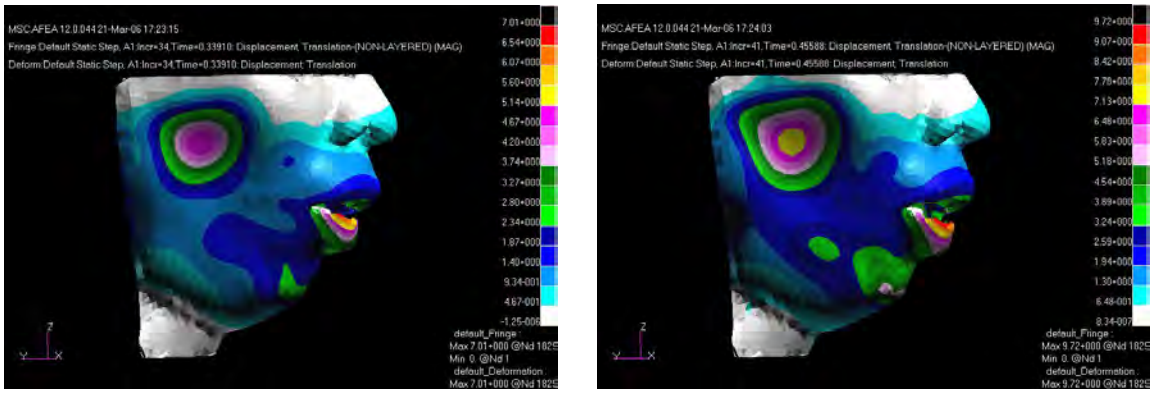

(i) (j)

Figure 4.5: Simulation of postoperative appearance in MSC.AFEA with increment of time (a): 0 at undeformed state, (b): 21, (c): 22, (d): 24, (e): 26, (f): 31, (g): 32, (h): 33, (i): 34, (j): 41

The various colors on the facial skin in **Figure 4.5** and **4.6** determine the stress distribution calculated throughout the simulation. Hot colors such as red, orange and yellow represent higher value stresses while cold colors such as blue, green and pink represent lower value stresses. A closer view of **Figure 4.5** is presented in **Figure 4.6**.

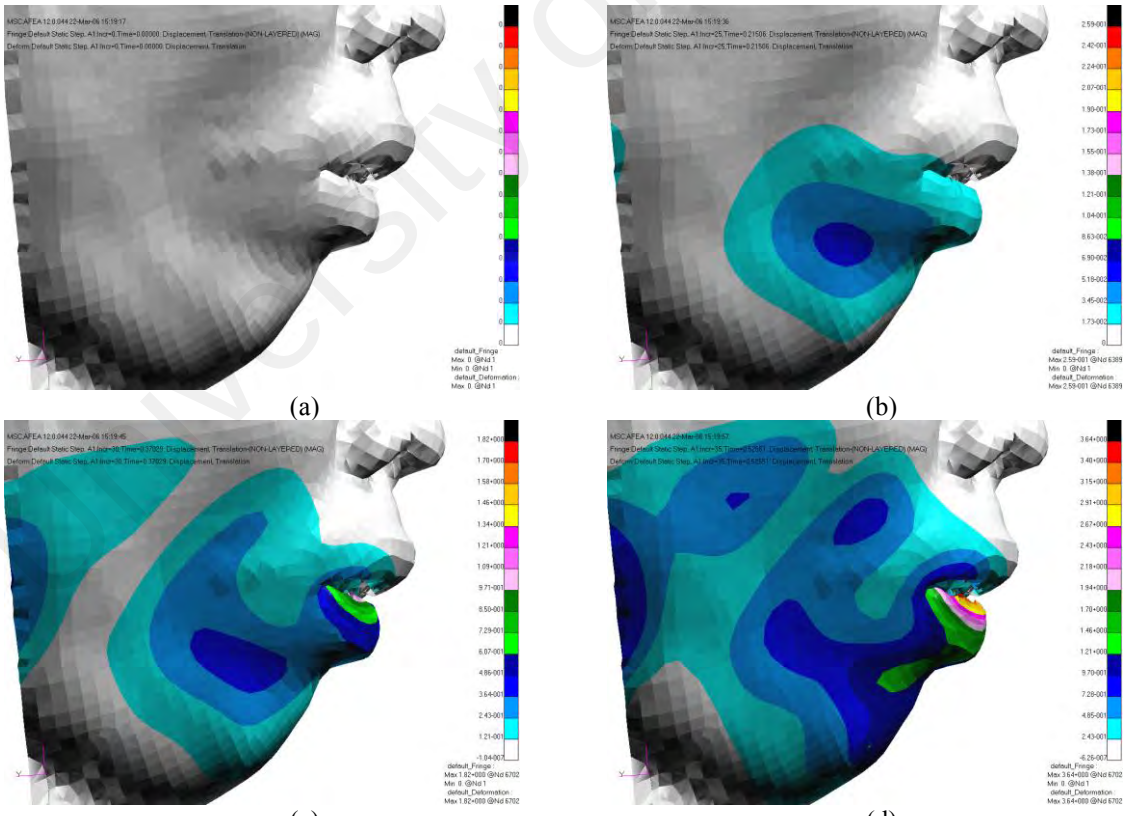

(a) (b)

(c) (d)

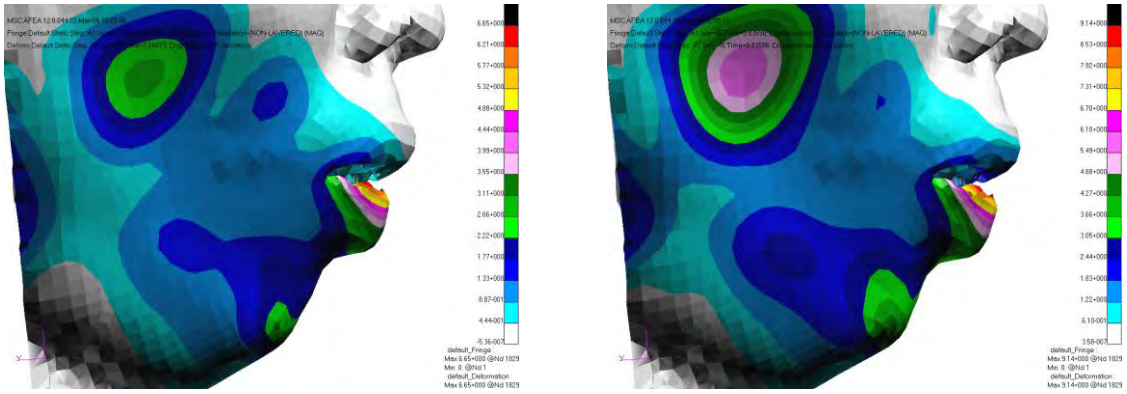

(e) (f)

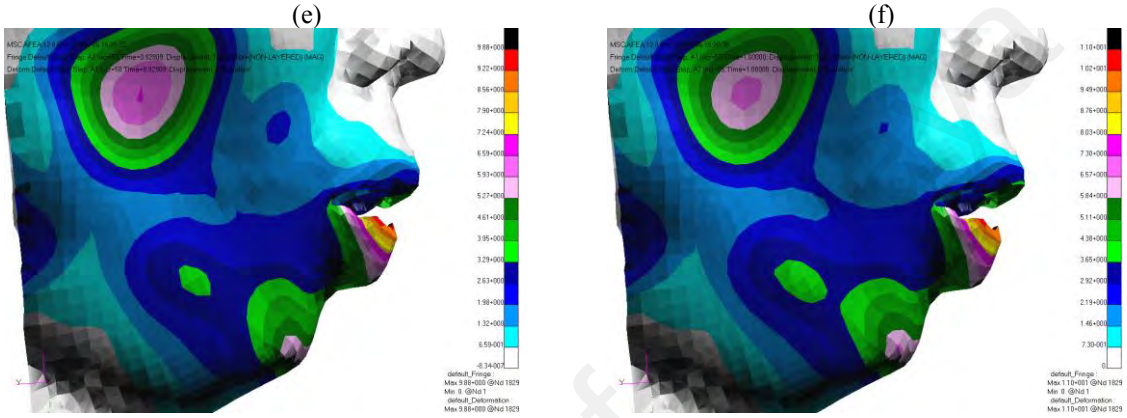

(g) (h)

Figure 4.6: Upclose view of the soft tissue prediction at increment of time (a): 0 at undeformed state, (b): 25, (c): 30, (d): 35, (e): 40, (f): 45, (g): 50, (h): 55

Figure 4.7 and **Figure 4.8** illustrate the general simulation of soft tissue prediction by using the wireframe option. The difference of undeformed and deformed state is observed between the images.

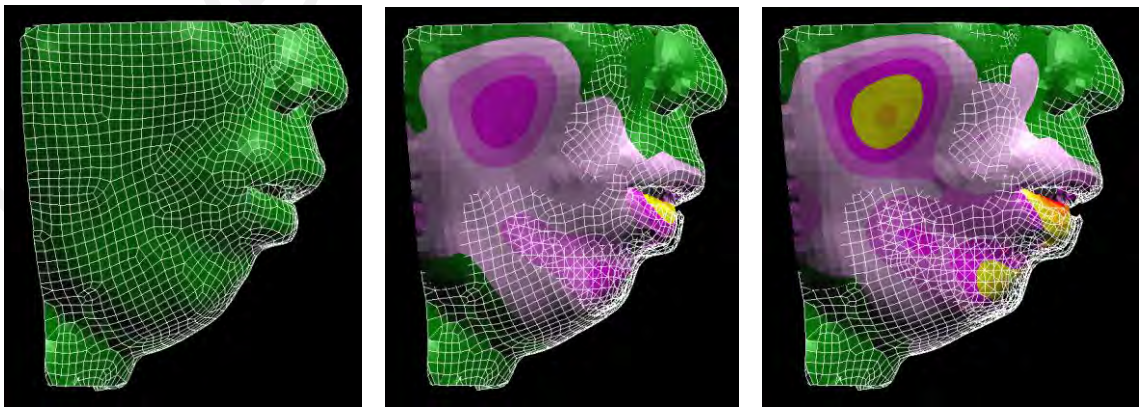

(a) (b) (c)

Figure 4.7: Differences of the undeformed and deformed soft tissue during simulation can be seen in a)undeformed skin, b)skin during simulation and c)deformed skin

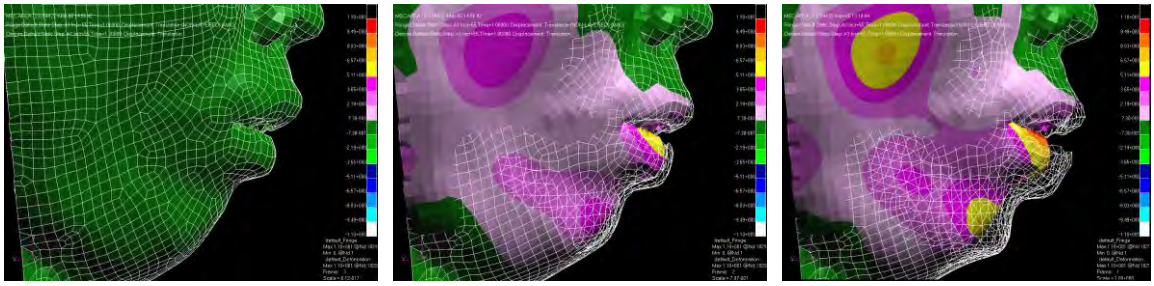

(a) (b) (c)

Figure 4.8: Closer inspection on variation for the (a): undeformed, (b) simulated and (c): deformed soft tissue

4.3. Static Soft Tissue Prediction from Amira

Due to the reason of enhanced visual display and simulation, Amira (Mercury Computer Systems 1999), a commercial visualization software is used. The experimental results of the soft tissue prediction within the orthognathic facial surgery planning from section 3.5.2: *Definition of osteotomies* is presented. Since postoperative computer tomography is not available, much focus relies on the qualitative validation of the simulated outcome. For this reason, the orthognathic surgeons are consulted.

In the given case, the patient suffered from *bimaxilliary protrusion*, *long face* and *left lateral scissor bite*, a condition where the upper jaw and lower jaw were not aligned to each other as illustrated in **Figure 4.9**. The actual postoperative pictures in **Figure 4.10** were taken 4 years after surgery. Surgical planning including the soft tissue prediction was simulated. This suggestion is innovative to minimize error and chances of nerve and other vital structure damage during the actual surgery. The correcting surgical impact for the patient consists of *right body of mandible osteotomy* and *left unilateral sagittal split*. **Figure 4.11** shows the predicted postoperative appearance of the patient based on finite element analysis simulation initially executed on MSC.AFEA.

(a) (b)

Figure 4.9: (a): Frontal view and (b): Side view of the patient specific preoperative picture

Figure 4.10: Postoperative picture

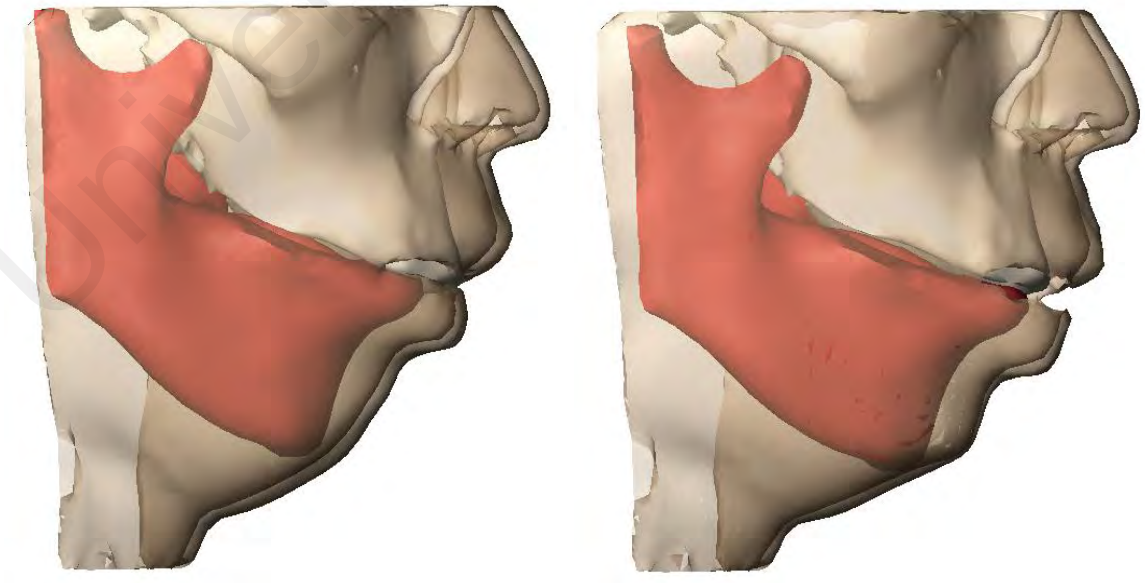

(a) (b)

Figure 4.11: Simulated prediction of postoperative appearance in (b) based on available preoperative data in (a)

In **Figure 4.12(a)** the simulated postoperative is superimposed on the actual preoperative facial appearance. The realigned mandible superposed on the actual mandible before surgery is illustrated in **Figure 4.12(b)**.

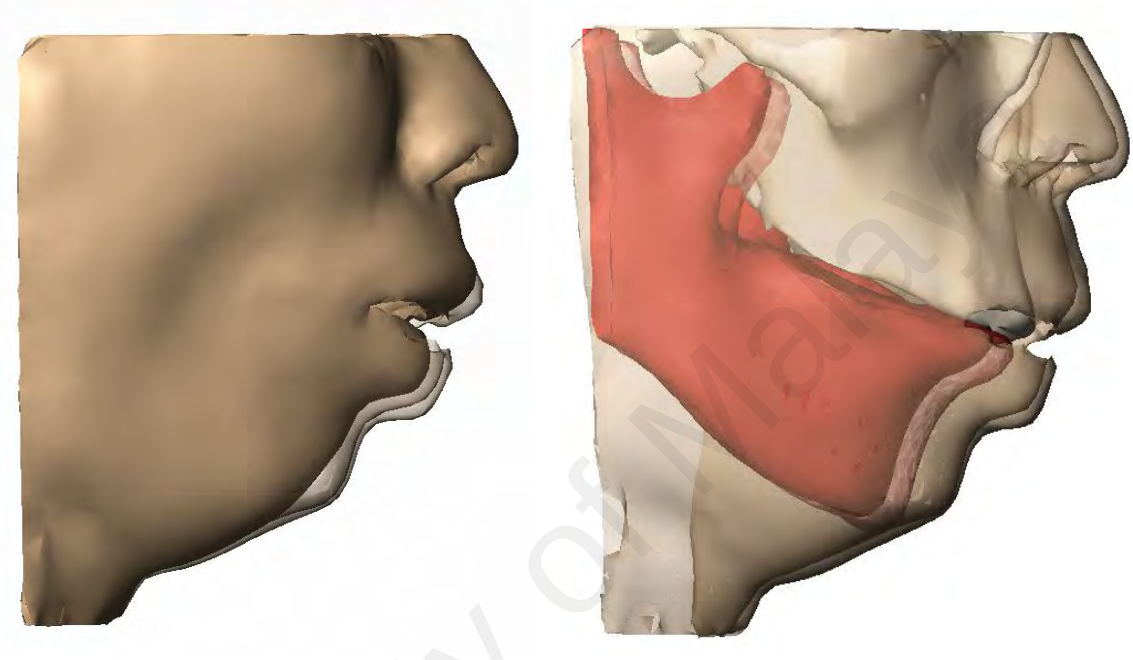

(a) (b)

Figure 4.12: Postoperative results overlaid on (a): Actual facial tissue and (b): Actual mandible of the simulated surgery

In the following **Figure 4.13** and **4.14**, the frontal view and side view of the entire simulation results is shown for time step at which there appears shape changes to the facial skin. As regards to improvement in the postoperative appearance, variation in the facial area is perceivable. These variations are achieved through various parameters such as the stress, strain, deformation and displacement in which each parameter relates to one another to give the predicted postoperative facial outlook. For instance, the facial deforms accordingly as the stress on certain area of the face increases. Thus, this gives differences in the changes of the skin at every increment of time as seen in **Figure 4.13** and **4.14**.

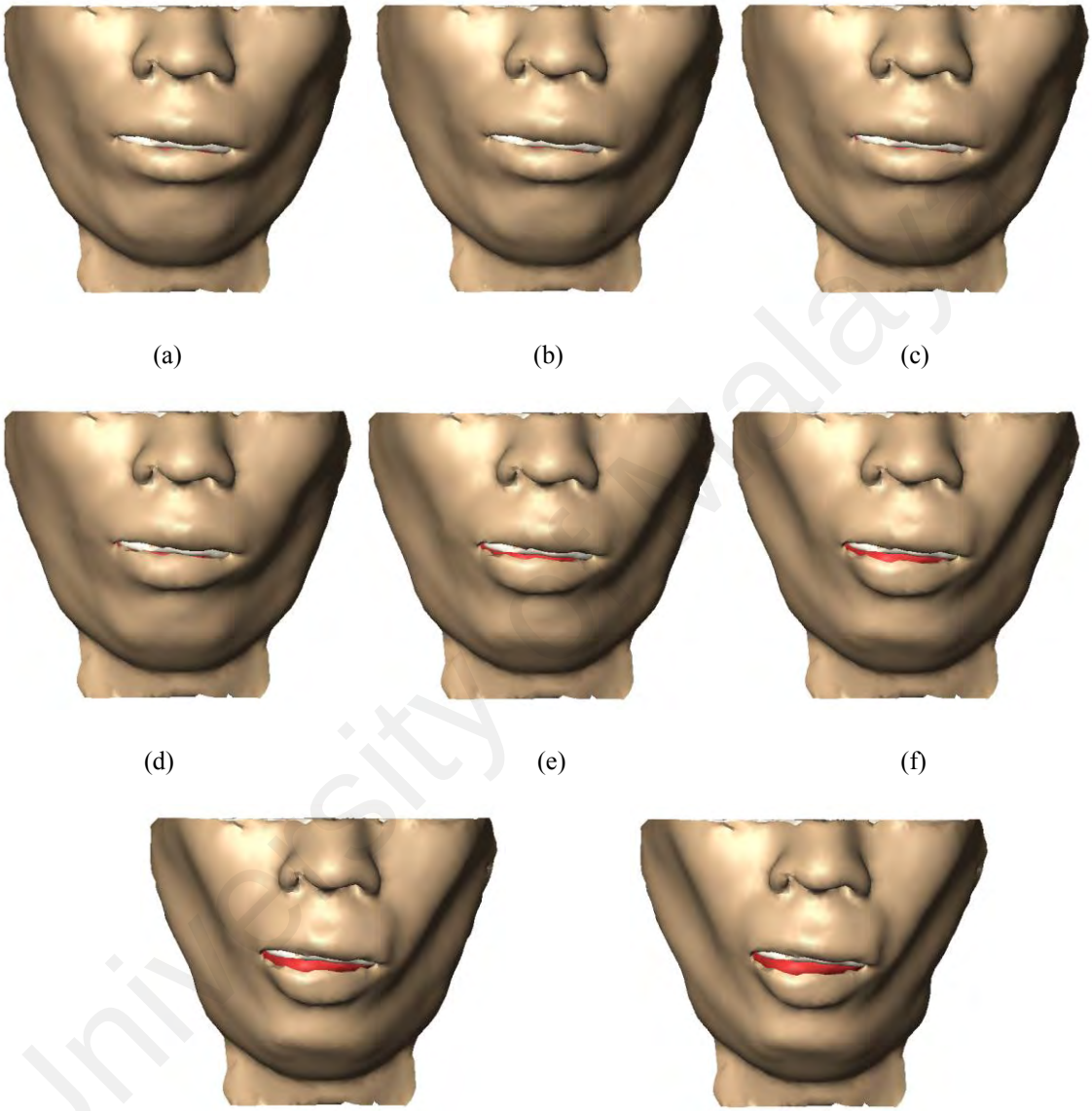

Figure 4.13: Front view of the entire simulated facial appearance for increment of time: (a): 0 for the actual appearance, (b): 25, (c): 30, (d): 35, (e): 40, (f): 45, (g): 50, (h): 55

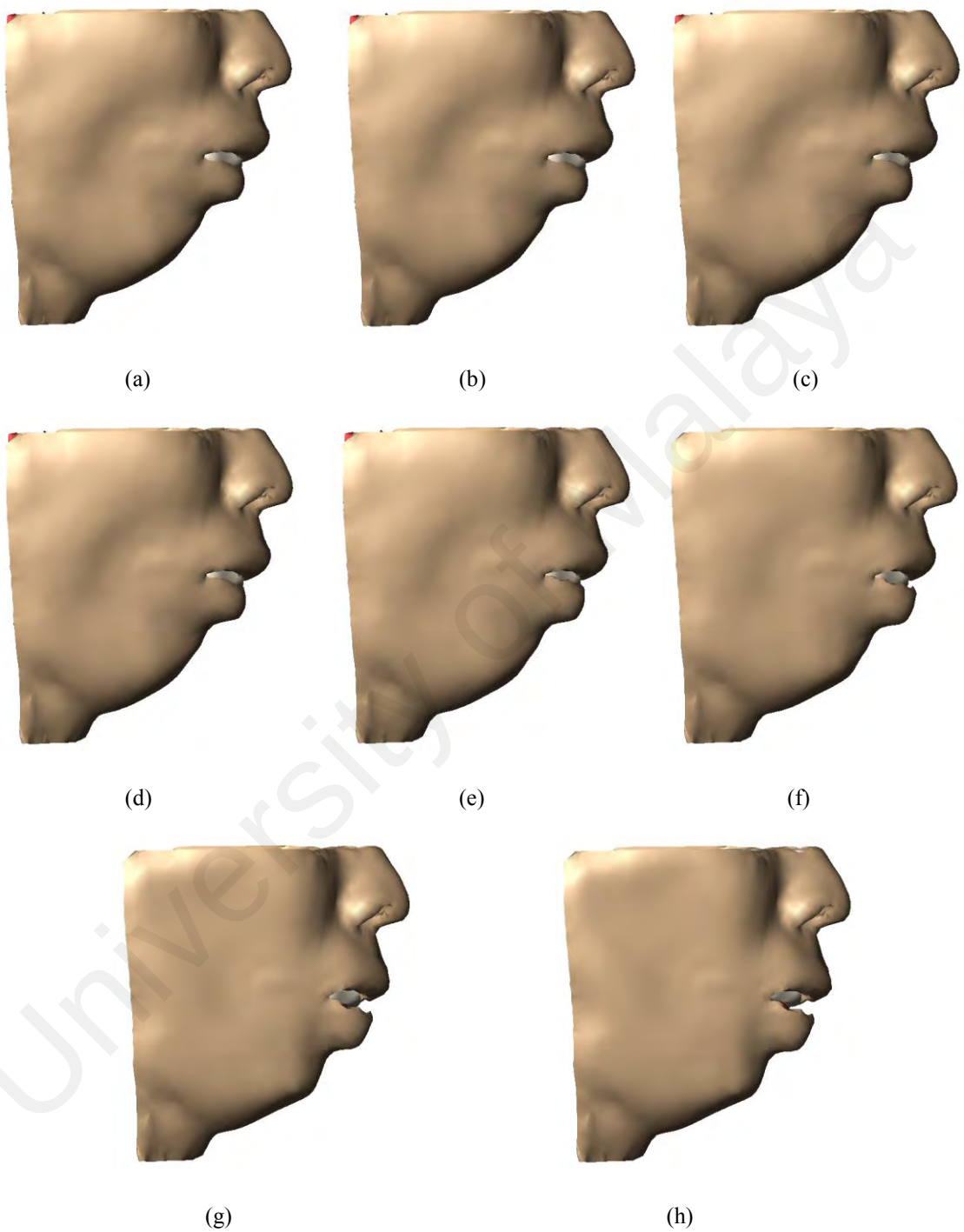

Figure 4.14: Side view of the entire simulated facial appearance for increment of time: (a): 0 for the actual appearance, (b): 25, (c): 30, (d): 35, (e): 40, (f): 45, (g): 50, (h): 55

5
DISCUSSION

This chapter evaluates the prediction capabilities for the simulated post surgical appearance. Evaluation is made with the actual image of the patient. The results are first presented before discussion on the numerical error measurement follows. Explanation continues with sources of errors during the surgery simulation which reveals the assumption and limitation throughout the research for this work.

5.1. Evaluation and Validation

In the view of validating the prototype in the context of orthognathic surgery simulation, the predicted post surgical appearance is compared with an actual picture of the example patient. The actual post operative photo image is used as the best measure of comparison because post operative computer tomography scan is against the medical ethics in this country. **Figure 5.1(a)** and **Figure 5.1(c)** shows the preoperative and postoperative picture of the patient respectively taken in 2001 and 2006.

5.1.1. Prediction Results

At the moment, the orthognathic surgery simulation within this work had been performed on one real patient case due to the reason that CT data was available only for one case throughout the research. In addition, the conducted work relying on elementary findings is carried out with intention as groundwork for further research. Therefore, accuracy is left for future work. The aim of this work focuses more on the practice and capability of engineering based software package to accommodate the need for predicting postoperative appearance of an orthognathic surgery by simulation accomplished through finite element analysis. In addition to the predicted postoperative result, **Figure 5.1** illustrates the pre- and post-operative picture of the patient.

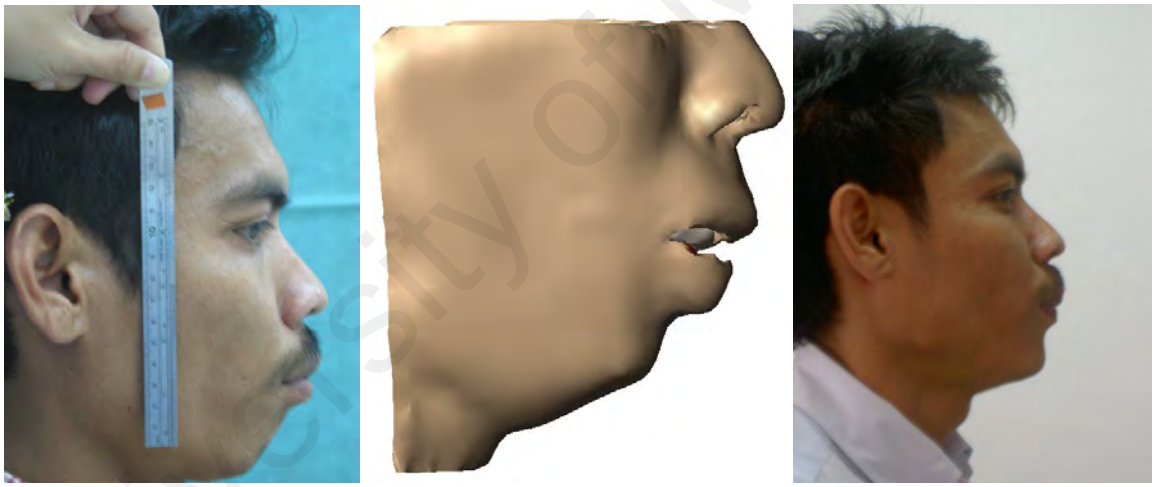

(a) (b) (c)

Figure 5.1: The (a): preoperative picture, (b): predicted results and (c): postoperative picture

5.1.2. Comparison

A graphical comparison is presented to obtain a visual impression regarding the exactness and quality of the predicted simulation to the actual postoperative picture. Due to the reason that the postoperative CT data is unavailable, the qualitative validation for this work is done by means of comparison of simulated results to the postoperative photograph of the same patient. A validation made with postoperative CT data would produce more accurate

evaluation as mapping on both simulated and actual findings gives persist differences between the two results. On the other hand, an evaluation of simulated results with the postoperative photograph prediction reduces the exactness of the simulated prediction as distances measurements are vague. However, this approach is acceptable.

As presented in **Figure 5.2**, the harmonizing of post surgical picture and the result of the simulation needed for qualitative evaluation is still far from precision and prone to errors. Better measurement could be achieved by comparison of actual post surgical CT data.

(a) (b)

(c)

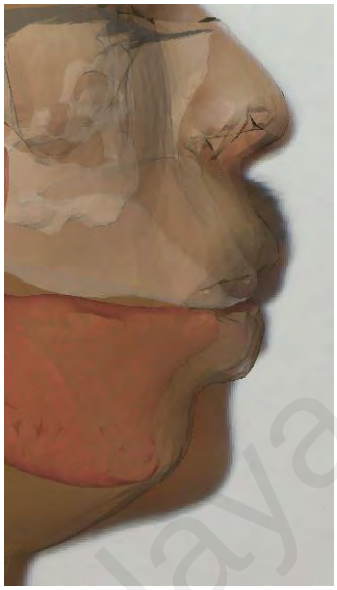

(d)

Figure 5.2: (a), (b), (c): Validation of predicted facial postoperative on actual postoperative picture with closer view in (d)

5.2. Error Measurements

In order to obtain numerical error measurement in between the actual simulated pre surgical data and simulated post surgical data, the two models had been superimposed with each other. The visualization of the error distribution on the surface facial models is presented in **Figure 5.3**.

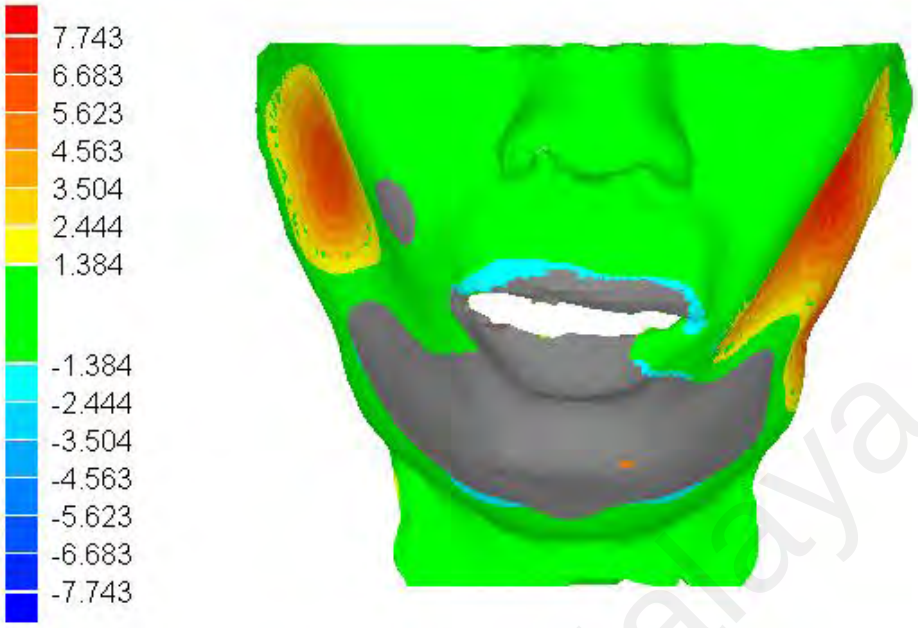

(a)

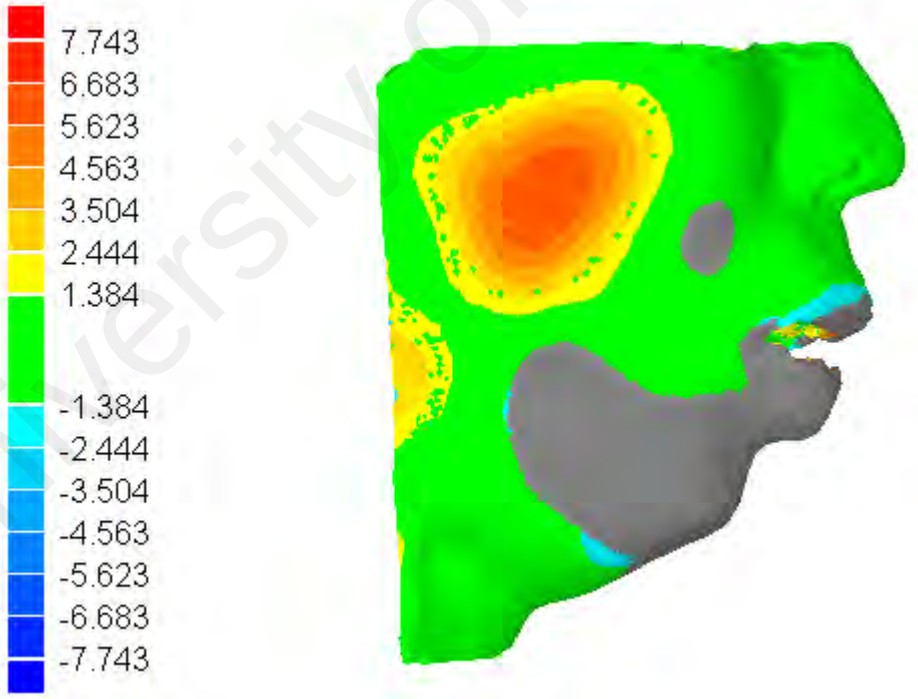

(b)

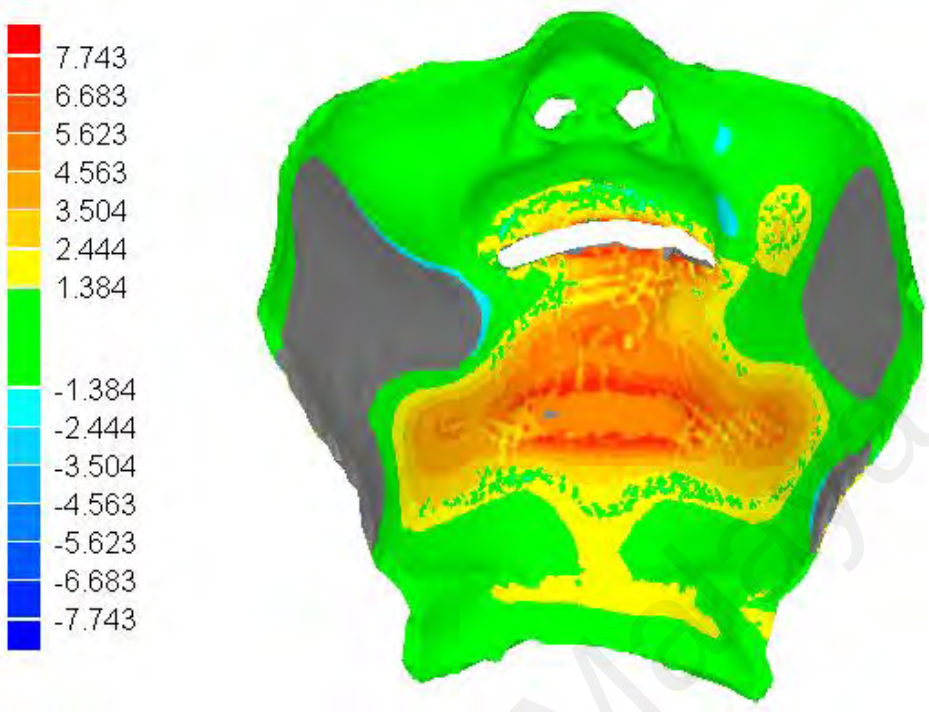

(c)

Figure 5.3: Error measurements between the simulated pre surgical and post surgical results for (a): front, (b): side and (c): top view

In reference to **Figure 5.4**, the highest deviation point on the post surgical soft tissue resides in the inner side around the chin facial skin. This supports the reason that movement of the mandible affects most within the chin area of the underlying skin surface. The statistical error measurement is listed in **Table 5.1**. The maximum distance value provides a quantitative evaluation on the differences of the pre- and post-surgical results. The value of 7.743mm shows that there is of 7.7mm distance difference in between the two results. The average distance finds the average of the distance between two distances calculated from pre- and post-surgical results. It is analyzed that the average distance value is 1.384mm. The standard deviation gives the quantitative evaluation values with a small numerical deviation value in terms of plus and minus for acceptable statistical findings. Based on the calculation, the standard deviation value is rounded to 1.6mm. The maximum and minimum parameters for positive and negative values represent the tolerance level for the quantitative results achieved by differences of the pre- and post-surgical results.

Table 5.1: Error measurement statistics

Statistics	Values
Maximum distance	7.743mm
Average distance	1.384mm
Standard deviation	1.597mm
Maximum positive	7.743mm
Minimum positive	1.384mm
Minimum negative	-1.384mm
Maximum negative	-7.743mm

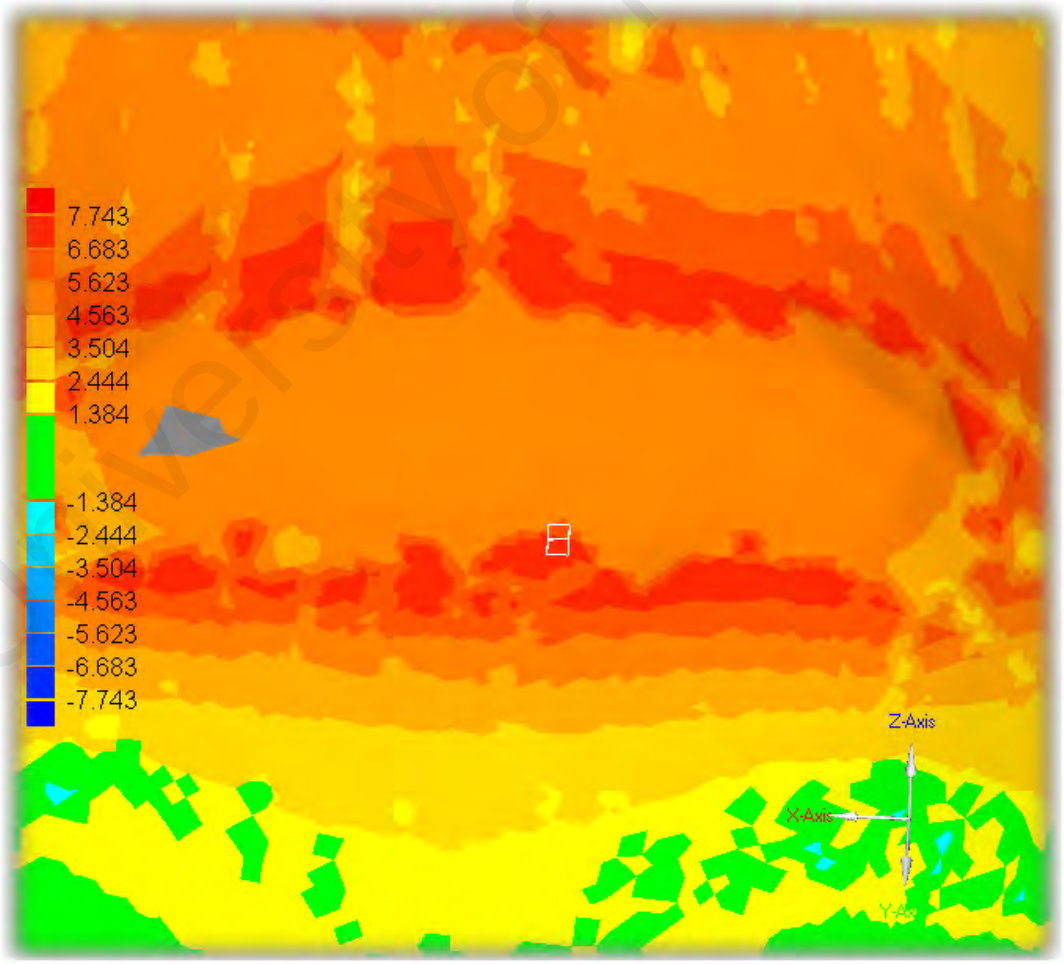

Figure 5.4: Red region on the inner chin area of the facial skin shows highest deviation point

5.3. Sources of Error

A number of assumptions engaged throughout the entire development process by reasons of limitations arising from data acquisition, data processing, simulation and evaluation. The sources of errors contributed to the inaccurate results are detailed in sequence during this work. In addition, a few possible suggestions to overcome the issues are discussed.

5.3.1. Data Acquisition

- The process of acquiring computer tomography data is one of the vital procedures which demands careful consideration. During scanning for the example case, the lower teeth and upper teeth of the patient were clenched, resulted to closed lips. Therefore, the generated 3D model around the teeth and lips region appeared connected to each other as seen in **Figure 3.5** and **Figure 3.7**. Thus introduces tedious process of separating the connecting teeth and lips. Hence, it is suggested that a patient keeps a gap in between the upper jaw and lower jaw during data acquisition.

- Quality of CT data is determined by factors emerging from noise produced by the CT scanner as well as during data transformation of scanning process, patient positioning and movement, also *amalgam* filling inside the teeth. Each of these factors contributes to various defects. Noise arises for every data acquirement from the CT scanner. Although the noise factor interferes with the process of producing a good quality model, minimal noise is negligible. Distorted image resultant to patient movement can be reduced by faster scan times under condition of patient holding a

single breath during scanning. On the other hand, artifacts caused by metallic objects illustrated in **Figure 3.4** producing streaks attributable to scattered radiation of dental restoration were unavoidable. However, this defect was resolved by recreating meshes during model improvement explained in section 3.4: *Model Improvement*.

5.3.2. Facial Model

- Due to the reason of simplicity for numerical calculation within limit, only major tissues comprising of skin surface, mandible and maxilla were considered. The remaining materials for example water and air along with tissues such as fat, muscular anatomy, blood, nerves, arteries to name a few were absent as their presence would produce too densed elements. Nevertheless, better results are definite if these materials are incorporated.

- Shell facial models composed of element whose geometry is defined by a surface were employed instead of volumetric models to ensure success of the utilized techniques in addition to acceptable duration for a solution of an analysis. Simulating volumetric models were very time consuming and was prohibited by the current hardware resources due to massive number of discrete nodes and elements.

- The setup for rigid body for contact analysis does not accept triangular elements very well. For that reason quadrilateral elements were employed. The conversion of triangular elements to quadrilateral elements was aided by the “mesh on mesh” option available in MSC.AFEA.

- In reality every type of material deforms. Thus requiring the simulation of deformable-deformable contact analysis. Nevertheless, the rigid-deformable contact was employed, assuming bone as rigid while the skin as deformable. This is because in MSC.AFEA, movement of the mandible is not within the capability of deformable-deformable contact analysis.

- The skin varies between individuals and there lies differences of skin depending on the location on the body of an individual (Gibson et al. 1965). This means that the skin has neither single *Young's modulus* nor shear modulus throughout the different region (Cook 1989, 205-225). Nevertheless, a single value *Young's modulus* was used for the simulation of the predicted postoperative appearance.

- It had been detailed in section 2.4: *Biomechanics and soft tissue properties* that the characteristics of a soft tissue including skin in general are inelastic, *viscoelastic*, *hysteresis*, *creep*, *anisotropic* and nonlinear. An inelastic mathematical equation which close resembles the tissue is best applied. However, due to limited intellectual capacity in terms of comprehension of the optimum mathematical formulation for the representation biological tissue properties within the two years of research period, the linear elastic constitutive equation was used to define the material properties of the skin. The use of linear elastic models had been supported by a number of previously published researches in the biomechanics and soft tissue prediction field (Koch et al. 2000, Zachow et al. 2000, Gladilin et al. 2001a, Schmidt et al. 2004). A more suitable mathematical equation called *hyperelastic*

constitutive equation is available in MSC.AFEA. However, the main reason this equation was not used for the soft tissue simulation is because numerous constants obtainable from comprehensive laboratory experiments were needed. Thus requires more time for research.

- The constraints of the skin were assigned based on assumptions from several tests where the best possible outcome for a given constraint is selected. The actual facial skin deformation is restricted by the interaction of various *boundary conditions* such as muscles, nerve, fat, water and a few other tissues. Further study on muscles which causes movement or deformation of skin is essential to achieve better soft tissue prediction. Therefore, such studies are dedicated to future works.

5.3.3. Medical Sources

- Inconsistencies between the simulated surgery planning and actual surgery are unavoidable for practical reasons. The actual surgery as explained by surgeons involved during the surgery included two types of bone cuts on the mandible with three plates and screws used to reconnect the semi sliced bone. On the other hand, the simulated surgery minutes did not consider the different steps of the performed *osteotomy* and the addition of plates and screws on the realigned mandible. Instead, focus of this work relies more on the prediction of a postoperative facial appearance rather than replicating the actual surgical steps. The simulated surgery used the entire mandible to change the shape of the underlying skin based on a defined forward movement.

5.3.4. Human Factors

- The facial muscular activity between CT scans and photographs are unavoidable. The process of capturing data would produce errors such as distortion and noise. Several reasons which cause these errors are the head alignment, head motion and pulse.

- At the moment, the research project only one example case is considered. This is because no further suitable data was available from the data resource. It is hoped that in the future, more data will be made available for stimulating research.

5.3.5. Hardware Resources

- Completing a successful analysis on the current hardware specification of Intel Pentium 4 desktop with 2Gb RAM is very time consuming. The CPU time took considerable period due to expensive computation for the large number of nodes and elements comprised in the facial models. Simulation could be achieved at a shorter length of time if such analysis runs on SGI.

- In addition to faster computation on SGI, the facial models can be refined with global edge length value of 1.0, as shown in **Figure 3.25(e)**. This would produce a more reliable prediction results. The current mesh density value used for the finite element analysis is 4.0.

- Another approach which can be considered for faster numerical computation is through the use of distributed parallel computing where analysis solution is divided into a number of tasks computed by several processors housed in separate computers. This technique is approachable for the reason of lower price computing platform.

5.3.6. Evaluation

- The simulation result was matched with the postoperative photograph of the patient because postoperative CT data was unavailable due to medical ethics established by this country. Matching was carried out based on mapping between the two postoperative simulation results and postoperative actual photograph. Hence, the qualitative evaluation is prone to errors as no proper reference points were employed during validation. Thus, proper validation tool that deals with enhanced mapping using landmarks between the two results is left for future work.

- The quantitative evaluation is carried out to find the differences of the simulated and postoperative results. The validation is done by using color map, a range of various colors which defines the findings differences at areas on the skin facial appearance. Although this method is acceptable, the evaluation can be further improved by employing more meaningful parameters such as the point at which the facial region is most sensitive and should be given attention during the actual surgery.

- The research project was taken up 4 years after the actual orthognathic surgery had been performed. Therefore, the evaluation directed to inaccurate error measurements because there are tendencies whereby after healing, the mandible of the patient would revert to its normal condition before surgery, even though there are slight retrude changes to the mandible. This is an issue of comfort to the patient. Therefore, small changes called as standard deviation are acceptable. Hence, fully accurate results between the simulated and postoperative findings are impossible. Nevertheless, the small differences measurement between the findings is tolerable.

6

CONCLUSION

6.1. Conclusion

In this dissertation, we have introduced a prototype system that is capable of performing mandibular advancement surgery planning, facial soft tissue simulation for the corrected appearance and comparison of the simulated results with the actual postoperative photographs. Prediction of the surface based facial model was performed by means of finite element method.

We developed a physics based facial system that incorporates features closely related to the real human facial anatomy. Firstly, the facial model consists of skull and facial skin are derived from CT data. The diverse tissue types are determined by threshold value assigned to the tomography data during segmentation. Subsequently, surface based model are constructed from these data slices. Relying on these models, cuts and bone repositions on the mandible, in line with clinical procedures are involved in the initial step of the surgery planning.

The surface based models comprised of triangular meshes are then converted to quadrilateral meshes and further characterized with displacements of the facial skin and properties describing the soft tissue behavior such as elasticity, stiffness, thickness and density. The simplified tissue model of our work is based on *isotropic*, *homogeneous* and

linear elastic approximation of tissue mechanics portrayed by two elastic constants called *Young's modulus*, *E* and *Poisson's ratio*, *v*. The contact bodies analysis approach is a significant contribution of this work. The skin layer is deformed or changed in terms of shape by the movement of the underlying mandible where such motion is numerically calculated by the finite element method of the MSC.AFEA software program. Error minimization is automatically reduced by the respective solver, MSC.Marc.

The development of simulation for the facial model had been experimentally compared with the FEM theory and validated with artificial objects. Simulated results are finally measured up with the actual patient's postoperative photograph. In addition, the facial soft tissue prediction had been evaluated by the collaborating craniofacial surgeons.

6.2. Future Directions

The facial surgery prediction problem can be divided into a number of tasks which can be individually solved. For every task, several solution alternatives are evaluated and the best method has to be chosen to achieve a robust and reliable surgery planning and soft tissue prediction system. We propose a few alternatives to the current approach that could improve the performance of our system.

Our surface based models used for simulation could be improved by introducing tetrahedral elements. In the current approach, our experiments proved that the MSC.AFEA finite element software was not able to simulate volumetric modeling due to insufficient hardware resources. This is because simulation was carried out on a typical personal

computer. Therefore, incorporation of powerful computing resources such as SGI, supercomputer or grid computing would produce solutions at a more accurate and reduced time. Models with finer mesh are also possibly performed with better computing resources.

The most noticeable disadvantage of this work is seen in the inaccurate postoperative simulation results. The reason is dependent on the allocated material properties parameters which describes the soft tissue behavior and the robustness of linear elastic FEM. Hence, further studies and laboratory work is mandatory to define more detailed constitutive models to suit the need of real tissue characteristics. In addition, displacement parameters assigned to our facial model is a subject to improvement if a concise study on the facial function is understood.

We have discovered that simulating facial soft tissue by means of the movement of underlying bone through the contact analysis is possible with MSC.AFEA. However, by expanding soft tissue information such as the muscular anatomy in the future work, one step system improvement on dynamic facial expression simulation is guaranteed.

Furthermore, the growing research in the area of haptic devices could incorporate this work that could assist surgeons during surgery planning. This is realized by giving measurement of best location to cut a bone when one part is pointed to the bone with another supporting device. This suggestion is innovative to minimize error and chances of dead nerves, cells or neurology damage during surgery as offline planning and simulation is impossible to show such impairment. Thus, for obvious reasons, the use of haptic device is potential to simplify and improve interaction between surgeons and virtual patient during surgery planning.

Sophisticated biological computer modeling for FEM is still in its infancy in biological research partly due to the great complexity of biological organs although researches nationwide are active discovering new techniques to achieve a perfect surgery planning and simulation systems, due to endless obstacle phenomena of the human anatomy for example defining soft tissue properties in differences in gender ethnicity and age among other numerous possibilities; a broad range of research collaboration is of major requirement.

The success of future surgery planning applications embedded on dedicated workstations relies profoundly on interdisciplinary open-mindedness. Results of a victorious application is served by the integration of a variety scientific researches from computational vision, 3D geometric modeling, knowledge engineering, computer–assisted decision making, 3D graphics display, intelligent human-computer interaction, natural language processing, communication systems, computer architecture and of course image processing and related clinical disciplines. Otherwise, the long term challenge of collaborating diversity requirements and methodology into a functional system which has to benefit the patient can hardly be met.

APPENDICES

I. Schematic Solution Procedure

Diagrams below show the schematic solution procedure undertaken by MSC.Marc solver to solve a problem submitted for analysis. (MSC.Software 2003)

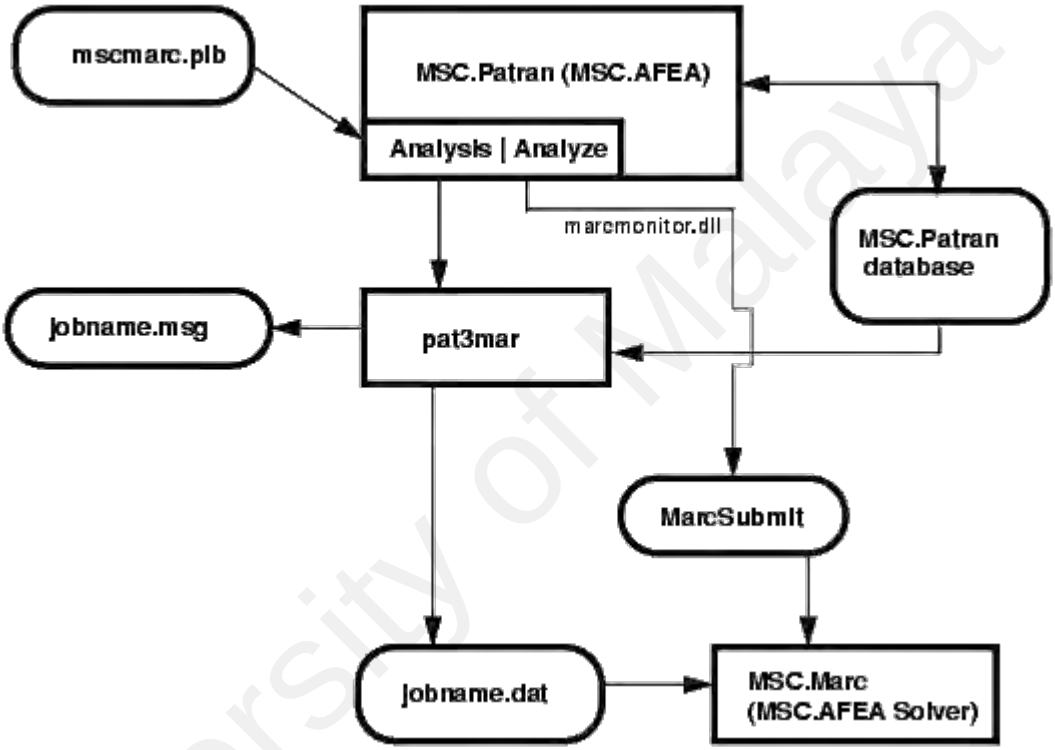

Figure I-1: Forward translation and analysis execution diagram (MSC.Software 2003)

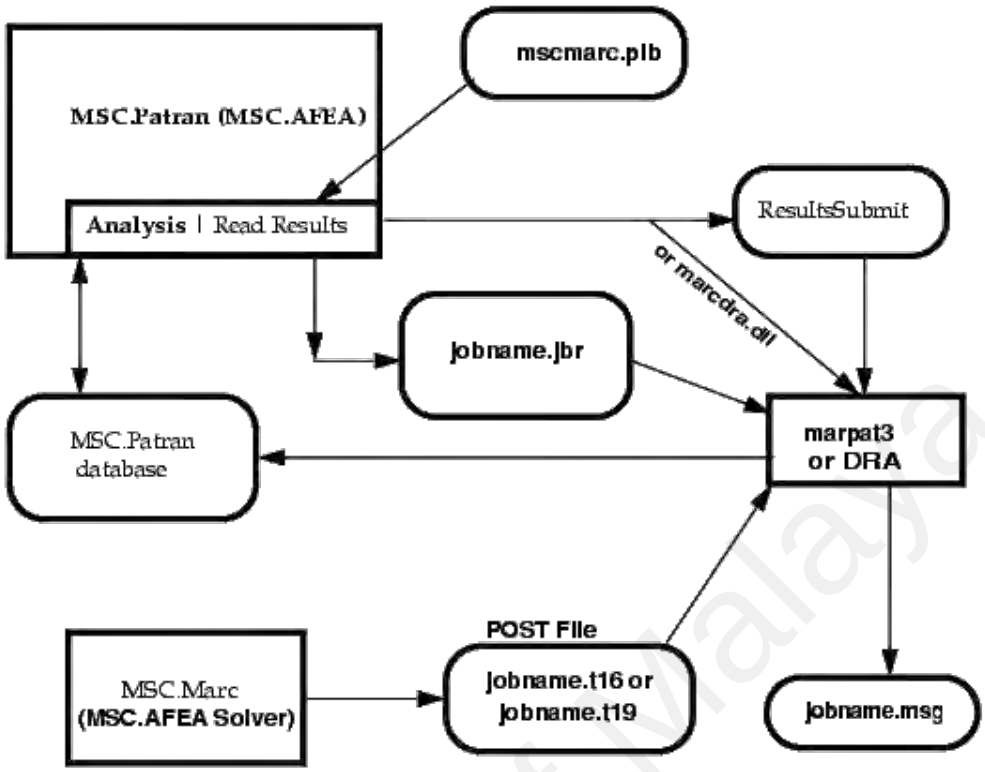

Figure I-2: Results translation diagram (MSC.Software 2003)

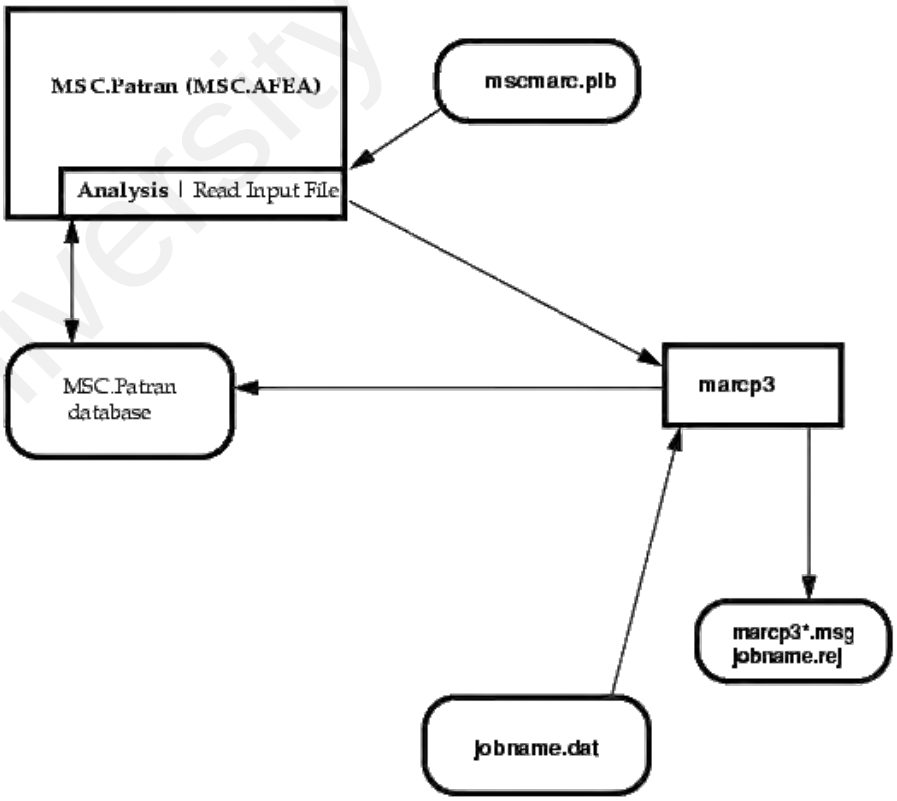

Figure I-3: Input file translation diagram (MSC.Software 2003)

II. MSC.AFEA Results Files

Figure II-1a: Output file showing contact information

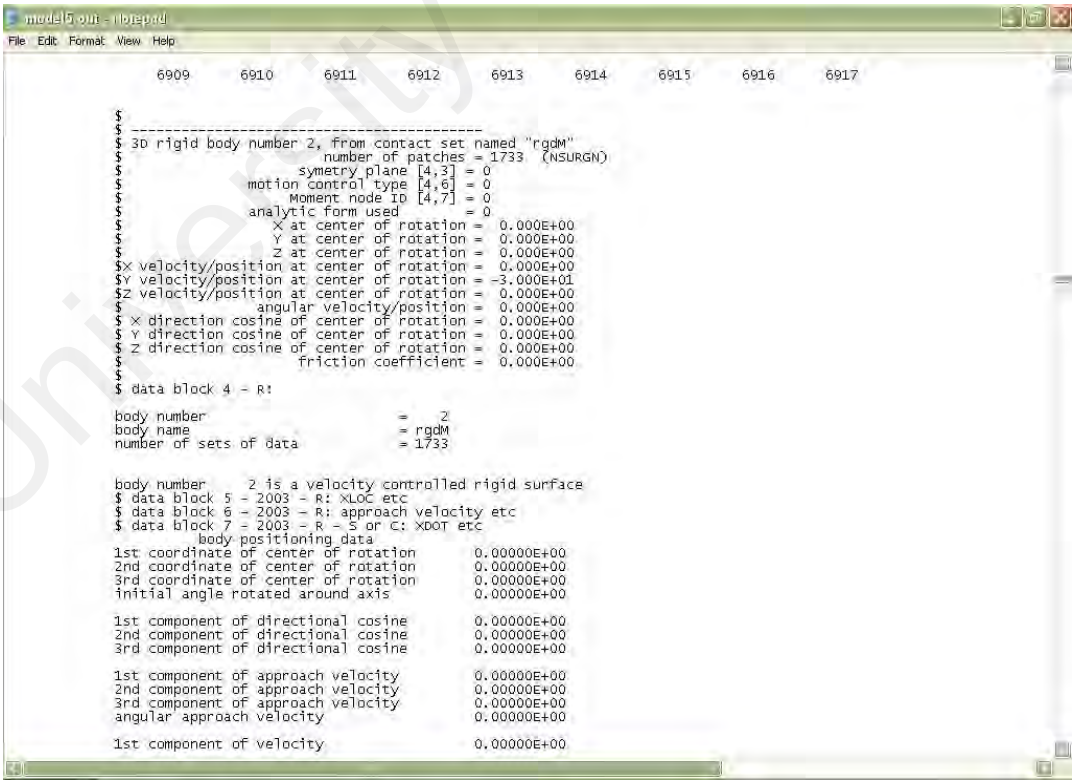

Figure II-1b: Output file showing contact information

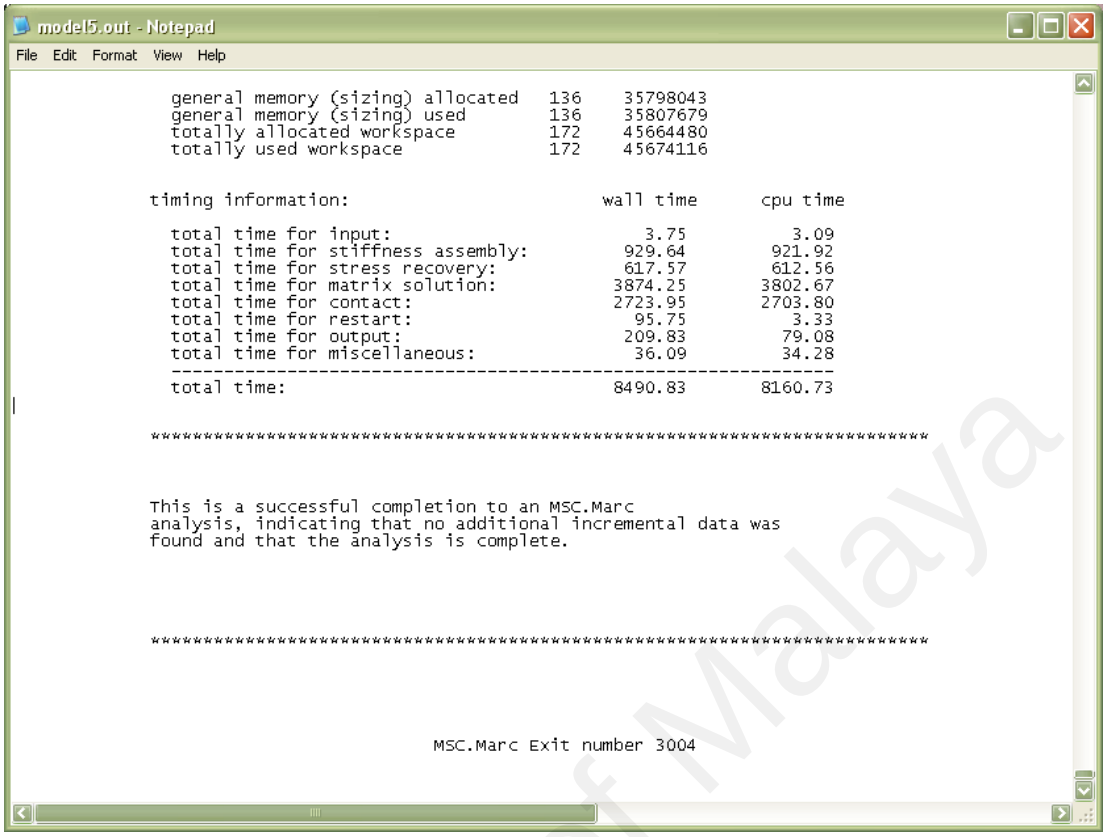

model5.out - Notepad

File Edit Format View Help

```
  general memory (sizing) allocated   136    35798043
  general memory (sizing) used        136    35807679
  totally allocated workspace         172    45664480
  totally used workspace              172    45674116


timing information:                          wall time      cpu time

  total time for input:                          3.75          3.09
  total time for stiffness assembly:           929.64        921.92
  total time for stress recovery:              617.57        612.56
  total time for matrix solution:             3874.25       3802.67
  total time for contact:                     2723.95       2703.80
  total time for restart:                       95.75          3.33
  total time for output:                       209.83         79.08
  total time for miscellaneous:                 36.09         34.28
  ------------------------------------------------------------------
  total time:                                 8490.83       8160.73

*****************************************************************************


This is a successful completion to an MSC.Marc
analysis, indicating that no additional incremental data was
found and that the analysis is complete.



*****************************************************************************



                              MSC.Marc Exit number 3004
```

Figure II-2: Output file reports whether an analysis is success or unsuccessful

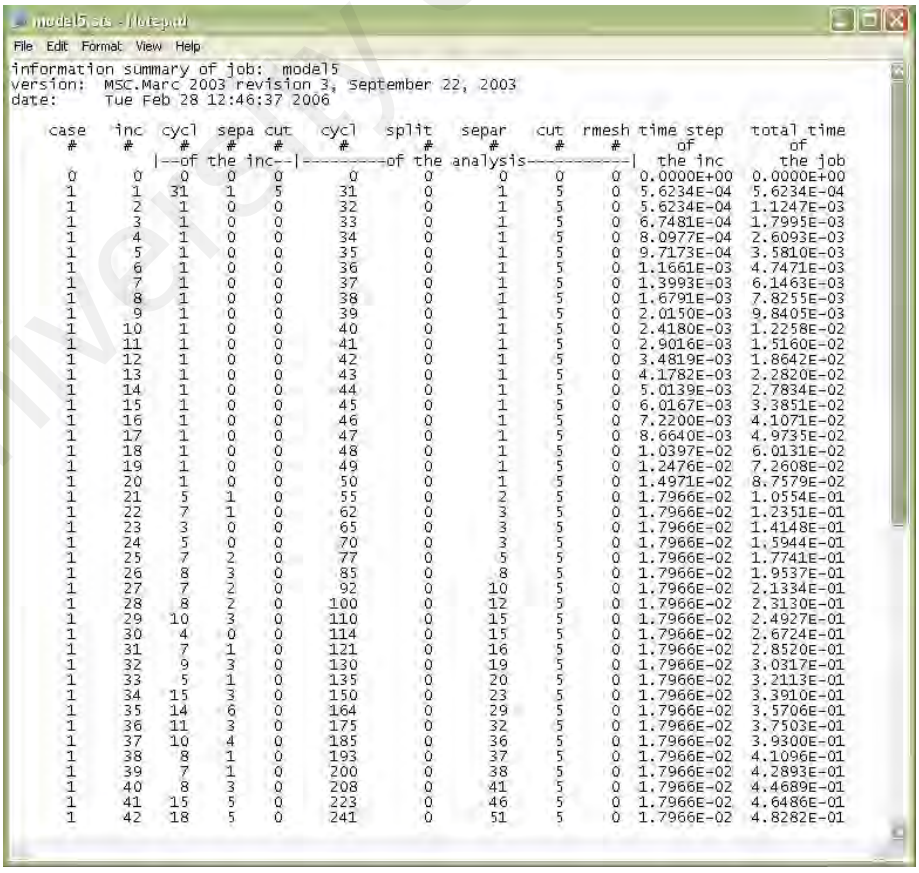

model5.sts - Notepad

File Edit Format View Help

```
information summary of job:  model5
version:  MSC.Marc 2003 revision 3, September 22, 2003
date:     Tue Feb 28 12:46:37 2006

    case    inc   cycl   sepa cut    cycl    split    separ    cut   rmesh time step    total time
      #      #      #      #   #       #        #        #      #      #      of           of
             |--of the inc--|---------of the analysis-----------|   the inc      the job
       0      0      0      0   0       0        0        0      0      0  0.0000E+00   0.0000E+00
       1      1     31      1   5      31        0        1      5      0  5.6234E-04   5.6234E-04
       1      2      1      0   0      32        0        1      5      0  5.6234E-04   1.1247E-03
       1      3      1      0   0      33        0        1      5      0  6.7481E-04   1.7995E-03
       1      4      1      0   0      34        0        1      5      0  8.0977E-04   2.6093E-03
       1      5      1      0   0      35        0        1      5      0  9.7173E-04   3.5810E-03
       1      6      1      0   0      36        0        1      5      0  1.1661E-03   4.7471E-03
       1      7      1      0   0      37        0        1      5      0  1.3993E-03   6.1463E-03
       1      8      1      0   0      38        0        1      5      0  1.6791E-03   7.8255E-03
       1      9      1      0   0      39        0        1      5      0  2.0150E-03   9.8405E-03
       1     10      1      0   0      40        0        1      5      0  2.4180E-03   1.2258E-02
       1     11      1      0   0      41        0        1      5      0  2.9016E-03   1.5160E-02
       1     12      1      0   0      42        0        1      5      0  3.4819E-03   1.8642E-02
       1     13      1      0   0      43        0        1      5      0  4.1782E-03   2.2820E-02
       1     14      1      0   0      44        0        1      5      0  5.0139E-03   2.7834E-02
       1     15      1      0   0      45        0        1      5      0  6.0167E-03   3.3851E-02
       1     16      1      0   0      46        0        1      5      0  7.2200E-03   4.1071E-02
       1     17      1      0   0      47        0        1      5      0  8.6640E-03   4.9735E-02
       1     18      1      0   0      48        0        1      5      0  1.0397E-02   6.0131E-02
       1     19      1      0   0      49        0        1      5      0  1.2476E-02   7.2608E-02
       1     20      1      0   0      50        0        1      5      0  1.4971E-02   8.7579E-02
       1     21      5      1   0      55        0        2      5      0  1.7966E-02   1.0554E-01
       1     22      7      1   0      62        0        3      5      0  1.7966E-02   1.2351E-01
       1     23      3      0   0      65        0        3      5      0  1.7966E-02   1.4148E-01
       1     24      5      0   0      70        0        3      5      0  1.7966E-02   1.5944E-01
       1     25      7      2   0      77        0        5      5      0  1.7966E-02   1.7741E-01
       1     26      8      3   0      85        0        8      5      0  1.7966E-02   1.9537E-01
       1     27      7      2   0      92        0       10      5      0  1.7966E-02   2.1334E-01
       1     28      8      2   0     100        0       12      5      0  1.7966E-02   2.3130E-01
       1     29     10      3   0     110        0       15      5      0  1.7966E-02   2.4927E-01
       1     30      4      0   0     114        0       15      5      0  1.7966E-02   2.6724E-01
       1     31      7      1   0     121        0       16      5      0  1.7966E-02   2.8520E-01
       1     32      9      3   0     130        0       19      5      0  1.7966E-02   3.0317E-01
       1     33      5      1   0     135        0       20      5      0  1.7966E-02   3.2113E-01
       1     34     15      3   0     150        0       23      5      0  1.7966E-02   3.3910E-01
       1     35     14      6   0     164        0       29      5      0  1.7966E-02   3.5706E-01
       1     36     11      3   0     175        0       32      5      0  1.7966E-02   3.7503E-01
       1     37     10      4   0     185        0       36      5      0  1.7966E-02   3.9300E-01
       1     38      8      1   0     193        0       37      5      0  1.7966E-02   4.1096E-01
       1     39      7      1   0     200        0       38      5      0  1.7966E-02   4.2893E-01
       1     40      8      3   0     208        0       41      5      0  1.7966E-02   4.4689E-01
       1     41     15      5   0     223        0       46      5      0  1.7966E-02   4.6486E-01
       1     42     18      5   0     241        0       51      5      0  1.7966E-02   4.8282E-01
```

Figure II-3a: Status file lists step, increment and iteration information during analysis

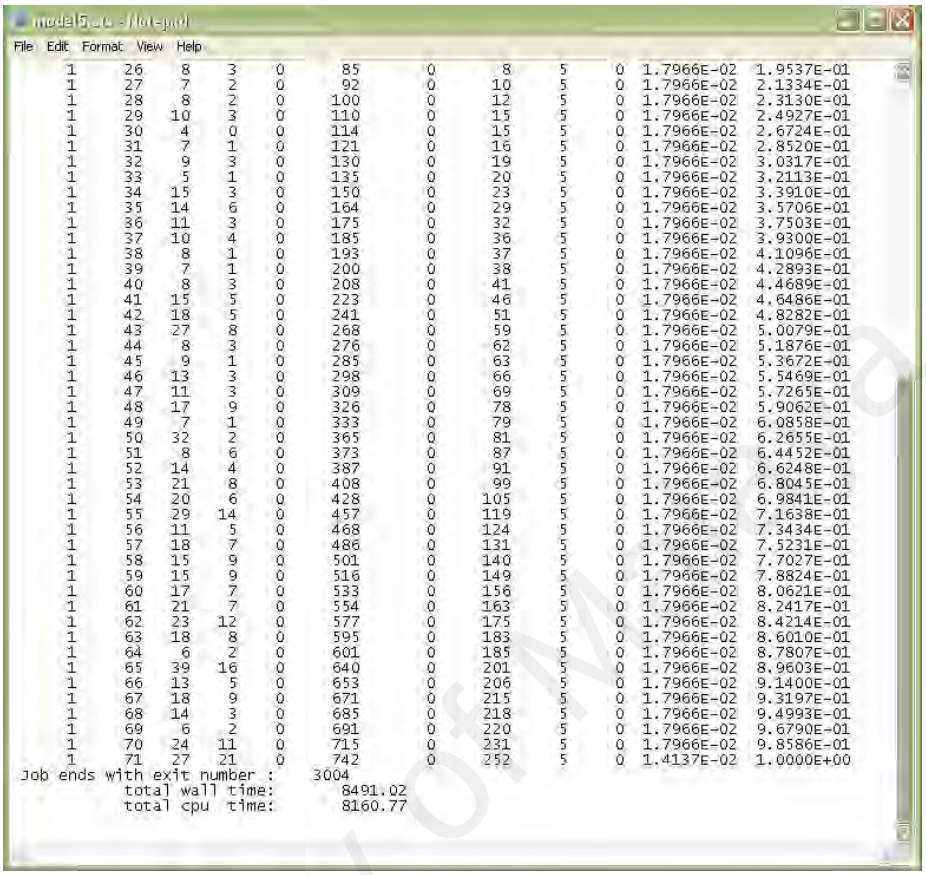

```
File  Edit  Format  View  Help
     1     26    8    3    0      85       0       8     5     0  1.7966E-02  1.9537E-01
     1     27    7    2    0      92       0      10     5     0  1.7966E-02  2.1334E-01
     1     28    8    2    0     100       0      12     5     0  1.7966E-02  2.3130E-01
     1     29   10    3    0     110       0      15     5     0  1.7966E-02  2.4927E-01
     1     30    4    0    0     114       0      15     5     0  1.7966E-02  2.6724E-01
     1     31    7    1    0     121       0      16     5     0  1.7966E-02  2.8520E-01
     1     32    9    3    0     130       0      19     5     0  1.7966E-02  3.0317E-01
     1     33    5    1    0     135       0      20     5     0  1.7966E-02  3.2113E-01
     1     34   15    3    0     150       0      23     5     0  1.7966E-02  3.3910E-01
     1     35   14    6    0     164       0      29     5     0  1.7966E-02  3.5706E-01
     1     36   11    3    0     175       0      32     5     0  1.7966E-02  3.7503E-01
     1     37   10    4    0     185       0      36     5     0  1.7966E-02  3.9300E-01
     1     38    8    1    0     193       0      37     5     0  1.7966E-02  4.1096E-01
     1     39    7    1    0     200       0      38     5     0  1.7966E-02  4.2893E-01
     1     40    8    3    0     208       0      41     5     0  1.7966E-02  4.4689E-01
     1     41   15    5    0     223       0      46     5     0  1.7966E-02  4.6486E-01
     1     42   18    5    0     241       0      51     5     0  1.7966E-02  4.8282E-01
     1     43   27    8    0     268       0      59     5     0  1.7966E-02  5.0079E-01
     1     44    8    3    0     276       0      62     5     0  1.7966E-02  5.1876E-01
     1     45    9    1    0     285       0      63     5     0  1.7966E-02  5.3672E-01
     1     46   13    3    0     298       0      66     5     0  1.7966E-02  5.5469E-01
     1     47   11    3    0     309       0      69     5     0  1.7966E-02  5.7265E-01
     1     48   17    9    0     326       0      78     5     0  1.7966E-02  5.9062E-01
     1     49    7    1    0     333       0      79     5     0  1.7966E-02  6.0858E-01
     1     50   32    2    0     365       0      81     5     0  1.7966E-02  6.2655E-01
     1     51    8    6    0     373       0      87     5     0  1.7966E-02  6.4452E-01
     1     52   14    4    0     387       0      91     5     0  1.7966E-02  6.6248E-01
     1     53   21    8    0     408       0      99     5     0  1.7966E-02  6.8045E-01
     1     54   20    6    0     428       0     105     5     0  1.7966E-02  6.9841E-01
     1     55   29   14    0     457       0     119     5     0  1.7966E-02  7.1638E-01
     1     56   11    5    0     468       0     124     5     0  1.7966E-02  7.3434E-01
     1     57   18    7    0     486       0     131     5     0  1.7966E-02  7.5231E-01
     1     58   15    9    0     501       0     140     5     0  1.7966E-02  7.7027E-01
     1     59   15    9    0     516       0     149     5     0  1.7966E-02  7.8824E-01
     1     60   17    7    0     533       0     156     5     0  1.7966E-02  8.0621E-01
     1     61   21    7    0     554       0     163     5     0  1.7966E-02  8.2417E-01
     1     62   23   12    0     577       0     175     5     0  1.7966E-02  8.4214E-01
     1     63   18    8    0     595       0     183     5     0  1.7966E-02  8.6010E-01
     1     64    6    2    0     601       0     185     5     0  1.7966E-02  8.7807E-01
     1     65   39   16    0     640       0     201     5     0  1.7966E-02  8.9603E-01
     1     66   13    5    0     653       0     206     5     0  1.7966E-02  9.1400E-01
     1     67   18    9    0     671       0     215     5     0  1.7966E-02  9.3197E-01
     1     68   14    3    0     685       0     218     5     0  1.7966E-02  9.4993E-01
     1     69    6    2    0     691       0     220     5     0  1.7966E-02  9.6790E-01
     1     70   24   11    0     715       0     231     5     0  1.7966E-02  9.8586E-01
     1     71   27   21    0     742       0     252     5     0  1.4137E-02  1.0000E+00
Job ends with exit number :    3004
          total wall time:      8491.02
          total cpu  time:      8160.77
```

Figure II-3b: Status file lists step, increment and iteration information during analysis

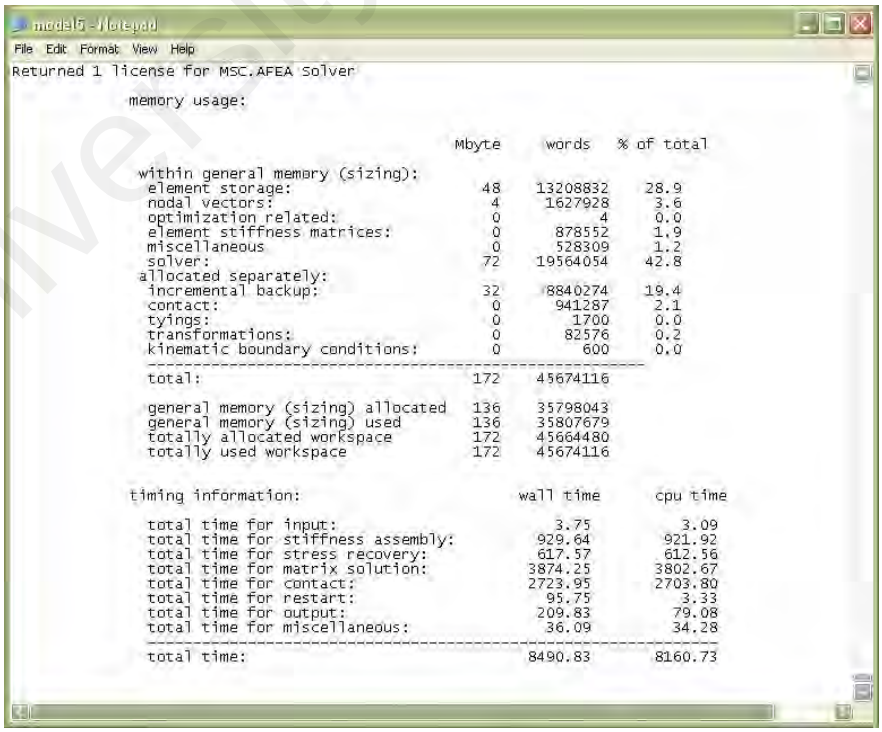

```
File  Edit  Format  View  Help
Returned 1 license for MSC.AFEA Solver

          memory usage:

                                                Mbyte      words   % of total

        within general memory (sizing):
         element storage:                          48   13208832     28.9
         nodal vectors:                             4    1627928      3.6
         optimization related:                      0          4      0.0
         element stiffness matrices:                0     878552      1.9
         miscellaneous                              0     528309      1.2
         solver:                                   72   19564054     42.8
        allocated separately:
         incremental backup:                       32    8840274     19.4
         contact:                                   0     941287      2.1
         tyings:                                    0       1700      0.0
         transformations:                           0      82576      0.2
         kinematic boundary conditions:             0        600      0.0
         ------------------------------------------------------------------
         total:                                   172   45674116

         general memory (sizing) allocated        136   35798043
         general memory (sizing) used             136   35807679
         totally allocated workspace              172   45664480
         totally used workspace                   172   45674116


        timing information:                              wall time      cpu time

         total time for input:                              3.75          3.09
         total time for stiffness assembly:               929.64        921.92
         total time for stress recovery:                  617.57        612.56
         total time for matrix solution:                 3874.25       3802.67
         total time for contact:                         2723.95       2703.80
         total time for restart:                           95.75          3.33
         total time for output:                           209.83         79.08
         total time for miscellaneous:                     36.09         34.28
         ------------------------------------------------------------------
         total time:                                     8490.83       8160.73
```

Figure II-4: Log file checks for error possibilities for the specific job

A

REFERENCES

A References

Ahmadian M.T., Nikooyan A. Asadi. 2005. Modeling and Prediction of Soft Tissue Directional Stiffness Using In Vitro Force-Displacement Data. *The First UAE International Conference on Biological and Medical Physics* 1: 123-126.

Akin, J.E. 1994. *Finite Elements for Analysis and Design.* New York: Academic Press.

Alcalde, R.E., Jinno T., Pogrel M.A., Matsumura T. 1998. Cephalometric norms for orthognathic surgery in Japanese adults. *J Oral Maxillofac Surg.* 56: 129-134.

Baraff, D. and Witkin A. 1998. Large steps in cloth simulation. *Proceedings of ACM SIGGRAPH '98, ACM Press*: 43-54.

Barr, A.H. 1984. Global and local deformations of solid primitives. *Computer Graphics* 18(3): 21-30.

Bhachu, D.S. and Kanal E. 2000. Implantable pulse generators (pacemakers) and electrodes: Safety in magnetic resonance imaging scanner environment. *Journal of Magnetic Resonance Imaging* 12: 201-204.

Bickford, William B. 1989. *A First Course in the Finite Element Method*. Illinois: McGraw-Hill.

Birk, D.E., Silver F.H., Trelstad R.L. 1991. *Cell Biology of Extracellular Matrix, Second Edition.* New York : Plenum Press.

Black, P.M., Moriarty T., Alexander E. III, Stieg P., Woodard E.J., Gleason P.L., Martin C.H., Kikinis R., Schwartz R.B., Jolesz F.A. 1997. The development and implementation of intraoperative MRI and its neurosurgical applications. *Neurosurgery*, 41(4): 831-842.

Blatz, P.L., Chu B.M. and Wayland H. 1969. On the mechanical behaviour of elastic animal tissue. *Trans. Soc. Rheol.* 13: 83-102.

Bohner, P., Pokrandt P., Haßfeld S. 1996. Simultaneous planning and execution in cranio-maxillo-facial surgery. In *Medicine Meets Virtual Reality4 (MMVR4)*.

Bourguignon, D. and Cani M.-P. 2000. Controlling anisotropy in mass-spring systems. *Computer Simulation and Animation*: 113-123.

Boutin, R.D., Briggs J.E., Williamson M.R. 1994 .Injuries associated with MR imaging: Survey of safety records and methods used to screen patients for metallic foreign bodies before imaging. *AJR Am J Roentgenol* 162: 195-199.

Bro-Nielsen, M. 1998. Finite element modeling in surgery simulation. *Proceedings of the IEEE: Special Issue on Virtual & Augmented Reality in Medicine* 86(3): 524-530.

Bro-Nielsen, M. and Cotin S. 1996. Real-time volumetric deformable models for surgery simulation using finite elements and condensation. *Computer Graphics Forum(Eurographics'96)* 15(3): 57-66.

Brooks, S.L. 2001. Basic principles of MR imaging. *Oral and Maxillofacial Surgery Clinics of North America* 13: 569-584.

Brown, J., Sorkin S., Bruyns C., Latombe J.C., Montgomery K., Stephanides M. 2001. Real-time simulation of deformable objects: tools and applications. In *Computer Animation publication*.

Burnett, D.S. 1987. *Finite Element Analysis – From Concepts to Applications*. Mass.: Addison-Wesley.

Carnegie-Mellon. 2000. Volume Rendering. http://www.cs.cmu.edu/afs/cs.cmu.edu/academic/class/15462/web.00f/notes/15-volren(4%20up).pdf (accessed on February 11, 2006).

Chabanas M. 2002. *Modélisation des tissue mous de la face pout la chirurgie orthognatique assistée par ordinateur*. Ph.D. diss., Université Joseph Fourier, Grenoble, France.

Chandrupatla, T.R. and Belegundu, A.D. 1997. *Introduction to Finite Elements in Engineering*. New Jersey: Prentice-Hall.

Cook, R.D., Malkus D.S., Plesha M.E. 1989. *Concepts and Applications of Finite Element Analysis*. New York: John Wiley & Sons.

Cook, T.H. 1989. Mechanical properties of human skin with aging. In *Aging and the skin*. Edited by Balin A.K. and Kligman A.M. New York: Raven Press.

Daniel, B.L., Jeffery S.S., Birdwell R.L., Ikeda D.M., Sawyer-Glover A.M., Herfkens R.J. 1998. Three-dimensional shaded-surface rendering of MR images of the breast: Technique, applications and impact on surgical management of breast disease. *Radiographics* 18: 483-496.

Danielson, D.A. 1973. Human skin as an elastic membrane. *J. Biomechanics 6*: 539-546.

Delcker, A. and Diener H.C. 1994. Quantification of atherosclerotic plaques in carotid arteries by three-dimensional ultrasound. *The British Journal of Radiology* 67: 672-678.

Delingette, H. 1998. Toward realistic soft-tissue modeling in medical simulation. *Proc. of IEEE : Special Issue on Surgery Simulation* 86(3): 512-523.

Delingette, H., Subsol G., Cotin S., Pignon J. 1994. A craniofacial surgery testbed. *Technical Report 2119, Institut National de Recherche en Informatique et Automatique, France*.

Deng, X.Q. 1988. A finite element analysis of surgery of the human facial tissue. Ph.D. diss., Columbia University.

Deuflhard, P., Leinen P., Yserentant H. 1989. Concepts of an adaptive hierarchical finite element code. *IMPACT Comp. Sci. Eng. 1*: 3-35.

Farkas, L.G. 1994. *Anthropometry of the Head and Face, Second edition*. New York: Raven Press 1994.

Fung, Y.C. 1967. Elasticity of soft tissues in simple elongation. *Am. J. Physiol.* 213: 1532-1544.

Fung, Y.C. 1981. *Biomechanics: Mechanical properties of living tissues.* Berlin: Springer-Verlag.

Gibson, T., Kenedi R.M., Craik J.E. 1965. The mobile micro-architecture of dermal collagen. *Br J Surg* 53: 764-770.

Gibson, S.F.F., and Mirtich, B. 1997. A survery of deformable modeling in computer graphics. *Technical Report TR-97-19,* Mitsubishi Electric Research Laboratory, Cambridge, MA, USA.

Girod, S., Keeve E., Girod B. 1993. Soft tissue prediction in orthognathic surgery by 3D CT and 3D laser scanning. *Journal of Oral and Maxillofacial Surgery Suppl. 51*: 167.

Gladilin, E., 2003. Biomechanical modeling of soft tissue and facial expressions for craniofacial surgery planning. Ph.D. diss., Free University Berlin.

Gladilin, E., Zachow S., Deuflhard P., Hege H.-C. 2001a. A biomechanical model for soft tissue simulation in craniofacial surgery. *In Proc. of MIAR*: 137-141.

Gladilin, E., Zachow S., Deuflhard P., Hege H.-C. 2001b. Towards a realistic simulation of individual facial mimics. In *Proc. of VMV*: 129-133.

Gladilin, E., Zachow S., Deuflhard P., Hege H.-C. 2001c. Validation of a linear elastic model for soft tissue prediction in craniofacial surgery. In *Proc. of SPIE Medical Imaging Conference* 4319: 27-35.

Gladilin, E., Zachow S., Deuflhard P., Hege H.-C. 2002. A nonlinear elastic soft tissue model for craniofacial surgery simulations. In *Proc of ESAIM* 12: 61-66.

Gladilin, E., Zachow S., Deuflhard P., Hege H.-C. 2004. Anatomy and physics based facial animation for craniofacial surgery simulations. In *Medical & Biological Engineering & Computing*, 42(2): 167-170.

Gray, H. 1918. *Gray's Anatomy of the Human Body, 20th Edition*. www.bartleby.com (accessed March 8, 2006).

Hager J.C. 2003. DataFace: Psychology, Appearance and Behavior of the Human Face. http://face-and-emotion.com/dataface/general/homepage.jsp (accessed February 20, 2006).

Han, L., Noble A., Burcher M. 2002. The elastic reconstruction of soft tissue. In *Proc. of IEEE International Symposium on Biomedical Imaging*: 1035-1038.

Harris, M. and Reynolds I.R. 1991. *Fundamentals of orthognathic surgery*. London: W.B. Saunders.

Hata, N., Dohi T., Warfield S., Wells III W., Kikinis R., Jolesz F. 1998. Multimodality deformable registration of pre- and intraoperative images for MRI-guided brain surgery." *In MICCAI'98, Lecture Notes in Computer Science* 1496: 1067-1074.

Hemmy, D.C., David D.J., Herman G.T. 1983. Three-dimensional reconstruction of craniofacial deformity using computer tomography. *Neurosurgery* 13: 534-541.

Hilderbrandt, J., Fukaya H., Martin C.J. 1969. Stress-strain relations of tissue sheets undergoing uniform two-dimensional strecth. *J. App. Physiol.* 27: 758-762.

Horace, H.S.I., Christy S.B.K, Xia J. 2000. Simulated patient for orthognathic surgery. *Computer Graphics International*: 239-246.

Hounsfield, G.N., Ambrose J.A. 1973. Computerized Transverse Axial Scanning (Tomography). *British Journal of Radiology* 46: 1016-1022.

Huebner, K.H. *The finite element method for engineers*. New York: John Wiley & Sons, 2001.

Ingervall, B., Mohlin B., Thilander B. 1978. Orevalence and awareness of malocclusion in Swedish men. *Community Dent Oral Epidemiol 6*: 308-314.

Joedicke, A., Deinsberger W., Erbe H., Kriete A., Boeker D.K. 1998. Intraoperative three-dimensional ultrasonography: an approach to register brain shift using multidimensional image processing. *Minim Invasive Neurosurg*, 41(1): 13-19.

Kähler, K., Haber J., Seidel H-P. 2001. Geometry-based muscle modeling for facial animation. *In Proc of Graphics Interface* : 27-36.

Karlamangla, A.S., Young J.T., Huang M., Greendale G.A. 2002. Differences in measures of femoral neck strength between Japanese-American and Caucasian-American woman. *Journal of Bone and Mineral Research* 17: Abstract 1207.

Kawamata, A., Ariji Y, Langlais R.P. 2001. Three-dimensional imaging for orthognathic surgery and orthodontic treatment. *Oral and Maxillofacial Surgery Clinics of North America* 13: 713-725.

Kawamata, A., Ariji Y., Langlais R.P. 2000. Three-dimensional computed tomography imaging in denstistry. *Dental Clinics of North America* 44: 395-410.

Keeve, E. and Kikinis R. 1999. Deformable modeling of facial tissue. *Proceedings of the First Joint BMES/EMBS Conference Serving Humanity, Advancing Technology*: 502.

Keeve, E., 1996a. Visualisierungs und Simulationsverfahren zur interaktiven Planung kraniofazialer Korrektur-operationen. Ph.D. diss., University of Erlangen.

Keeve, E., Girod S., Augustin A., Binner A., Girod B. 1996. Interactive craniofacial surgery simulation. *Proc. 3D Image Analysis and Synthesis*: 219-224.

Keeve, E., Girod S., Girod B. 1996. Computer-aided craniofacial surgery. *Computer Assisted Radiology (CAR) 3(2*): 66-70.

Keeve, E., Girod S., Girod B. 1996. Craniofacial surgery simulation. In *Proceedings of the 4th International Conference on Visualization in Biomedical Computing (VBC '96)* 4: 541-546.

Keeve, E., Girod S., Kikinis R., Girod B., 1998. Deformable modeling of facial tissue for craniofacial surgery simulation. Invited paper. *Computer Aided Surgery* 3(5): 228-238.

Keeve, E., Girod S., Neukam F.-W., Girod B. 1997. Biomechanic-based modeling of facial tissue for craniofacial surgery simulation. *Proc. 1st Int. Congress on Computer Integrated Surgery CIS'97,* in *Computer Aided Surgery,* 2(3/4).

Keeve, E., Girod S., Pfeifle S., Girod B. 1996. Anatomy based facial tissue modeling using the finite element method. *Proc. of IEEE Visualization '96*: 1-10.

Kenedi, R.M., Gibson T., Daly C.H. 1965. Bioengineering studies of the human skin. *Proc. Symp. On Biomechanics and Related Bioengineering Topics*: 147.

Kenedi, R.M., Gibson T., Evans J.H., Barbenel J.C. 1975. Tissue Mechanics. *Physics in Medicine and Biology 20*: 699-717.

Kikinis, R., Cline H., Altobelli D., Halle M., Lorensen W., Jolesz F. 1992. Interactive visualization and manipulation of 3D reconstructions for the planning of surgical procedures. In *Proceedings of Visualization in Biomedical Computing VBC '92*: 559-563.

Koch R.M. 2000. Methods for physics based facial surgery prediction. Ph.D. diss., Department of Computer Science, ETH Zürich.

Koch, R.M., Gross M.H., Carls F.R., von Büren D.F., Fankhauser G., Parish Y.I.H. 1996. Simulating facial surgery using finite element models. In *SIGGRAPH'96 Conference Proceedings, Annual Conference Series, ACM SIGGRAPH* 4(9):421-428.

Koch, R.M., Roth S.H.M., Gross M.H., Zimmermann A.P., Sailer H.F. 2002. A framework for facial surgery simulation. *Proceedings of ACM Spring Conference on Computer Graphics*.

Kolston, Paul J. 2000. Finite element modeling: a new tool for the biologist." *Philosophical Transactions of the Royal Society (Series A: Mathematical, Physical and Engineering Sciences) 358*: 611-631.

Kwan, M.K. and Woo S.L-Y. 1989. A structural model to describe the non-linear stress-strain behavior for parallel-fibered collagenous tissues. *J. Biomech. Engng. 111*: 361-363.

Lanir, Y. 1987. *Handbook of Bioengineering*. New York: McGraw-Hill.

Larrabee, W. 1986. A finite element model of skin deformation. *Laryngoscope 96*: 406-412.

Lee, Y. and Terzopoulos D. 1995. Realistic modeling for facial animation. *Proceedings of SIGGRAPH '95, Computer Graphics Proceedings, Annual Conference Series*: 55-62.

Liu, Y., Kerdok A.E., Howe R.D. 2004. A nonlinear finite element model of soft tissue indentation. *Proceedings of International Symposium on Medical Simulation* 2: 67-76.

Lorensen, W.E., Cline H.E. 1987. Marching cubes: A high resolution 3D surface construction algorithm. *SIGGRAPH 1987, ACM Computer Graphics 21*: 163-169.

Maciel, A., Nedel L.P., Freitas C.M.D.S. 2002. Anatomy-based joint models for virtual humans skeletons. In *Proceedings of Computer Animation 2002*: 220-224.

Maciel, A., Ronan B., Thalmann D. 2003. Deformable tissue parametrized by properties of real biological tissue. *In Proc of Surgery Simulation and Soft Tissue Modeling: International Symposium, IS4TM,* 4: 74-87.

Marc Analysis Research. "Automated Contact Analysis Using Marc". <http://www.techsavvy.com/industry/file/national/08fqj/mrc02.html> (accesed July 13, 2005).

Masel R. 1999. A Dictionary of Dental Terms. http://www.bracesinfo.com/glossary.html (accessed on March 5, 2006).

Materialise. 1991. *Mimics 8.1 Software Manual*. Belgium.

Materialise. 1991. *Mimics 8.1 Software*. Belgium.

Maue-Dickson, W., Trefler M. and Dickson D.R. 1979. Comparison of dosimetry and image quality in computed and conventional tomography. *J. of Radiology* 131: 509-514.

Mercury Computer Systems Inc. 1999. *Amira 3.0 demo* (available in software). USA.

Mercury Computer Systems Inc. 1999. *Amira 3.0 software*. USA.

Miloro, M., Ghali G.E., Larsen P.E., Waite P.D., Decker B.C. 2004. *Principles of oral and maxillofacial surgery Second edition Volume 2*, Canada: Peterson.

MSC.Software Corporation. 1999. *MSC.AFEA software ver. 2004*. Santa Ana, USA.

MSC.Software Corporation. 1999. *MSC.Marc Introductory Course Manual*. Santa Ana, USA.

MSC.Software Corporation. 2003. *Interface to MSC.Marc Preference Guide*. Santa Ana, USA.

MSC.Software Corporation. 2003. *MSC.Patran 2003 MSC.Documentation*. Santa Ana, USA.

Müller, J., Sahni O., Jansen K.E., Shephard M.S., Taylor C.A. 2005. A tool for the efficient FE-simulation of cardio-vascular flow. *Proc. of Second NAFEMS CFD Seminar: Simulation of Complex Flows (CFD)* 2: 1-10.

Nastri, V. Marcio, Baptista Luciana P.S., Baroni, Ronaldo H., Blasbalg Roberto, de Ávila Luis F., Leite Claudia C., de Castro Claudio C., Cerri Giovanni G. 2004. Gadolinium-enhanced three-dimensional MR angiography of Takayasu Arteritis. *Radiographics* 24: 773-786.

Nedel, L.P. and Thalmann D. 1998. Real time muscle deformations using mass-spring systems. *Computer Graphics International*: 156-165.

Nikishkov, G.P. 2004. Introduction to the finite element method. University of Aizu. http://www.u-aizu.ac.jp/~niki/feminstr/introfem/introfem.html (accessed March 10, 2005).

Ottosen, N. and Petersson H. 1992. *Introduction to the Finite Element Method.* New York: Prentice Hall.

Parks, E.T. 2001. Basic principles of Computed Tomography. *Oral and Maxillofacial Surgery Clinics of North America* 13: 547-567.

Pieper, S.D. 1991. CAPS: Computer-aided plastic surgery. Ph.D. diss., MIT, Media Arts and Sciences, Cambrigde, MA.

Rao, S.S. 1989. *The Finite Element Method in Engineering*. England: Pergamon Press.

Reddy, J.H. 1992. *An Introduction to the Finite Element Method.* New York: McGraw Hill.

Reddy, J.N. 1993. *An Introduction to Finite Element Method, Second Edition*. New York: McGraw-Hill.

Richter, M., Goudot P., Laurent F., Jaquinet A., Bidaut L. 1998. *Chirurgie correctrice des malformations ou dysmorphies maxillomandibulaires: bases chirurgicales*. In *Encyclopédie médico-chirurgicale*, *Stomatologie*, Paris: Elsevier. Quoted in Chabanas M. 2002. *Modélisation des tissue mous de la face pout la chirurgie orthognatique assistée par ordinateur*. Ph.D. diss., Université Joseph Fourier, Grenoble, France.

Roberts, J.C. 1993. An overview of rendering from volume data - including surface and volume rendering. *Technical Report 13-93, Computing Laboratory, University of Kent, Canterbury, UK.*

Roth, S.H.M., Gross M.H., Turello S., Carls F.R. 1998. A Bernstein-Bézier based approach to soft tissue simulation. *Technical Report 282, Institute of Scientific Computing, ETH Zurich*.

Salonen, L., Mohlin B., Gotzlinger B., Hellden L. 1992. Need and demand for orthodontic treatment in an adult Swedish population. *Eur J Orthod 14*: 359-368.

Samii V. 2005. Introduction to Magnetic Resonance Imaging (MRI). www.vet.ohio-state.edu/assets/courses/vm526/mri/vm526mri.pdf (accessed Mac 17, 2005).

Sarni, S., Maciel A., Boulic R., Thalmann D. 2004. Evaluation and visualization of stress and strain on soft biological tissues in contact. In *Proceedings of International Conference on Shape Modeling and Applications*: 255- 262.

Schmidt, J.G., Berti G., Fingberg J., Cao J. Wollny G. 2004. A finite element based tool chain for the planning and simulation of maxillo-facial surgery. In *Proc. of European Congress on Computational Methods in Applied Sciences and Engineering, ECCOMAS*: 1-17.

Schutsyer, F., Cleynenbreugel J.V., Schoenaers J., Marchal G., Suetens P. 1999. A simulation environment for maxillofacial surgery including soft tissue implications. *Medical Image Computing & Computer-Assisted Intervention, Second International Conference* 2: 65-70.

Seeman, E. 1998. Growth in bone mass and size – are racial and gender differences in bone mineral density more apparent than real?. *The Journal of Clinical Endocrinology & Metabolism 83*: 1414-1419.

Shen, G., Hagg U., Rabie A.B.M. and Zhao Z.H. 2000. Quantitative assessment of the condylar chondrogenesis triggered by bite-jumping appliance. *Chinese Journal of Orthodontics 7*: 7-11.

Shirkhoda, A., Brashear H.R., Zelenik M.E., Burke D.C. 1984. Sacral abnormalities--computed tomography versus conventional radiography. *J Comput. Tomogr.* 8(1): 41-51.

Snell, J.W., Merickel M.B., Ortega J.M., Goble J.C., Brookeman J.R., Kassell N.F. 1994. Segmentation of the brain from 3D MRI using a hierarchical active surface template. *Proc. of the International Society for Optical Engineering (SPIE). Medical Imaging 1994: Image Processing* 2167: 2-9.

Soh, J., Sandham A., Chan Y.H. 2005. Occlusal status in Asian male adults: prevalence and ethnic variation. *The Angle Orthodontist* 75(5): 814-820.

Soyama, Y., Yasuda, T. and Yokoi, S. et al. 1989. A hip joint surgical planning system using 3-D images, (In Japanese). *Japanese Journal of Medical Electronics and Biological Engineering*, 27(2): 70-78.

Stalling, D., Hege H.-C., Zöckler M. et al. *1999. Amira-An advanced 3D visualization and modeling system*. *http://amira.zib.de (accessed August 20, 2004).*

Taylor K. and Molly S. 2003. The dermis and epidermis. http://www.sad61.k12.me.us/~andrea_capano/2003Webproject/pera/webAtaylork/dermisandepidermis.html (accessed February 9, 2005).

Terai, H., Shimahara M., Sakinaka Y., Tajima S. 1999. Accuracy of integration of dental casts in three-dimensional models. *J Oral Maxillofac Surg.* 57(6): 662-665.

Terzopoulos, D. and Waters K. 1990. Physically-based facial modeling, analysis and animation. *The Journal of Visualization and Computer Animation* 1: 73-80.

Terzopoulos, D. and Waters K. 1993. Analysis and synthesis of facial image sequences using physical and anatomical models. *IEEE Transactions on Pattern Analysis and Machine Intelligence* 15(6): 569-579.

Teschner, M., Girod S., Girod B. 1999. Interactive osteotomy simulation and soft-tissue prediction. In *Proc Vision, Modeling and Visualization, VMV'99*: 405-412.

Teschner, M., Girod S., Girod B. 1999. Optimization approaches for soft-tissue prediction in craniofacial surgery simulation. *Proc. MICCAI '99*: 1183-1190.

Teschner, M., Girod S., Girod B. 2000. Direct computation of nonlinear soft-tissue deformation. In *Proc. of Vision, Modeling and Visualization, VMN'00* : 383-390.

Tod, M.A. and Taverne A.A. 1997. Prevalence of malloclusion traits in an Australian adult population. *Aust Orthod J.* 15: 16-22.

Vannier, M.W., Marsh J.L., Warren J.O. 1983. Three dimensional computer graphics for craniofacial surgical planning and evaluation. *Computer Graphics* 17(3): 263-273.

Veronda, D.R. and Westmann R.A. 1970. Mechanical characteristics of skin—finite deformations. *J. Biomech.* 3: 111-124.

Viidik, A. 1987. Properties of tendons and ligaments. *Handbook of Bioengineering*. New York: McGraw-Hill.

Viidik, A., Vuust J. 1980. *Biology of collagen*. London: Academic Press.

Wang, X.F., Beck T.J., Duan Y., Seeman E. 2002. Racial differences in hip fracture risk are established during growth: structural and biomechanical determinants of strength at the proximal femur in Asians and Caucasians. *Journal of Bone and Mineral Research* 17: Abstract 1167.

Watanabe, M., Suda N., Ohyama K. 2005. Mandibular prognathism in Japanese families ascertained through orthognathically treated patients. *Am J Orthod Dentofacial Orthop.* 128(4): 466-70.

Waters, K., Frisbie J. 1995. A coordinated muscle model for speech animation. Proceeding of Graphics Interface 95 :163-170.

Woon, K.C., Thong Y.L., Abdul Kadir R. 1989. Permanent dentition occlusion in Chinese, Indian and Malay groups in Malaysia. *Aust Orthod J. 11*: 45-48.

Xia, J., Horace Ip. H.S., Nabil S., Helena W.T.F., Jaime G., Dongfeng W., Richie Y.W.K, Christy K.S.B. and Henk T. 2001. Three-dimensional virtual-reality surgical planning and soft-tissue prediction for orthognathic surgery. *Proceedings of IEEE Transactions on Information Technology in Biomedicine.* 5(2) : 97-107.

Xia, J., Qi F., Yuan W., Wang D., Qiu W., Sun Y., Huang Y., Shen G., Wu H. 1995. Computer Aided Simulation System for Orthognathic Surgery. *Proceedings of Eight IEEE Symposium on Computer-based Medical Systems, IEEE Computer Society Press.* 11: 386-393.

Yasuda, T., Hashimoto Y., Yokoi S., Toriwaki J. 1990. Computer system for craniofacial surgical planning based on CT images. *IEEE Transactions on Medical Imaging 9(3)*: 270-280.

Zachow, S. 2006. ZIB: Computer assisted cranio-maxillofacial surgery. Zuse Institute Berlin. http://www.zib.de/Visual/projects/cas/cas-gallery.html (accessed March 03, 2006).

Zachow, S., Gladilin E., Hege H.-C., Deuflhard P. 2000. Finite-element simulation of soft tissue deformation." *Proceedings of the 14th International Symposium: Computer Assisted Radiology and Surgery,* 14: 23–28.

Zachow, S., Hege H.-C., Deuflhard P. 2006. Computer assisted planning in cranio-maxillofacial surgery. *Journal of Computing and Information Technology - Special Issue on Computer-Based Craniofacial Modelling and Reconstruction*: 53-64.

Zachow, S., Hierl, Th., Erdmann, B. 2004. A quantitative evaluation of 3D soft tissue prediction in maxillofacial surgery planning. In *Proc. 3 Jahrestagung der Deutschen Gesellschaft für Computer- und Roboter-assistierte Chirurgie(CURAC*) 3: 75-79.

Zienkiewics, O.C. and Taylor R.L. 1989. *The Finite Element Method, Vol. 1 and 2*. New York: McGraw Hill.